CENTER FOR
TRANSPORTATION STUDIES

UNIVERSITY OF MINNESOTA

RESEARCH REPORT

A Computational Study of the I-35W Bridge Collapse

Minmao Liao
Taichiro Okazaki

CTS 09-29

Technical Report Documentation Page

1. Report No. CTS 09-29	2.	3. Recipients Accession No.	
4. Title and Subtitle A Computational Study of the I-35W Bridge Collapse		5. Report Date October 2009 6.	
7. Author(s) Minmao Liao and Taichiro Okazaki		8. Performing Organization Report No.	
9. Performing Organization Name and Address Department of Civil Engineering University of Minnesota 500 Pillsbury Drive, SE Minneapolis, MN 55455-0116		10. Project/Task/Work Unit No. CTS Project # 2008049 11. Contract (C) or Grant (G) No.	
12. Sponsoring Organization Name and Address The National Science Foundation 4201 Wilson Boulevard Arlington, Virginia 22230 Center for Transportation Studies University of Minnesota 511 Washington Avenue SE, Suite 200 Minneapolis, Minnesota 55455		13. Type of Report and Period Covered Final Report 14. Sponsoring Agency Code	
15. Supplementary Notes http://www.cts.umn.edu/Publications/ResearchReports/			

16. Abstract (Limit: 250 words)

Reported evidence suggests that failure of gusset plates initiated the collapse of the I-35W Bridge in Minneapolis, Minnesota. The particular gusset plates were at a panel point designated as U10. Therefore, a computational study was conducted on the condition of the U10 gusset plates at the time of bridge collapse. The primary objectives of this study were: (1) to evaluate previous research and existing design methods for gusset plate connections; (2) to examine the mechanical condition of the U10 gusset plates at the time of the collapse; (3) to examine possible scenarios that led to the collapse of the entire bridge; and (4) to identify research needs to improve the design methods for gusset plate connections. The forces delivered to panel point U10 were reproduced using available information of the bridge. The truss forces were introduced to detailed nonlinear, three-dimensional finite element models to calculate stress and strain states of the gusset plates. The results indicate that substantial portions of the U10 gusset plates were yielded at the time of collapse, confirming earlier findings from federal and state investigations. Insufficient strength of the gusset plate, along with weight increase due to past deck reconstruction and construction material and equipment staged on the day of collapse, were identified as the main contributing factors to the substantial yielding. It is important to note that, even with the weight increase, the gusset plates would not have yielded substantially if the gusset plates had adequate thickness. The results also suggest that the interaction of compression and shear played an important role in the gusset plate failure and should be addressed in gusset plate design. This interaction is not well understood based on available research.

17. Document Analysis/Descriptors I-35W Bridge, Gusset plates, Finite element method, Bolted connection, Structural connection		18. Availability Statement No restrictions. Document available from: National Technical Information Services, Springfield, Virginia 22161	
19. Security Class (this report) Unclassified	20. Security Class (this page) Unclassified	21. No. of Pages 95	22. Price

A Computational Study of the I-35W Bridge Collapse

Final Report

Prepared by

Minmao Liao
Taichiro Okazaki

Department of Civil Engineering
University of Minnesota

October 2009

Published by

Center for Transportation Studies
University of Minnesota
511 Washington Avenue SE, Suite 200
Minneapolis, Minnesota 55455

ACKNOWLEDGEMENTS

The financial support for this study was provided by the National Science Foundation (CMMI-0753666) and by the Center of Transportation Studies of the University of Minnesota. Computing resources were provided by the Minnesota Supercomputing Institute.

The authors would like to thank Dr. Roberto Ballarini, Dr. Arturo E. Schultz, and Dr. Theodore V. Galambos for their suggestions and comments on this study and report. Alicia Forbes and Tor Oksnevad constructed the original 2D and 3D bridge models.

TABLE OF CONTENTS

LIST OF TABLES

LIST OF FIGURES

EXECUTIVE SUMMARY

On Wednesday, August 1, 2007, about 6:05 p.m. CDT, the bridge carrying Interstate Highway 35W (I-35W, National Bridge Inventory Structure No. 9340) over the Mississippi River in Minneapolis, Minn., suffered a tragic collapse within a matter of seconds. The 456-foot-long center span of the deck truss portion fell into the Mississippi River. According to a post-accident investigation, at the time of the collapse, a total of 111 vehicles were on the collapsed portion, and of these, 17 vehicles fell into the water. Thirteen people died, and 145 people were injured because of the collapse.

After the collapse, an investigation led by the National Transportation Safety Board (NTSB) concluded that inadequate design of gusset plates played a key role in the collapse of the bridge. The particular gusset plates were at a panel point designated as U10. At this panel point, a pair of gusset plates connected top chord truss members, two diagonal members, and a vertical member. This report describes a computational study on the condition of the U10 gusset plates at the time of the collapse. The primary objectives of this study were: (1) to evaluate previous research and existing design methods for gusset plate connections; (2) to examine the mechanical condition of the U10 gusset plates at the time of the collapse; (3) to examine possible scenarios that led to the collapse of the entire bridge; and (4) to identify research needs to improve the design methods for gusset plate connections.

To achieve the above objectives, first, the bridge condition was carefully analyzed using available information on the loading conditions at the time of the collapse. The loading included dead loads from original construction, added dead loads due to renovations in later years, live loads due to traffic, construction loads placed on the bridge on the day of the collapse, and thermal effects. Two and three-dimensional truss bridge models were created to reproduce the truss forces. The analysis suggested that renovations conducted in 1977 and 1998 substantially increased the weight of the concrete slab, and consequently increased the truss forces by 30%. The construction loads, which were concentrated near panel point U10, caused another 10 to 15% increase in the truss forces applied on panel point U10.

The truss forces obtained from the bridge analysis were then used to check the adequacy of individual truss members and the U10 gusset plates using conventional design methods. The design check indicated that all truss members were reasonably sized. However, the U10 gusset plates were found to be inadequate according to these design checks. It is noted that panel point U10 was located at the inflection point of the continuous-span truss bridge. The force in the top chord changed from tension on one side of the panel point to compression on the other side, and accordingly, one diagonal delivered compression, while the other diagonal delivered tension to the panel point. According to the design checks, the U10 gusset plates were not adequately sized to carry the net shear force produced by the combined forces, and they were not adequate to carry the compression delivered by the compression diagonal.

The truss forces computed from the bridge analysis were introduced to a detailed nonlinear finite element model of the U10 gusset plate connection. Available experimental data was used to establish a finite element modeling procedure that reliably captures the behavior of gusset plates under tension or compression. The computed mechanical condition of the U10 gusset plates was compared to available forensic evidences. For example, the locations and

directions of high principal stress in the finite element model were found to correspond well with the observed fractures. The computation results suggest that a substantial portion of the U10 gusset plates may have yielded at the time of the collapse, confirming earlier findings from federal and state investigations, and the simple design checks mentioned above. Insufficient strength of the gusset plate, along with addition of dead loads during service life, and construction loads placed on the day of the collapse were identified as the main contributing factors to the substantial yielding. It is important to note that, even with the weight increase, the gusset plates would not have yielded substantially if the gusset plates had adequate thickness. Temperature gradient between the two sides of the gusset plate connection may have produced additional stress and strain in the U10 gusset plates, but they were clearly a secondary factor. It is also noted that the effect of temperature gradient is difficult to quantify because the computed results are highly dependent on the assumed boundary conditions for the analysis model.

The finite element analysis results also suggest that the interaction between compression and shear played an important role in the gusset plate failure. On the other hand, based on a literature survey, this interaction is not well understood from previous research. Standard design methods do not explicitly account for the interaction. Therefore, further research is recommended to clarify the effect of interaction between compression (or tension) and shear in gusset plate behavior.

Finally, the bridge collapse sequence was studied based on a video image captured by a monitoring camera and analysis of truss force redistribution after failure of the U10 gusset plate connection. The proposed sequence might be explained as follows: first, the west U10 gusset plate connection failed; truss force redistribution led to overload and failure of the east U10 gusset plate connection; the center span of the deck truss portion now acted as a cantilever with the south end free and north end fixed; due to large bending moment produced at the north end, the north end of the center span also failed; the entire center span fell and pulled down the north side span toward the river in the process.

CHAPTER 1: INTRODUCTION

1.1 General

On Wednesday, August 1, 2007, about 6:05 p.m. central daylight time, the bridge carrying Interstate Highway 35W (I-35W, National Bridge Inventory Structure No. 9340) over the Mississippi River in Minneapolis, Minnesota, suffered a tragic collapse within a matter of seconds. Figure 1.1 shows a comparison of the bridge before and after the collapse. The photographs are from a report by the National Transportation Safety Board (NTSB 2008a). The 456-foot-long center span of the deck truss portion of the bridge fell into the Mississippi River. According to a post-accident investigation by the NTSB (NTSB 2008b), at the time of the collapse, a total of 111 vehicles were on the collapsed portion, and of these, 17 vehicles fell into the water. Thirteen people died, and 145 people were injured because of the collapse.

(a) Before collapse

(b) After collapse

Figure 1.1 Photographs of I-35W Bridge (from NTSB 2008a).

The collapse of an interstate highway bridge in a major U.S. downtown area was unprecedented. What makes the event peculiar is that the bridge was a very typical structure and that the collapse occurred under what was thought to be normal operating conditions except for minor deck, joint, lighting, and guardrail repairs. In addition, steel truss bridges such as the I-35W Bridge are a very common form for long-span bridges in the U.S. and worldwide. Until the current event occurred, steel truss bridges had earned the reputation of being economical and reliable. While the small redundancy of the trusses may be of concern, it is believed that mandated maintenance procedures assure that this structural system is as safe and reliable as any other.

After the collapse, an investigation led by the NTSB (2008b) concluded that the bridge failure initiated at a gusset plate connection that connected the top chord members to a compression diagonal and tension diagonal. The critical gusset plate connection was at a panel point designated as U10. The location of this panel point is indicated in Figure 1.1(a). The NTSB (2008b) suggests that inadequate design of the U10 gusset plates was a major contributing factor to the collapse, and "lack of guidance" with regard to the construction loads placed on the bridge may have been the trigger that initiated the collapse.

Considering the large number of steel truss bridges in service, and the common use of the truss system in buildings and facilities, further understanding of the behavior of the U10 gusset plates is essential. Therefore, this report describes a computational study on the condition of the U10 gusset plates at the time of the bridge collapse. Based on available information, the loading condition of the bridge at the time of the collapse was estimated. Two and three-dimensional (2D and 3D) truss bridge models were created to evaluate truss forces and to examine the collapse scenarios that followed the gusset plate failure. The forces obtained from the bridge models served as loading conditions for a detailed finite element model of the critical gusset plate connection. The finite element modeling procedure was validated using available experimental data. Results from the gusset plate analyses were used to gain insight into probable causes of the gusset plate failure, possible failure mechanism, and improvement of gusset plate connection design. Design implications of the results were examined.

1.2 Objectives

The primary objectives of this study were as follows:

- To evaluate previous research and existing design methods for gusset plate connections.
- To examine the mechanical condition of the U10 gusset plates at the time of the collapse.
- To examine possible scenarios that led to collapse of the entire bridge.
- To identify research needs to improve the design methods for gusset plate connections.

1.3 Outline

The remaining part of this report is divided into the following six chapters:

- Chapter 2 describes factual information of the bridge, including the structural system, condition changes during its service life, and forensic evidences after the bridge collapse. The second half of the chapter is a literature review of topics relevant to gusset plate connections in truss bridges.
- Chapter 3 describes the bridge analyses conducted in this study. The loading condition of the bridge at the time of the collapse was estimated based on available construction drawings and reported data. Subsequently, the 2D and 3D truss bridge models are discussed. These models were used to estimate the truss forces that acted on panel point U10 at the time of the collapse. Design checks of truss members and gusset plates are discussed.
- Chapter 4 validates the finite element modeling procedure for the U10 gusset plate connections using existing test data. Two verification studies are discussed: one based on a tension gusset plate connection test and one based on a compression gusset plate connection test.
- Chapter 5 focuses on nonlinear finite element analyses of a detailed U10 gusset plate connection model. The results are compared against observed fractures from reported forensic studies. Comments are made on the effect of using thicker gusset plates and the interaction between compression and shear acting in the gusset plates.
- Chapter 6 describes possible sequence of the bridge collapse. Assuming that the U10 gusset plates failed at the connection with compression diagonal L9/U10, the resulting truss force redistribution is discussed. The collapse sequence is described based on truss force redistribution, and is compared against a video image recording of the bridge collapse.
- Chapter 7 summarizes findings of this study and gives recommendations for future research.

CHAPTER 2: BACKGROUND

2.1 Introduction

Chapter 2 describes background information for this study. Section 2.2 describes the known and reported facts of the I-35W Bridge. The history and configuration of the bridge are described. In addition, forensic evidences after the collapse, including fracture locations and orientations at panel point U10 are described. A more detailed description of the bridge is provided in Appendix A. Section 2.3 describes a literature review of previous research and design methods of gusset plate connections.

2.2 Reported Facts of the I-35W Bridge

According to the Minnesota Department of Transportation (Mn/DOT 2008) and the NTSB (2008b; 2008c), construction of the I-35W Bridge began in 1964, and the bridge was opened to traffic in 1967. The bridge was designed based on the 1961 American Association of State Highway Officials (AASHO) *Standard Specifications for Highway Bridges*, the 1961 and 1962 *Interim Specifications*, and the 1964 Minnesota Highway Department *Standard Specifications for Highway Construction*.

The bridge had 14 spans and 13 piers including the south approach spans, north approach spans, and central deck truss spans. The total length from the south abutment to the north abutment was 1,907 feet. Figure 2.1 shows a plan and elevation view of the entire bridge, drawn based on original construction drawings released by the Mn/DOT (2008).

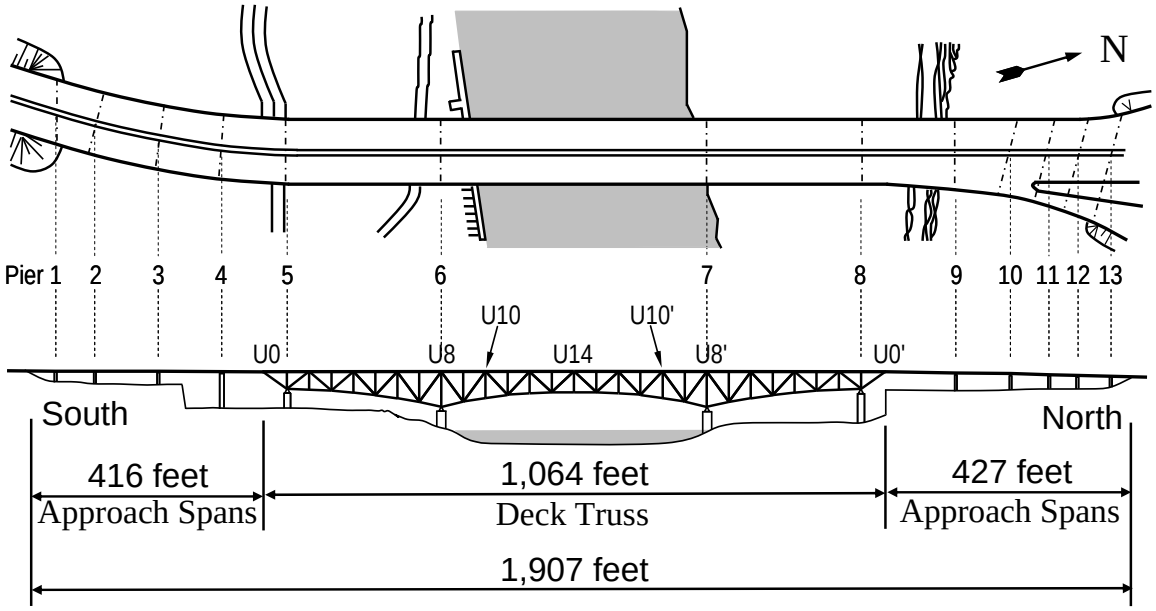

Figure 2.1 Plan and elevation view of I-35W Bridge (based on Mn/DOT 2008).

The south and north approach spans rested at the ends of the two (west and east) main trusses, at panel points U0 and U0', respectively. Starting from the South end, the panel points of the main truss were counted from U0 up to U14 at the center of the bridge, and then from U14, U13' down to U0'. The main truss rested on roller supports at piers 5, 6, and 8, and a hinge support at pier 7. The main truss consisted of 28 panels, each of which was 38 feet long. Figure 2.2 is a photograph from NTSB (2008b), showing the floor trusses, sway frames, and bracing members transversely connecting the two main trusses. The floor trusses supported longitudinal stringers, which in turn supported the reinforced concrete deck and traffic. Underneath the floor trusses, sway frames in a chevron configuration connected the two main trusses. The lateral bracings spanned between the upper chords and lower chords of the main trusses.

The reinforced concrete deck was separated for the southbound and northbound traffic. Each deck accommodated four 12-foot-wide traffic lanes and two 2-foot-wide shoulders. The original concrete deck was designed as 6.5 inches thick, but the thickness was increased by about 2 inches by an overlay added in later years. Outside barriers and median railings were also added to address maintenance and operational issues. At the time of the collapse, a bridge patching and overlay project had been underway since June of 2007. Figure 2.3 is an aerial photograph from NTSB (2007), taken on the day the bridge collapsed. As shown in the photo, two southbound inside lanes and two northbound outside lanes were closed for traffic. Construction materials and equipment were staged on the closed southbound traffic lanes near panel point U10.

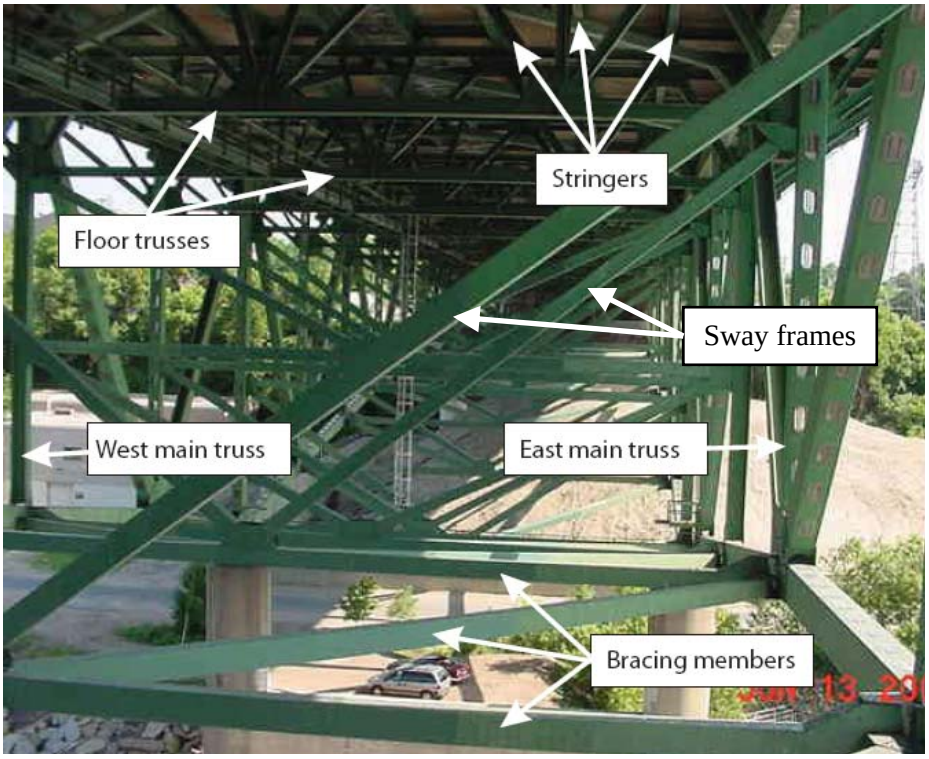

Figure 2.2 Structural system of I-35W Bridge (from NTSB 2008b).

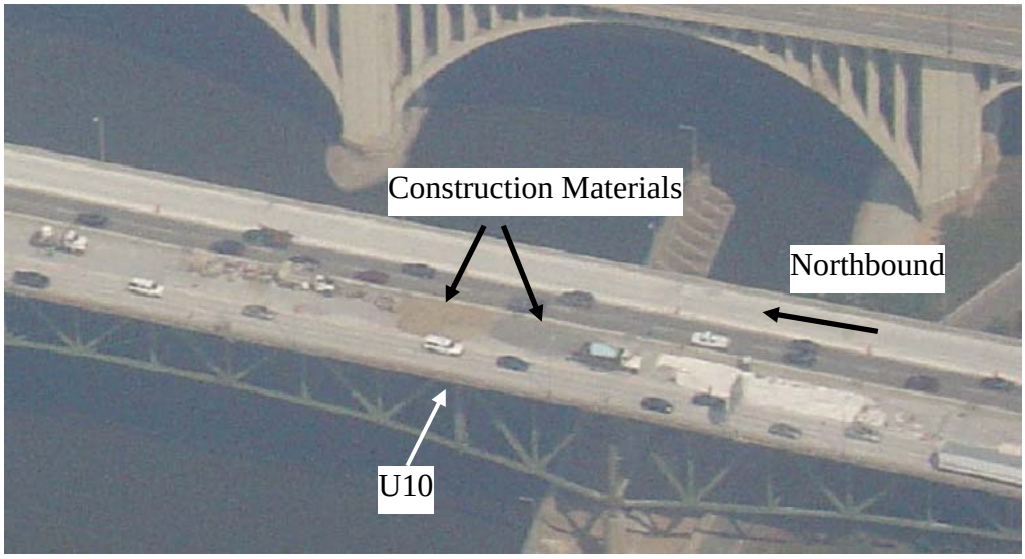

Figure 2.3 Photograph of I-35W Bridge taken prior to collapse on August 1, 2007 (from NTSB 2007).

After the bridge collapsed, field investigation was conducted by the Mn/DOT and the NTSB. Reported observations (Hill et al. 2008; NTSB 2008a; NTSB 2008b), summarized in the following, indicate that the failure initiated at panel point U10. Figure 2.4(a) is a photograph taken prior to the collapse (NTSB 2008a), showing a pair of gusset plates connecting five truss members at the panel point U10 of the west main truss (U10W). Figure 2.4(b) identifies the five truss members: upper chords U9/U10 and U10/U11, diagonals L9/U10 and U10/L11, and a vertical U10/L10. The five truss members were connected through a pair of 0.5-inch-thick gusset plates of ASTM A441 grade 50 steel (Beshah et al. 2008) and using 1-inch diameter rivets (Mn/DOT 2008). The upper chords U9/U10 and U10/U11 and compression diagonal L9/U10 were box sections, while the tension diagonal U10/L11 and vertical U10/L10 were W-sections. All members were welded built-up sections.

Figure 2.5(a) shows a photograph of panel point U10W taken after the collapse (NTSB 2008a), while Figure 2.5(b) illustrates the three primary fractures seen in Figure 2.5(a) and that were commonly observed in all four U10W and U10E gusset plates (NTSB 2008c). These fractures are listed below:

(A) Diagonal fracture along rivet holes connecting the gusset plate to the compression diagonal L9/U10. The fracture occurred along the perimeter holes of the rivet group adjacent to U10/L10.

(B) Horizontal fracture below the lower edge of upper chord U9/U10.

(C) Vertical fracture near the separation between the upper chords U9/U10 and U10/U11.

Fracture of gusset plates was uniquely observed in panel point U10. This observation combined with the fact that the design strength of the U10 gusset plates was insufficient to carry the design forces (Holt and Hartmann 2008) strongly suggests that failure of the I-35W Bridge initiated in the U10 gusset plates.

(a) Photograph of U10W before collapse (from NTSB 2008a)

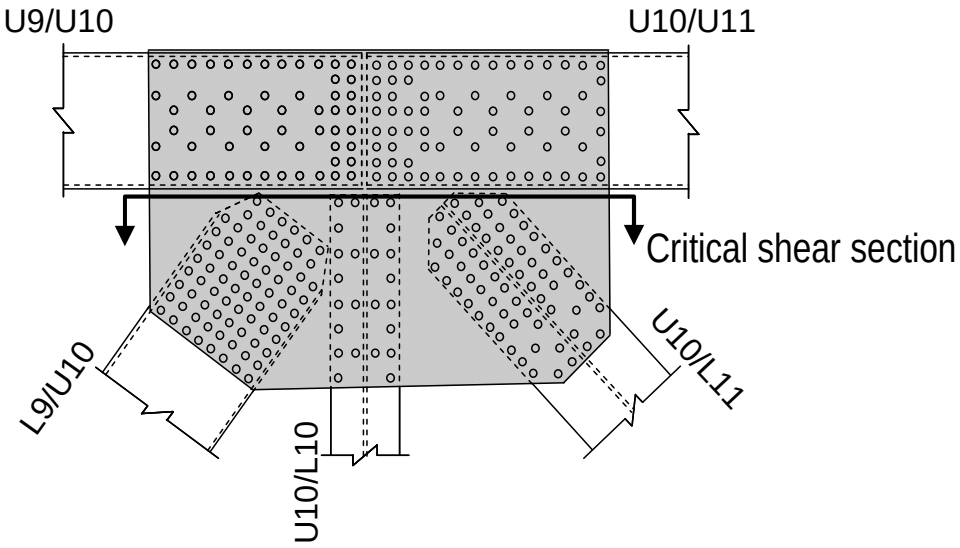

(b) Member designation

Figure 2.4 Panel point U10.

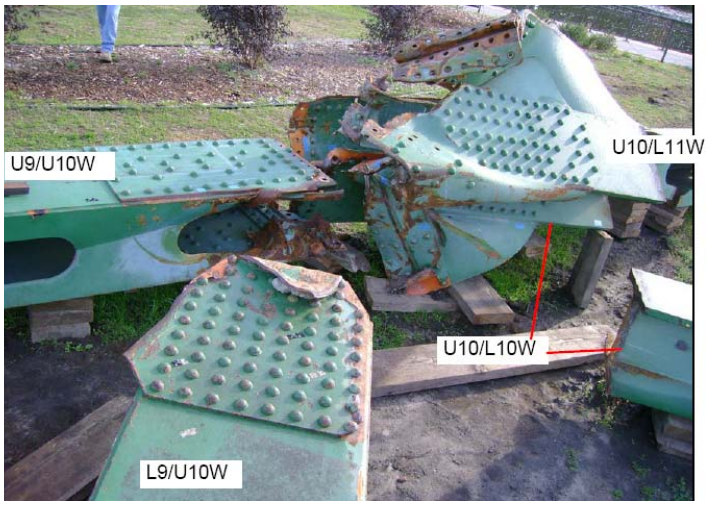

(a) Photograph of U10W (from NTSB 2008a)

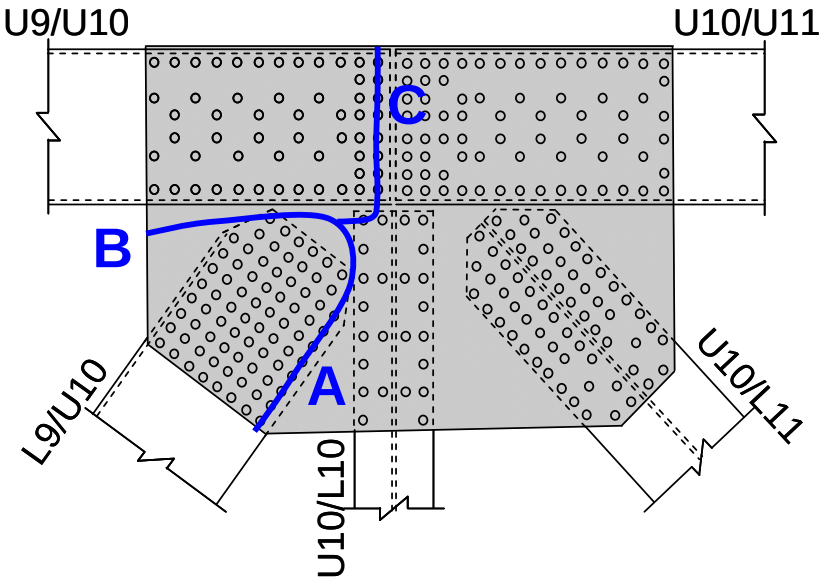

(b) Reported locations of fracture

Figure 2.5 Panel point U10 after collapse.

2.3 Literature Review

Although the earliest gusset plate research can be dated back more than fifty years, the current design methods are based on simple analysis and the engineers' intuition and experience. In current practice, gusset plates are designed for the stresses at the Whitmore section, block shear in tension, buckling in compression, and stresses at critical sections (for example, the critical shear section indicated in Figure 2.4(b)) calculated based on simple beam equations, in addition to constructability considerations. The design procedure is described, for example, by Gross (1990) and Kulicki et al. (2006).

The design rules are justified by both laboratory tests and analytical studies. Hardash and Bjorhovde (1985) tested a series of gusset plates loaded in tension. Figure 2.6 sketches the common failure mode that consisted of a tensile fracture across the last row of bolts and shear yielding along the bolt lines parallel to the applied load. By utilizing the concept of block shear, which was introduced previously for shear failure of coped beam webs, design equations were developed to predict the ultimate strength of the gusset plates. Bjorhovde and Chakrabarti (1985) performed further tests to consider the effects of realistic boundary conditions on the gusset plates in braced frames, that is, the edges defined by the flanges of beams and columns. As in tests by Hardash and Bjorhovde (1985), the gusset plate specimens failed due to tensile fracture across the last row of bolts and shear yielding/tearing along the bolt lines parallel to the tensile force. This failure mode, again, may be viewed as block shear failure.

The compressive strength of gusset plates may be governed by buckling. Thornton (1984) described a rational procedure for checking gusset plate stability. As shown in Figure 2.7, Thornton's model assumes that the Whitmore section acts as a column, and that a uniform compressive stress acts at the Whitmore section. The length of the column is defined by the larger of l_1, which is measured along the action line of the compressive force, or the average of the lengths l_1, l_2 and l_3. Thornton recommended an effective length factor of 0.65. Thornton's method tends to be conservative because it neglects the restraining effects of the material outside of the Whitmore section, and ignores post-buckling strength. Yam and Cheng (1993) conducted a series of full-scale tests to investigate the compression behavior of gusset plates. The common failure mode was sidesway buckling, involving deformation of the gusset plate in the direction perpendicular to itself. The measured capacity was compared against the strength evaluated by Whitmore's method (yield strength of the Whitmore section) and Thornton's method. Yam and Cheng observed that Whitmore's method may produce conservative estimates for large size specimens (gusset plate size of 19.7 × 15.7 inches (500 × 400 mm) in the tests) but unconservative estimates for small size specimens (gusset plate size of 33.5 × 27.6 inches (850 × 700 mm) in the tests), while Thornton's method generally produces conservative estimates.

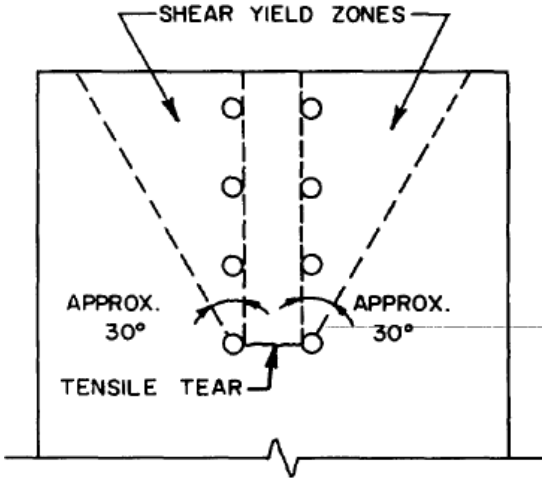

Figure 2.6 Common failure mode for tension gusset plates (from Hardash and Bjorhovde 1985). Copyright © American Institute of Steel Construction. Reprinted with permission. All rights reserved.

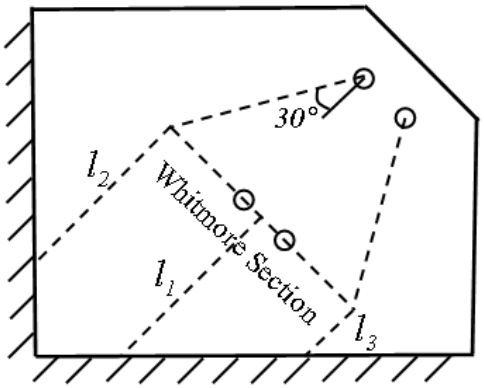

Figure 2.7 Buckling length of Thornton's method.

These earlier studies focused mainly on gusset plate connections designed for tension and/or compression behavior, as seen in braced frames for building systems. Little research data is available on gusset plate connections in truss bridge systems, where the gusset plates may connect multiple diagonal members and chord members. The stress distribution in such gusset plates differs substantially from that in simple tension or compression connections, and varies with member arrangement. To the knowledge of the author, Yamamoto et al. (1985) were the first to report realistic tests of gusset plates subjected to loads applied simultaneously in multiple directions. The tests examined the elastic stress distribution in gusset plates for a range of member arrangements. Based on the experimental findings, a design equation was developed for the required thickness of gusset plates to meet allowable stress design requirements. However, these tests were terminated before failing the specimens, and hence, did not examine the strength limit state of gusset plates.

Therefore, Yamamoto et al. (1988) tested another series of gusset plates to examine the behavior leading to failure. One of the eight specimens tested had a very similar member arrangement as seen in the U10 gusset plate connection, except that the vertical member was missing. The development of plasticity, local bucking, and failure of the gusset plate connection specimen was examined. It was observed that the initial yielding and local buckling occurred almost simultaneously, and that further load could be carried after reaching the local buckling load. Based on a simplified buckling analysis, the required thickness to control local buckling was proposed. However, the ultimate failure mechanism of the gusset plates is not clearly reported in the paper.

Tajima et al. (1984) tested a number of large-scale gusset plate connection specimens to improve gusset plate designs for fatigue performance. The study provides detailed data on stress distribution in gusset plates. However, because the objective of the study was to identify details that provide improved fatigue life, the tests did not examine the strength limit state of gusset plates.

The above literature review indicates that research information is lacking on behavior of gusset plates in truss bridges, where the gusset plates are subjected to combined loads. Effects of interactions among the loads on the strength limit state have not been explicitly investigated. There is very limited data that may help explain the gusset plate fracture that was observed in the I-35W Bridge. This study addresses these knowledge gaps through a computational study.

CHAPTER 3: BRIDGE ANALYSIS

3.1 Introduction

As a first step of investigating the cause of the I-35W Bridge collapse, a series of structural analyses were performed. The loads applied to the bridge structure at the time of the collapse were estimated. Two and three-dimensional (2D and 3D) truss bridge models were created and analyzed, using the estimated loads, to compute the forces in each member. The forces were used to examine whether any of the truss members or the U10 gusset plate connection may have been overstressed due to the applied loads.

First, Section 3.2 describes the 2D and 3D structural models, including the overall geometry, dimensions, and material properties. Section 3.3 describes the estimated loading condition at the time of the collapse based on publically available information. Section 3.4 describes the response of the 2D and 3D models to the estimated loading conditions. Section 3.5 examines the adequacy of the size of each truss member. Section 3.6 discusses the adequacy of the critical gusset plates at panel point U10.

3.2 Model Description

In order to study the overall response of the bridge, two and three-dimensional (2D and 3D) truss bridge models were constructed with varying levels of detail and analyzed using SAP 2000 version 11.0.8 (CSI 2007).

Figure 3.1 displays the two bridge models. Considering that the two main trusses were roughly identical, and subjected to similar loads, complete symmetry was assumed in the 2D model. The model consisted of one of the two main trusses. All members were pin-connected at both ends, and therefore, secondary moments in the members were neglected. The cross-sectional area of each member is listed in Table 3.1. Generic elastic properties of steel were assigned to the members. Secondary elements, such as floor trusses, stringers, and sway frames, were not included in the model. The model was supported by a roller at each pier, except at pier 7, which was supported by a hinge. This support condition represented the condition intended in the design.

The 3D model consisted of all significant steel components, including the main trusses, floor trusses, end floor beams (plate girders that replace the floor trusses at the end panel points of the main trusses, U0 and U0', see Figure A.8), sway frames, and lateral bracings. The concrete deck, expansion joints, stringers, stringer diaphragms, and kicker braces were not included in the model. The model dimensions were based on the original construction drawings disclosed by Mn/DOT (2008). Because all connections were modeled to be fully rigid, and the members were provided with bidirectional bending, St. Venant torsion, and shear properties, secondary moments in the members could be captured. The same as-designed support conditions as in the 2D model were used. The 3D model captured the 3D geometry of the bridge structure, including the gradual tilting of the floor trusses near the south end.

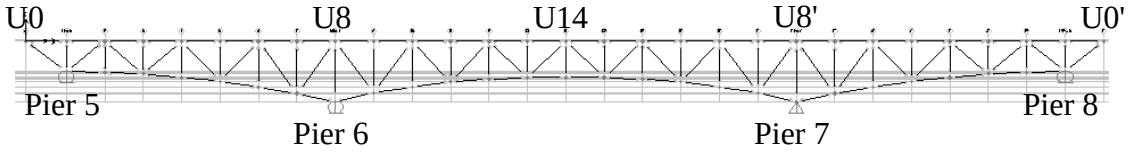

(a) 2D model

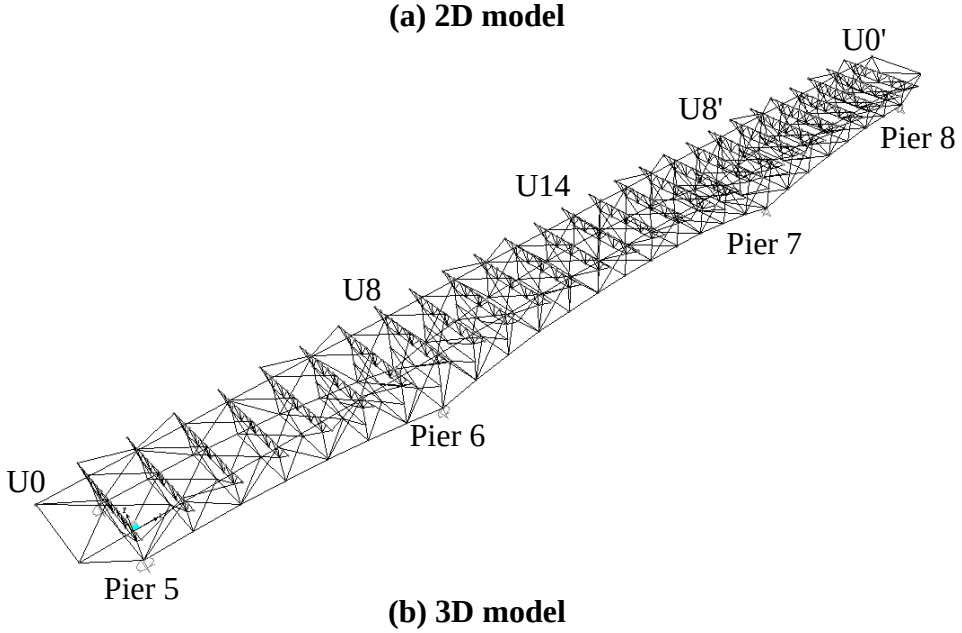

(b) 3D model

Figure 3.1 I-35W Bridge models.

Table 3.1 Cross-sectional area of truss members in 2D bridge model

Member	Area (inch^2)	Member	Area (inch^2)	Member	Area (inch^2)
U0/U2	55.00	U0/L1	61.25	U1/L1	42.50
U2/U4	76.00	L1/U2	74.00	U2/L2	22.50
U4/U6	55.00	U2/L3	27.70	U3/L3	42.50
U6/U8	111.00	L3/U4	35.44	U4/L4	22.50
U8/U10	100.50	U4/L5	65.00	U5/L5	45.00
U10/U12	76.00	L5/U6	57.70	U6/L6	22.50
U12/U14	141.50	U6/L7	110.00	U7/L7	50.50
U2'/U0'	72.50	L7/U8	73.98	U8/L8	194.19
		U8/L9	92.75	U9/L9	50.50
L1/L3	53.50	L9/U10	139.50	U10/L10	22.50
L3/L5	72.50	U10/L11	87.98	U11/L11	42.50
L5/L7	93.50	L11/U12	103.00	U12/L12	22.50
L7/L9	180.00	U12/L13	57.70	U13/L13	42.50
L9/L11	72.50	L13/U14	50.50	U14/L14	22.50
L11/L13	100.50	L3'/U2'	29.90		
L13/L14	139.00	U2'/L1'	80.00		
L3'/L1'	66.50	L1'/U0'	89.00		

3.3 Estimated Loads

Based on construction and reconstruction plans (Mn/DOT 2008), and vehicle, construction materials, equipment weights, and weather report data (NTSB 2007), the loading condition of the bridge at the time of the collapse was estimated. The loads were decomposed into the following five components:

- DL1: Dead loads at the time of original construction, including the weight of all concrete and steel components. The original thickness of the concrete deck was 6.5 inches. It is cautioned that the self-weight of the model components was assigned to those components and was not included as portion of the concentrated loads.
- DL2: Net increase in dead loads due to repair and reconstruction in 1977 and 1998 (Mn/DOT 2008). Added components included a 2-inch-thick overlay on the concrete deck and new concrete parapets.
- LL: Live loads including vehicle loads and impact effects. The vehicle loads were evaluated by uniformly distributing the total vehicle weight present at the time of the collapse, as reported by the NTSB (2007). Per highway bridge design specifications (AASHO 1973), impact effects were accounted for by adding 30% of the vehicle loads to the live loads.
- CL: Construction loads. Figure 3.2 shows a figure taken from NTSB (2007), which illustrates the locations of construction materials and equipment and traffic vehicles at the time of the collapse. Four piles of coarse aggregate (gravel), four piles of fine aggregate (sand), one water truck, one cement tanker, and one concrete mixer were placed near panel point U10 in preparation of a deck paving operation. The total weight of the construction materials and equipment was estimated as 577 kips.
- TH: Thermal effects, which were examined as two separate components as suggested by Barker and Puckett (2007): a uniform change in temperature due to daily change in ambient temperature and a temperature gradient expected in the immediate vicinity of panel point U10 due to solar radiation. The former was modeled based on the peak-to-peak difference in ambient temperature on the day of the collapse, which was reported to be 20 °F by NTSB (2007). The latter was estimated as 30 °F (between 80 °F and 110 °F) based on temperature monitored from a similar truss bridge in Cleveland, Ohio on October 11th, 1998 (Huckelbridge 2008). The uniform ambient temperature change was studied in the bridge model analysis in this chapter, and the temperature gradient was studied in a local gusset plate connection model analysis, which is described later in Chapter 5.

The estimated loads for DL1, DL2, LL, and CL were applied to the 2D bridge model as concentrated loads at panel points along the upper chord. Table 3.2 lists the load values. Panel point designations are indicated in Figure 3.1(a). The load values were obtained based on a tributary area calculation and assuming that the loads were shared evenly between the two main trusses. The self-weight of the main truss, which totaled 1,260 kips, was assigned to the members themselves. Loads on the south and north-end panel points (U0 and U0') included the loads transferred from the approach spans.

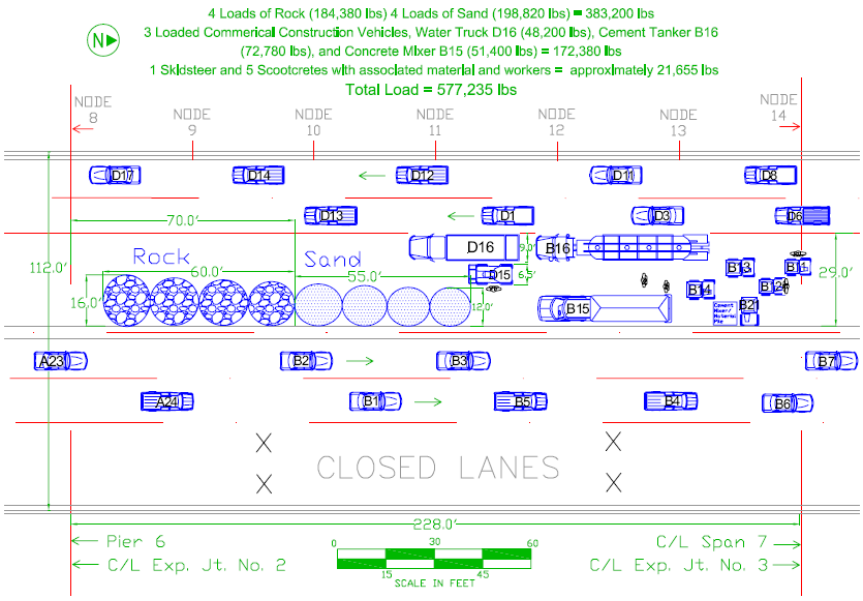

Figure 3.2 Locations of construction materials and equipment (from NTSB 2007).

Table 3.2 shows that the dead loads added during deck reconstruction (DL2) are on the order of 30% of the original dead loads (DL1). This increment is quite significant. The vehicle load and impact effects combined (LL) is less than 6% of DL1. The LL may have doubled if half of the traffic lanes had not been closed for traffic. Therefore, the live loads may have been a minor factor to the bridge collapse. Construction loads (CL) were applied only on panel points U9 through U14. The CL added on U10 is greater than 20% of that from DL1.

The loads applied to the 3D bridge model were also estimated based on tributary area calculations. For the structural members that were explicitly modeled, the self-weight was assigned to the members themselves. The estimated loads were applied as concentrated loads on the upper-chord panel points of the floor trusses and distributed loads on the end floor beams as shown in Figure 3.3(a). The estimation of DL1 and DL2 took into account the specific locations of median and outside parapets shown in Figure 3.4. As a result, a larger proportion of the DL1 and DL2 loads were applied on the middle and end parts of the floor trusses. Figure 3.4 also indicates that the modified parapets added in later years were substantially heavier than the original parapets. Because of traffic closures on the day of the collapse, the live loads were applied only on two southbound outside lanes and two northbound inside lanes, resulting in the non-symmetric loading shown in Figure 3.3(b). Figure 3.3(c) shows the locations of construction loads, which concentrated in the region between panel points U9 and U14, and on the west half of the deck. Therefore, the 3D model was analyzed using a more realistic loading condition than the 2D bridge model.

Table 3.2 Loads applied on panel points of 2D bridge model (unit in kips)

Panel Point	DL1	DL2	LL	CL
U0	419.9	101.0	14.8	0
U1	264.8	87.4	15.3	0
U2	268.2	87.4	15.3	0
U3	267.0	87.4	15.3	0
U4	324.0	87.4	15.3	0
U5	267.5	87.4	15.3	0
U6	274.0	87.4	15.3	0
U7	272.5	87.4	15.3	0
U8	330.1	87.4	10.9	0
U9	271.1	87.4	6.4	58.4
U10	272.0	87.4	6.4	65.2
U11	268.9	87.4	6.4	75.1
U12	267.4	87.4	6.4	40.4
U13	265.8	87.4	6.4	32.1
U14	322.2	87.4	6.4	3.6
U13'-U9'	Symmetric	Symmetric	Symmetric	0
U8'	330.1	87.4	6.2	0
U7'-U1'	Symmetric	Symmetric	5.9	0
U0'	622.5	164.7	18.4	0

Note: the listed values for DL1 do not include the self-weight of the explicitly modeled components.

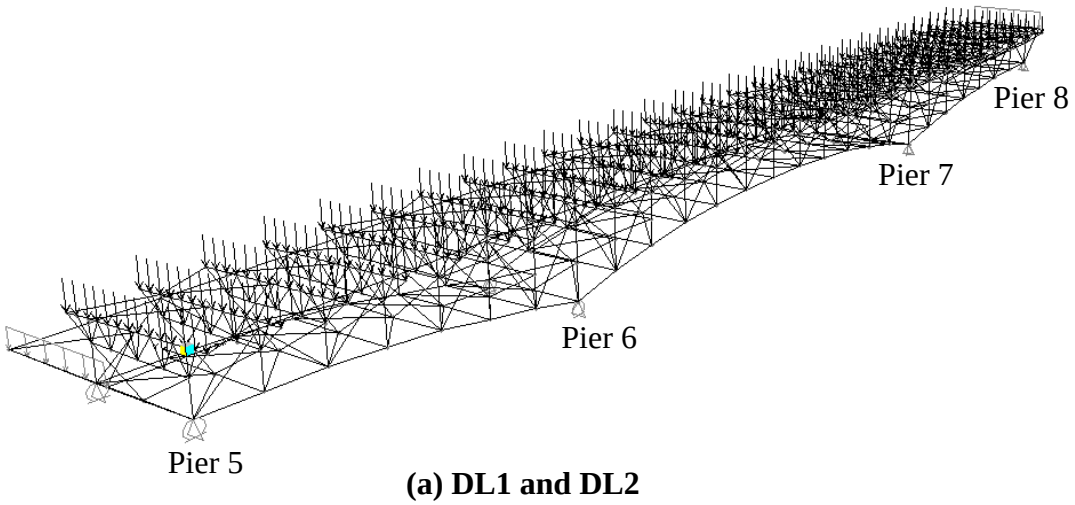

(a) DL1 and DL2

Figure 3.3 Locations of applied concentrated loads in 3D bridge model.

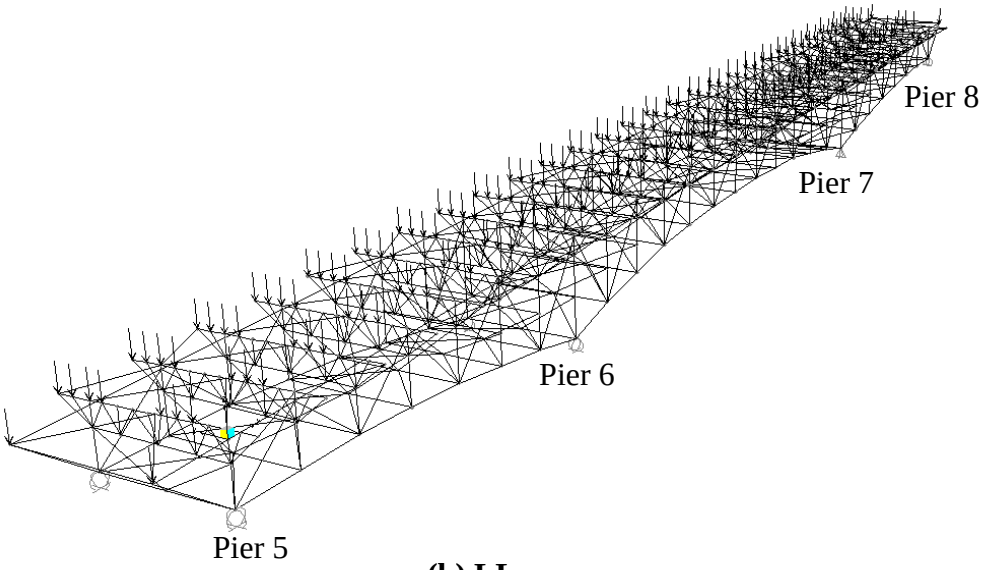

(b) LL

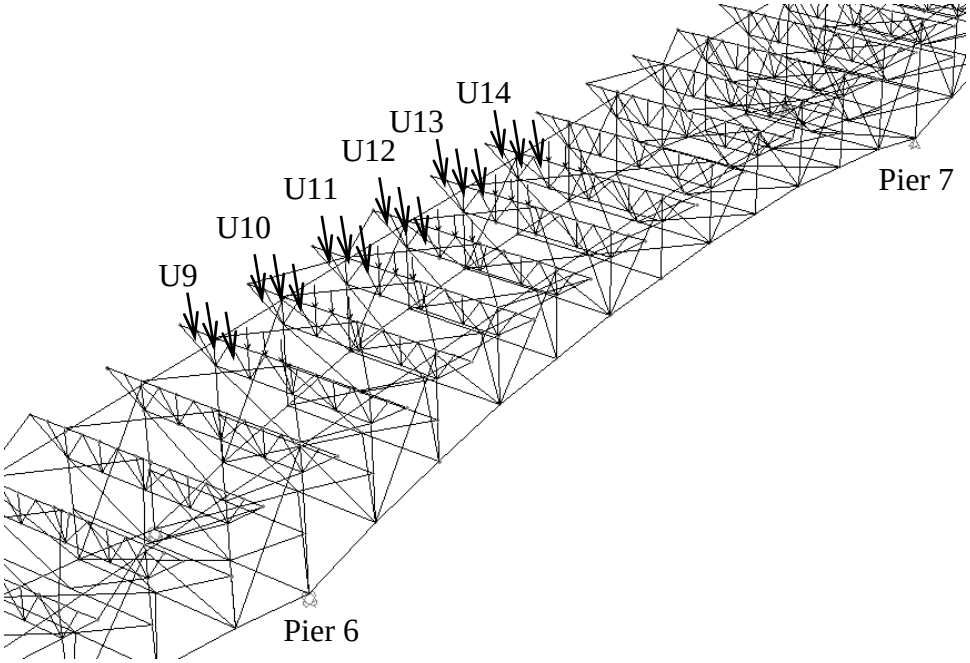

(c) CL

Figure 3.3 Locations of applied concentrated loads in 3D bridge model (continued).

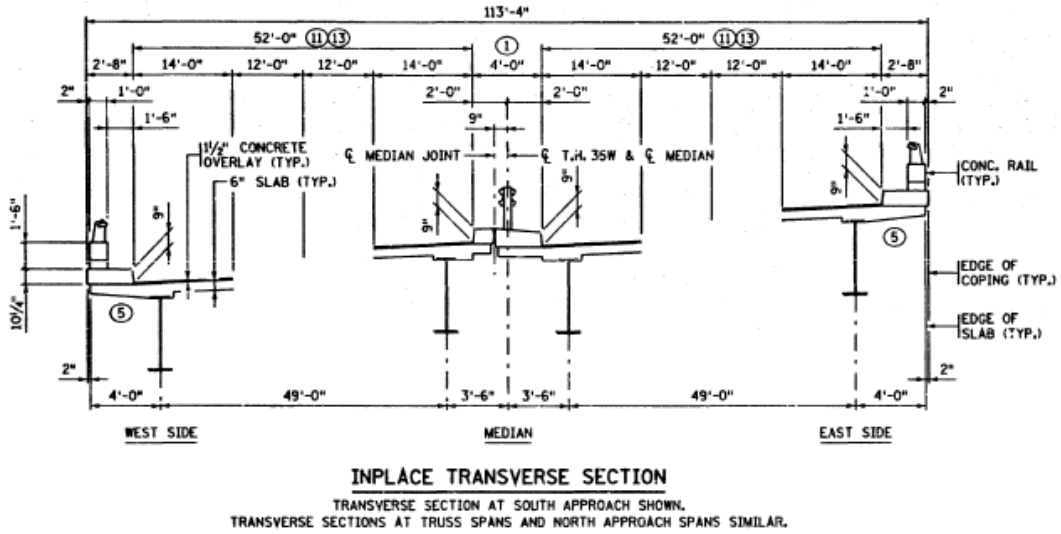

(a) Original construction

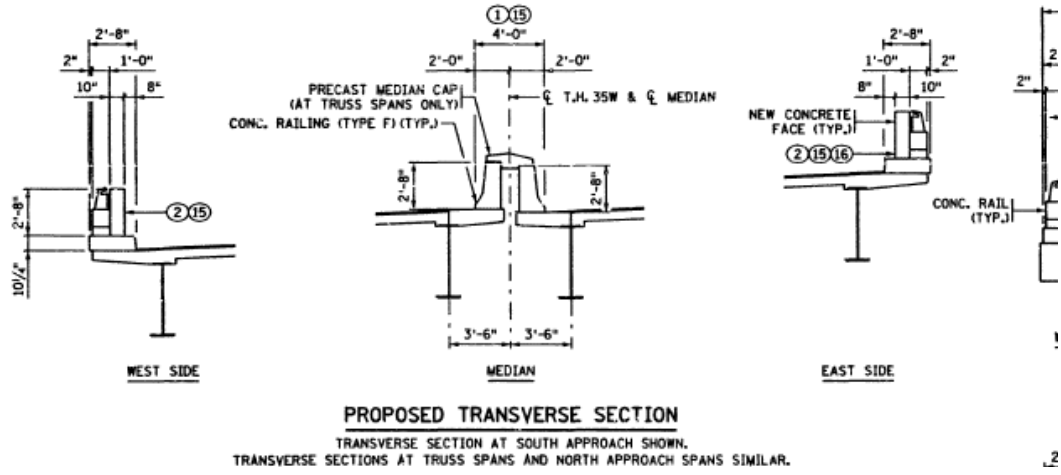

(b) After renovations

Figure 3.4 Locations of median and outside parapets (from Mn/DOT 2008).

3.4 Computed Member Forces

The loads described in the previous section were applied to the 2D and 3D models according to the following four combinations:

- Case 1: DL1
- Case 2: DL1 + DL2
- Case 3: DL1 + DL2 + LL
- Case 4: DL1 + DL2 + LL + CL

In addition, the following two cases were considered for the effects of uniform change in temperature.

- Case T1: Ambient temperature increase of 20 °F with as-designed support conditions.
- Case T2: Ambient temperature increase of 20 °F with hinge supports used at all four piers. This case addressed the extreme effects of frozen roller supports reported by URS (2006) that could have prevented motion of the roller supports.

Table 3.3 lists the axial forces (positive in tension) in the truss members framing into panel point U10, obtained from the 2D and 3D bridge models. For the 3D model, the forces are shown for both U10W and U10E. The dead load effects (corresponds to Case 1) and the strength demands (based on summation of unfactored dead load, live load, and impact effects) used in the original design are also listed for comparison. The results show that differences between the 2D and 3D bridge models are within 4%, and differences between U10W and U10E are within 6%. A more substantial difference between the 2D and 3D models is seen in the vertical U10/L10, because the 2D model does not take into account the transverse load paths in the floor trusses, which adds to the axial force in the top portion of U10/L10 in the 3D model. While the 3D model separated the U10/L10 member into two members, the larger force value obtained from the top portion is listed in Table 3.3. However, compared to the axial forces in the other four members, the magnitude of the force in U10/L10 is much smaller. The simplifying assumption that the loads are shared evenly between the two main trusses appears acceptable, and the 2D model predicted the 3D model response fairly well. This observation applied to the entire bridge.

Table 3.3 Truss forces at panel point U10 (unit in kips)

	Original Design		Bridge Model Analysis				
Member	Case 1	Demand		Case 1	Case 2	Case 3	Case 4
U9/U10	1,551	2,147		1,586	2,015	2,070	2,122
U10/U11	-486	-924		-455	-572	-559	-746
L9/U10	-1,680	-2,288	2D	-1,713	-2,175	-2,210	-2,431
U10/L11	1,432	1,975		1,475	1,868	1,898	2,054
U10/L10	271	540		14	14	14	14
U9/U10				1,568	1,996	2,068	2,141
U10/U11				-449	-568	-553	-763
L9/U10			3D U10W	-1,701	-2,166	-2,216	-2,504
U10/L11				1,448	1,838	1,878	2,058
U10/L10				241	318	326	406
U9/U10				1,570	1,998	2,034	2,064
U10/U11				-449	-568	-557	-720
L9/U10			3D U10E	-1,703	-2,168	-2,188	-2,369
U10/L11				1,448	1,838	1,856	1,970
U10/L10				242	319	321	365

The dead load effects in Table 3.3 agree well between the original design and estimation in this study, which suggests that the estimated dead loads (DL1) are reliable. The forces in Case 3 are smaller than the design strength demand, primarily because the design live load prescribed in AASHO (1973), 640 pound per foot per lane, is roughly 10 times greater than the live loads present at the time of the bridge collapse.

As observed in Table 3.3, the deck repair in later years (DL2) increased the truss forces by 30%. Live loads (LL) and construction loads (CL) increased the truss forces by another 10 to 15%. The forces produced in the diagonals L9/U10 and U10/L11 by Case 4, which represented the total estimated load on the bridge at the time of the collapse, exceeded the design strength demand by 5%. To quantify the effects of placement of construction materials and equipment, Figure 3.5 plots the influence lines for the truss forces (positive in tension) in the compression diagonal L9/U10 and tension diagonal U10/L11 from the 2D bridge model. The influence lines indicate that loads applied on the center span produces compression in L9/U10 and tension in U10/L11, and that loads placed near U10 produces very large response. Therefore, the temporary construction loads (CL), which were placed in the shaded region of Figure 3.5, may have significantly affected the forces imposed on the U10 gusset plate.

Figure 3.6 shows the effects of support conditions on the ambient temperature increase of 20 °F in the 2D model. The member is in tension if the force diagram is plotted above the member. Figure 3.6(a) shows that the temperature increase with as-designed support conditions (Case T1) caused tension in the upper chord members and compression in the lower chord members. However, the forces produced in this case were very small, at most 3.1 kips. Figure 3.6(b) shows that, if the roller supports were frozen (Case T2), the temperature increase could have caused compression in both the upper and lower chord members.

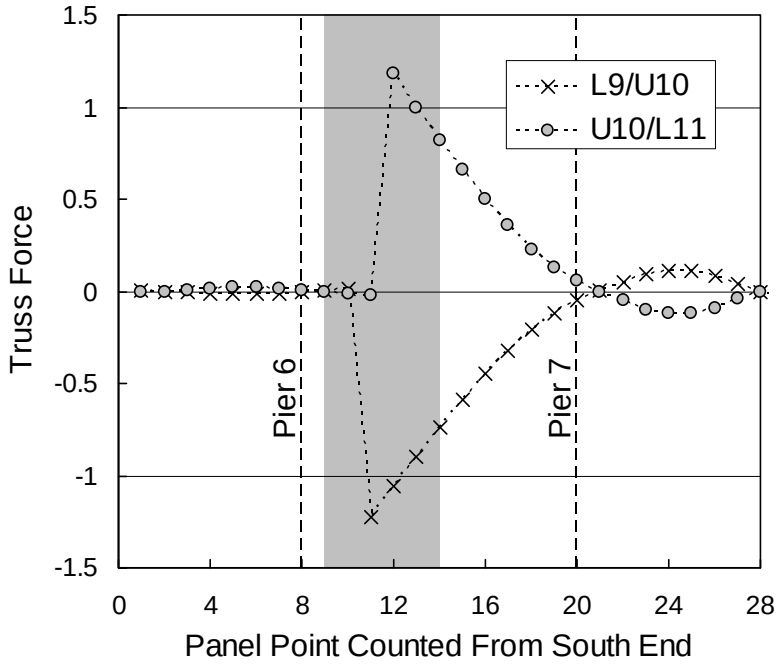

Figure 3.5 Influence lines of truss forces in L9/U10 and U10/L11.

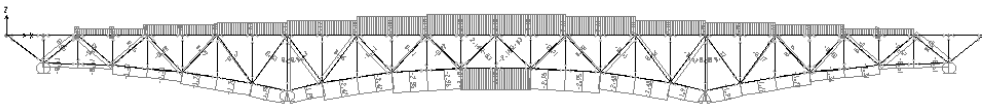

(a) Case T1

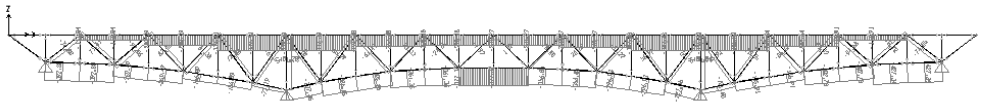

(b) Case T2

Figure 3.6 Truss force diagrams caused by ambient temperature change.

Table 3.4 lists the truss forces (positive in tension) at panel point U10 caused by the ambient temperature increase of 20 °F. The forces for Case T1 are negligible compared to the forces for Case 4. Case T2 produces tension in member L9/U10 and compression in U10/L11. Therefore, if the roller supports were frozen, it is likely that increase in ambient temperature relaxed the compression in member L9/U10, relaxed the tension in member U10/L11, and relaxed the shear force along the critical shear section shown in Figure 2.4(b).

Table 3.4 Truss forces at panel point U10 caused by ambient temperature change (unit in kips)

Case	U9/U10	U10/U11	L9/U10	U10/L11	U10/L10
T1	2.2	2.8	0.5	-0.5	0
T2	-338	-262	55	-61	0

3.5 Design Check of Member Sizes

To evaluate the original truss member design, a simple estimation of member capacity was conducted based on Equations (D2-1) and (E3-1) in the *AISC Specification for Structural Steel Buildings* (AISC 2005). For tension members, the nominal tensile strength was estimated as:

$$P_n = F_y A_g \tag{3-1}$$

where F_y is the yield stress of the steel, and A_g is the gross area of the member. For compression members, the nominal compressive strength was estimated as:

$$P_n = F_{cr} A_g \tag{3-2}$$

where F_{cr} is the flexural buckling stress defined as:

$$F_{cr} = \begin{cases} \left[0.658^{\frac{F_y}{F_e}} \right] F_y, & \text{if } F_e \geq 0.44F_y \\ 0.877F_e, & \text{if } F_e < 0.44F_y \end{cases} \quad (3\text{-}3)$$

where F_e is the elastic critical buckling stress defined as:

$$F_e = \frac{\pi^2 E}{\left(\frac{KL}{r} \right)^2} \quad (3\text{-}4)$$

In the above equation, E is the modulus of elasticity of steel (29,000 ksi), K is the effective length factor, L is the length of the member, measured as the distance between work points, and r is the radius of gyration about the weak axis. For the following calculations, K = 1.0 was assumed for all compression members.

Table 3.5 lists the design check for members in the main truss, excluding the vertical members, with as-designed support conditions. Two different demand values are listed in the table: the original design demands in the second column and the forces computed for Case 4 (representing the loading condition at the time of the collapse) in the third column. For most members, the latter value is smaller than the former. For those members whose truss force for Case 4 is larger than the design demand, the differences are within 6.5%. The design check was made based on the original design demands. Because information on the steel material properties is not available for all truss members, member capacity was estimated for both Grade 36 steel (F_y = 36 ksi) and Grade 50 steel (F_y = 50 ksi). The safety factor of each member was calculated by dividing the member capacity, either based on F_y = 36 or 50 ksi, by the original design demand. As shown in Table 3.5, the safety factor ranged between 1.6 and 3.8 if F_y = 36 ksi was assumed, and between 1.9 and 5.1 if F_y = 50 ksi was assumed. Therefore, the member sizes met the allowable stress design requirement reasonably well except for U6/U8, U12/U14, L7/L8, L8/L9, L5/U6, U6/L7, L7/U8, U8/L9, and L3'/U2' which may have registered a safety factor close to 1.6.

Considering the reported facts by URS (2006) that “the main truss expansion bearings have been found not to behave as intended,” the design check was performed again in Table 3.6 by altering the supports at the four piers. The member forces were reevaluated as follows: the forces from DL1 were computed from the as-designed support conditions, while the forces from DL2, LL, CL, and TH were computed from using hinges at all four supports. This procedure approximates the scenario that while the rollers functioned as intended when the bridge was originally constructed, the roller completely froze by the time subsequent loads were applied. The safety factor of each member was obtained by dividing the member capacity by the forces estimated using the above procedure. As shown in Table 3.6, the safety factor ranged between 1.4 and 13.2 if F_y = 36 ksi was assumed, and between 1.8 and 18.3 if F_y = 50 ksi was assumed. The combination of frozen roller supports and thermal effects reduced the safety factor values for many of the compression members. The compression members that were subjected to a force relatively close to its nominal strength were U12/U14, L7/L8, L8/L9 and L9/L11. For example, the safety factor for member L9/L11 reduced from 2.5 in Table 3.5 to 1.7 in Table 3.6. Therefore,

the assumed support conditions affect the force in L9/L11 significantly. In general, however, the truss members were reasonably sized.

Table 3.5 Design check of truss members with as-designed support conditions

Member	Design Demand (kips)	Case 4 (kips)	Capacity (kips)		Safety Factor	
			F_y =36 ksi	F_y =50 ksi	F_y =36 ksi	F_y =50 ksi
U0/U2	734	734	1,980	2,750	2.7	3.7
U2/U4	-942	-164	-2,456	-3,272	2.6	3.5
U4/U6	1,119	766	1,980	2,750	1.8	2.5
U6/U8	2,436	2,519	3,996	5,550	1.6	2.3
U8/U10**	2,147	2,122	3,618	5,025	1.7	2.3
U10/U12*	-924	-746	-2,456	-3,272	2.7	3.5
U12/U14	-2,790	-2,661	-4,494	-5,945	1.6	2.1
U4'/U2'	-855	-9	-2,456	-3,272	2.9	3.8
U2'/U0'	1,158	1,037	2,610	3,625	2.3	3.1
L1/L3	-456	-24	-1,733	-2,311	3.8	5.1
L3/L5	-828	-107	-2,345	-3,125	2.8	3.8
L5/L7	-1,696	-1,603	-2,990	-3,966	1.8	2.3
L7/L8	-3,407	-3,509	-5,583	-7,334	1.6	2.2
L8/L9	-3,420	-3,527	-5,577	-7,323	1.6	2.1
L9/L11*	-919	-676	-2,342	-3,119	2.5	3.4
L11/L13	2,011	1,883	3,618	5,025	1.8	2.5
L13/L13'	2,975	2,871	5,004	6,950	1.7	2.3
L5'/L3'	-955	-178	-2,345	-3,125	2.5	3.3
L3'/L1'	-722	-254	-2,149	-2,862	3.0	4.0
U0/L1	-936	-911	-1,701	-2,136	1.8	2.3
L1/U2	-1,184	-908	-2,106	-2,669	1.8	2.3
U2/L3	594	249	997	1,385	1.7	2.3
L3/U4	609	357	1,276	1,772	2.1	2.9
U4/L5	-1,007	-956	-1,753	-2,177	1.7	2.2
L5/U6	1,265	1,183	2,077	2,885	1.6	2.3
U6/L7	-1,635	-1,585	-2,669	-3,262	1.6	2.0
L7/U8	1,647	1,554	2,663	3,699	1.6	2.2
U8/L9	2,088	2,209	3,339	4,638	1.6	2.2
L9/U10**	-2,288	-2,431	-3,599	-4,392	1.6	1.9
U10/L11**	1,975	2,054	3,167	4,399	1.6	2.2
L11/U12	-1,725	-1,644	-2,916	-3,689	1.7	2.1
U12/L13	1,256	1,074	2,077	2,885	1.7	2.3
L13/U14	-552	-289	-1,351	-1,672	2.4	3.0
U4'/L3'	521	245	1,276	1,772	2.4	3.4
L3'/U2'	679	345	1,077	1,495	1.6	2.2
U2'/L1'	-1,315	-997	-2,262	-2,859	1.7	2.2
L1'/U0'	-1,474	-1,321	-2,494	-3,143	1.7	2.1

* Steel grade known as Grade 36 (Beshah et al. 2008)

** Steel grade known as Grade 50 (Beshah et al. 2008)

Table 3.6 Design check of truss members with all-hinged support conditions

Member	Estimate Force (kips)	Capacity (kips)		Safety Factor	
		F_y =36 ksi	F_y =50 ksi	F_y =36 ksi	F_y =50 ksi
U0/U2	734	1,980	2,750	2.7	3.7
U2/U4	-401	-2,456	-3,272	6.1	8.2
U4/U6	328	1,980	2,750	6.0	8.4
U6/U8	1,954	3,996	5,550	2.0	2.8
U8/U10**	1,602	3,618	5,025	2.3	3.1
U10/U12*	-1,120	-1,101	-3,272	2.2	3.0
U12/U14	-2,941	-4,494	-5,945	1.5	2.0
U4'/U2'	-246	-2,456	-3,272	10.0	13.3
U2'/U0'	1,037	2,610	3,625	2.5	3.5
L1/L3	-332	-1,733	-2,311	5.2	7.0
L3/L5	-190	-2,345	-3,125	12.3	16.4
L5/L7	-1,523	-2,990	-3,966	2.0	2.6
L7/L8	-3,333	-5,583	-7,334	1.7	2.2
L8/L9	-4,038	-5,577	-7,323	1.4	1.8
L9/L11*	-1,335	-2,342	-3,119	1.7	2.3
L11/L13	1,101	3,618	5,025	3.3	4.6
L13/L13'	2,052	5,004	6,950	2.4	3.4
L5'/L3'	-298	-2,345	-3,125	7.9	10.5
L3'/L1'	-601	-2,149	-2,862	3.6	4.8
U0/L1	-911	-1,701	-2,136	1.9	2.3
L1/U2	-1,065	-2,106	-2,669	2.0	2.5
U2/L3	398	997	1,385	2.5	3.5
L3/U4	206	1,276	1,772	6.2	8.6
U4/L5	-819	-1,753	-2,177	2.1	2.7
L5/U6	1,075	2,077	2,885	1.9	2.7
U6/L7	-1,482	-2,669	-3,262	1.8	2.2
L7/U8	1,484	2,663	3,699	1.8	2.5
U8/L9	2,079	3,339	4,638	1.6	2.2
L9/U10**	-2,338	-3,599	-4,392	1.5	1.9
U10/L11**	1,919	3,167	4,399	1.7	2.3
L11/U12	-1,600	-2,916	-3,689	1.8	2.3
U12/L13	1,024	2,077	2,885	2.0	2.8
L13/U14	-295	-1,351	-1,672	4.6	5.7
U4'/L3'	97	1,276	1,772	13.2	18.3
L3'/U2'	493	1,077	1,495	2.2	3.0
U2'/L1'	-1,150	-2,262	-2,859	2.0	2.5
L1'/U0'	-1,327	-2,494	-3,143	1.9	2.4

* Steel grade known as Grade 36 (Beshah et al. 2008)

** Steel grade known as Grade 50 (Beshah et al. 2008)

3.6 Design Check of Critical Gusset Plates

Figure 3.7(a) shows panel point U10 with the member forces computed for Case 4 using the 2D model (listed in Table 3.3). Because U10 was located near an inflection point of the continuous truss, the force in the upper chord switched from tension on one side of the panel point to compression on the other side. The diagonal members delivered substantial compression and tension to the connection. As a result, a large net shear force was produced along the horizontal critical section indicated in the figure. Based on commonly used, simplified design checks, Holt and Hartmann (2008) suggested that the gusset plates at panel point U10 needed to be twice as thick to safely transfer the shear force produced by the strength demands from the original design calculations.

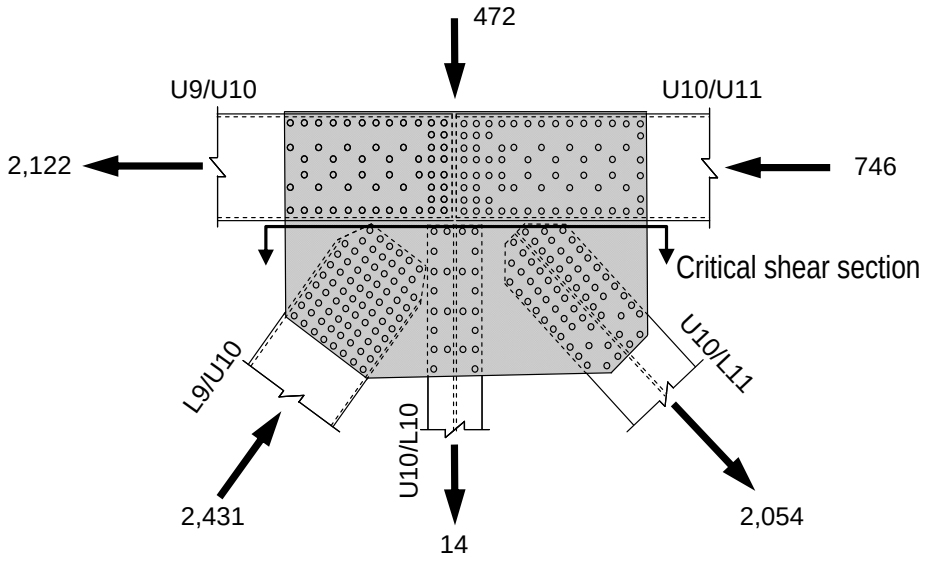

(a) Forces for Case 4 (unit in kips)

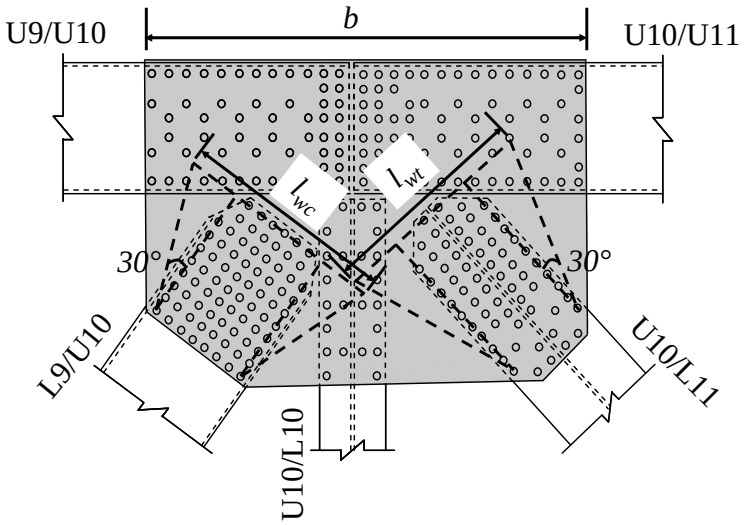

(b) Key dimensions

Figure 3.7 Gusset plate at panel point U10.

A design check of these critical gusset plates was conducted by the author based on the handbook procedure (Kulicki et al. 2006) and the *AISC Specification for Structural Steel Buildings* (AISC 2005). The following five limit states were checked:

- Shear yielding at the critical shear section indicated in Figure 3.7. The nominal shear strength was estimated as:

$$P_n = 2 \times \frac{2}{3} \times 0.6 F_y b t \tag{3-5}$$

  where F_y = 50 ksi is the nominal strength of the gusset plate steel (ASTM A 709), b = 100 inches is the width of the gusset plate along the critical shear section indicated in Figure 3.7(b), and t = 0.5 inches is the thickness of a single gusset plate. Because two gusset plates were used in the connection, the strength is multiplied by 2. Considering parabolic distribution of shear stress, the strength is multiplied by 2/3.

- Buckling at the connection with compression diagonal L9/U10. The nominal compressive strength was estimated as:

$$P_n = 2 F_{cr} l_{wc} t \tag{3-6}$$

  where F_{cr} is calculated by Equations (3-3) and (3-4), and assuming that the cross section of the column is represented by the Whitmore section. l_{wc} = 60 inches is the width of the Whitmore section indicated in Figure 3.7(b). Thornton's method was used to evaluate the effective length in Equation (3-4): K = 0.65 and L was taken as the length of l_1 shown in Figure 2.7. KL = 0.65 × 10 inches = 6.5 inches resulted in F_{cr} = 43 ksi.

- Tension yielding at the connection with tension diagonal U10/L11. The nominal tensile strength was estimated as:

$$P_n = 2 F_y l_{wt} t \tag{3-7}$$

  where l_{wt} = 62 inches is the width of the Whitmore section at the connection with tension diagonal indicated in Figure 3.7(b).

- Net section fracture at the connection with tension diagonal U10/L11 per the *AISC Specification* (2005) Sections D2 and D3:

$$P_n = 2 F_u A_n \tag{3-8}$$

  where A_n = 30 in^2 is the net area along the Whitmore section at the connection with tension diagonal. The diameter of a bolt hole was 1/16 inches greater than the nominal bolt diameter. F_u = 65 ksi is the specified minimum tensile stress of the steel.

- Block shear at the connection with tension diagonal U10/L11. The nominal block shear strength was estimated as:

$$P_n = 2\left(0.6 F_u A_{vn} + F_u A_{tn}\right) \le 2\left(0.6 F_y A_{vg} + F_u A_{tn}\right) \tag{3-9}$$

where A_{vn} = 30 in^2 is the net area along the shear paths, A_{tn} = 4.75 in^2 is the net area along the tension path, A_{vg} = 40 in^2 is the gross area along the shear paths, and F_u = 65 ksi is the specified minimum tensile stress of the steel.

Table 3.7 lists the capacity check for the above limit states. The corresponding force demands for loading Case 4 are also listed. The safety factor in the table is computed by dividing the nominal strength by the force demand for Case 4. The safety factor is less than 1.0 at the critical shear section and is very close to 1.0 at the compression connection with L9/U10. The design checks suggest that the estimated forces likely caused substantial yielding along the critical shear section and inelastic buckling in front of the compression connection with L9/U10. Therefore, the gusset plate may not have had adequate thickness to carry the forces produced by Case 4. The results listed in Table 3.7 are not identical, but agree with a previous statement by Holt and Hartmann (2008).

Table 3.7 Design check of gusset plate U10

	Limit State	Nominal Strength (kips)	Force for Case 4 (kips)	Safety Factor
Critical Shear Section	Shear Yielding	2,000	2,868	0.7
Connection with L9/U10	Buckling	2,585	2,431	1.1
Connection with U10/L11	Tension Yielding	3,100	2,054	1.5
	Net Section Fracture	3,900	2,054	1.9
	Block Shear	2,958	2,054	1.4

CHAPTER 4: VALIDATION OF FINITE ELEMENT MODELS

4.1 Introduction

Chapter 4 describes a validation study of a finite element modeling procedure that was applied to the U10 gusset plate connection. The validation was performed based on reported laboratory test behavior of two simple gusset plate connections. ABAQUS 6.8-1 (Simulia 2008) was used for all finite element analyses presented in this study. Nonlinear material behavior was modeled using the von Mises yield criteria and the isotropic hardening rule. A large strain-large displacement formulation, which is the default option for ABAQUS, was used to carry out the nonlinear analysis. For the validation studies presented in this chapter, the steel was modeled using the respective reported yield strength and a post-yield stiffness of approximately 0.01 times the Young's modulus.

Section 4.2 describes the simulation of a tension gusset plate connection. Section 4.3 describes the simulation of a compression gusset plate connection. Section 4.4 describes the modeling procedure established based on the two simulations.

4.2 Tension Gusset Plate Connection

The first validation used a bolted tension gusset plate connection reported by Hardash and Bjorhovde (1985). Figure 4.1(a) shows the test setup with a gusset plate specimen before testing, and Figure 4.1(b) shows the state of the gusset plate after testing. Figure 4.1(b) indicates failure due to block shear, composed of tensile fracture across the last row of bolts and elongation of bolt holes. Figure 4.2 plots the relationship between the applied tensile load and the deformation between the testing machine crossheads. The curve shows that the tension plate gradually softened until reaching a tensile strength of 125.7 kips.

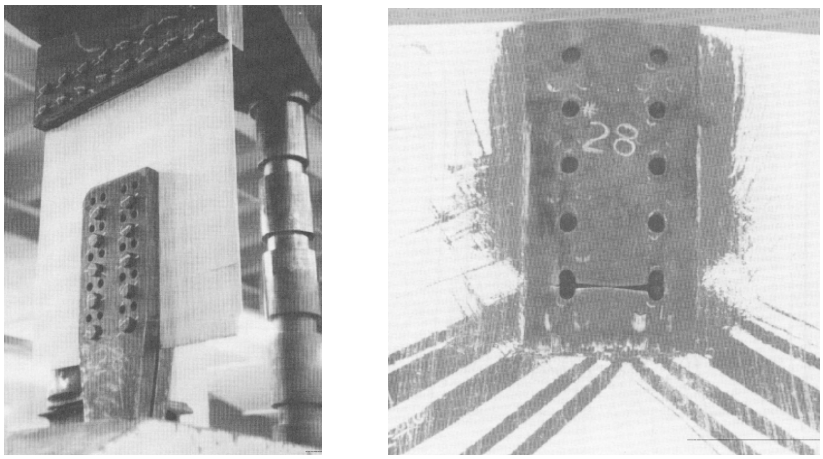

(a) Test setup **(b) State of gusset plate after testing**

Figure 4.1 Tension gusset plate connection (from Hardash and Bjorhovde 1985).

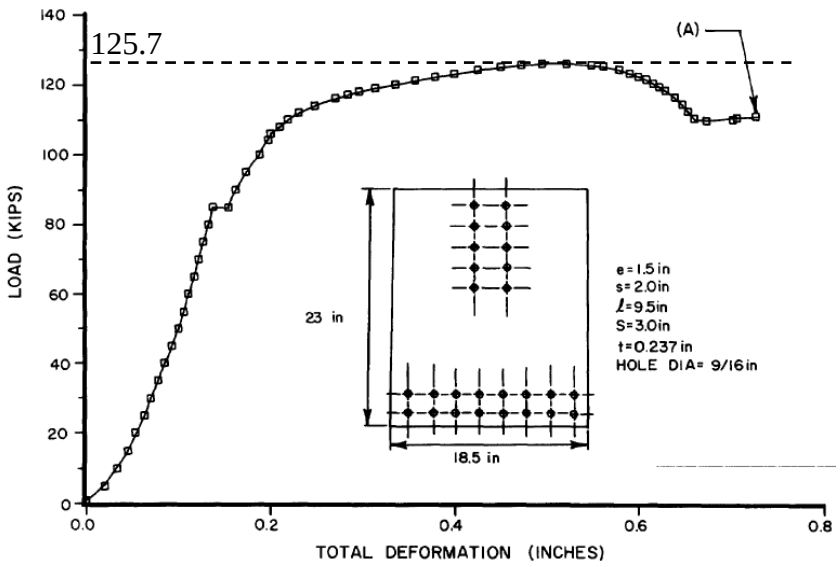

Figure 4.2 Load-deformation curve for tension gusset plate connection (from Hardash and Bjorhovde 1985). Copyright © American Institute of Steel Construction. Reprinted with permission. All rights reserved.

The finite element model of this gusset plate is shown in Figure 4.3 as the global model. Considering symmetry, only one half of the gusset plate was modeled. All nodes along the left edge of the model were restrained against translation in two transverse (X and Z) directions. All nodes at the bottom edge of the plate were restrained against translation in all three (X, Y, and Z) directions. The bolts were modeled as rigid cylindrical shells. The rigid shells were displaced equally in the upward (positive Y) direction to deliver load to the gusset plate. The remaining five degrees-of-freedom of the rigid shells were restrained.

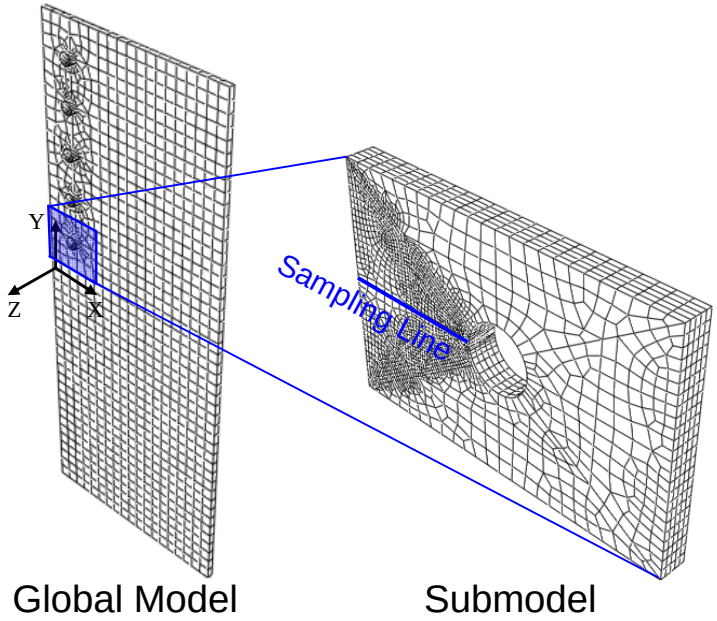

Figure 4.3 Finite element models for tension gusset plate connection.

A comparison study of element types and mesh refinement was conducted. Figure 4.4(a) compares the loading curve obtained from using different solid elements, designated as C3D8 (linear isoparametric brick element), C3D8R (linear brick element with reduced integration), and C3D4 (linear isoparametric tetrahedral element) in the ABAQUS element library. All analyses used a similar meshing strategy with 16 nodes surrounding each bolt hole. The models using C3D8 or C3D8R achieved the measured strength of 125.7 kips at 0.4 inches displacement

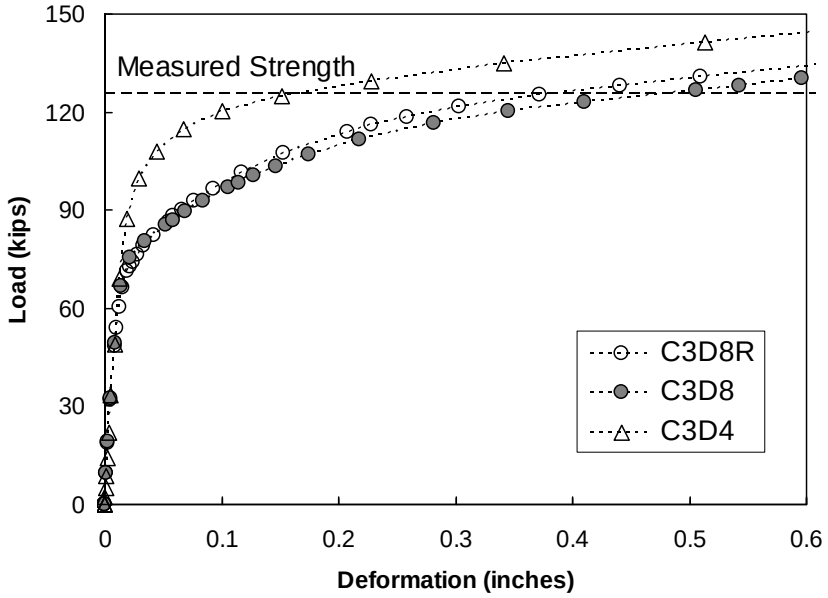

(a) Element types

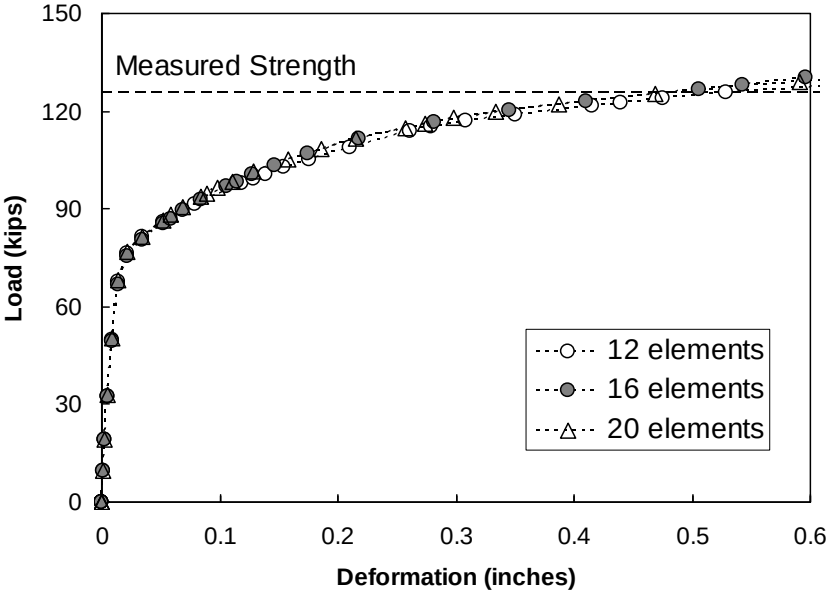

(b) Mesh refinement

Figure 4.4 A comparison study of modeling procedure.

(beyond the stage when the bolts contacted the hole perimeter), and continued to develop larger strength. The strength degradation observed in the experiment was influenced by fracture propagation between the last row of bolts. Therefore, the discrepancy between the experiment and analysis may be attributed to absence of fracture model in the analysis. The model using C3D4 exceeded the measured strength at a much smaller deformation of 0.15 inches, and therefore, was judged as less appropriate than the other two models. Figure 4.4(b) compares the loading curve obtained from using different number of elements surrounding each bolt hole. All analyses used C3D8. The discrepancy among the three models was negligible. Therefore, the comparison study led to the conclusion that the overall behavior of the tension connection may be modeled appropriately by using C3D8 and 16 elements surrounding the bolt holes.

Figure 4.5 shows the deformation of the gusset plate and the Mises stress distribution when the bolts were displaced by 0.4 inches. The Mises stress is a stress invariant defined as:

$$\sigma_{Mises} = \sqrt{3S_{ij}S_{ij}/2} \tag{4-1}$$

where S_{ij} are the deviatoric stress components, and the summation convention is applied over $i, j = 1, 2, 3$. The computed deformation and stress distribution resemble the photograph of the test specimen in Figure 4.1(b). Very high stresses were computed near the bearing side of the bolt holes, and also across the last row of bolt holes where fracture was observed in the test. Deformation of the plate was supplied by bolt hole elongation, most notably at the last bolt hole. Overall, the finite element model reproduced the behavior of the tension gusset plate connection reasonably well.

In order to examine the critical stress and strain condition that led to fracture in the gusset plate, a densely meshed model representing the region surrounding the last row of bolt hole, shown in Figure 4.3 as the submodel, was analyzed using the submodeling technique (Simulia 2008). The displacement field obtained from the global model was used as boundary conditions for the submodel analysis. Figure 4.6 plots the distribution of normal stress, σ_{YY}, and equivalent plastic strain, PEEQ, respectively, along the sampling line connecting the two bolt holes. PEEQ is defined as:

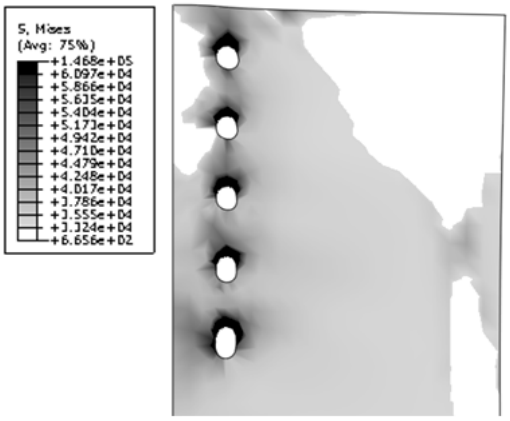

Figure 4.5 Deformation and Mises stress (unit in psi) distribution for tension gusset plate connection.

$$\varepsilon_{PEEQ} = \int \sqrt{\frac{2}{3} d\varepsilon_{ij}^{p} d\varepsilon_{ij}^{p}} \tag{4-2}$$

where ε_{ij}^{p} are the plastic strain components, and the summation convention is applied over i, j = 1, 2, 3. The integration is applied over the loading history. In Figure 4.6, the abscissa indicates the distance measured from the middle of the plate. The figures compare the results from the global model and submodel when the bolts were displaced by 0.4 inches (the loading stage when

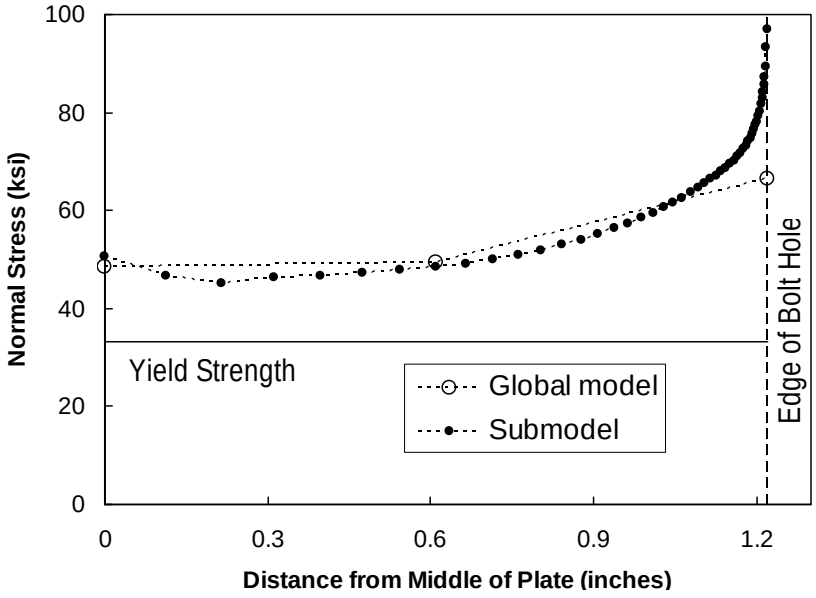

(a) Normal stress σ_{YY}

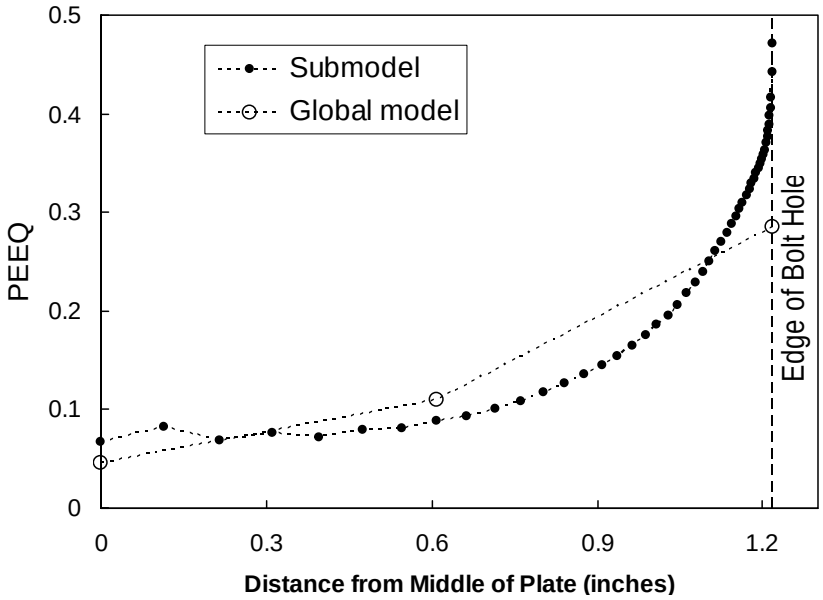

(b) Equivalent plastic strain PEEQ

Figure 4.6 Comparison between global model and submodel.

the measured strength was reached). The figures indicate that the yield strength (33 ksi) was exceeded along the entire length between the last row of bolts. Both σ_{YY} and PEEQ are largest at the edge of the bolt hole. The major difference between the global model and submodel occurs only near the edge of the bolt holes, where the global model does not capture the severe stress and strain concentration. The very large stress concentration obtained from the submodel indicates that fracture may initiate at the edge of the bolt hole at a load much lower than the tensile capacity of the gusset plate connection.

4.3 Compression Gusset Plate Connection

The second validation study used a bolted compression connection reported by Yam and Cheng (1993). Figure 4.7(a) shows the schematic of the gusset plate, while Figure 4.7(b) shows the test setup. The gusset plate had a slender, 28.5-inch (725-mm) long and 0.5-in (13.3-mm) thick, unbraced edge. The brace member delivering compression was restrained from torsion and rotation in the plane perpendicular to the gusset plate. The bottom and left edges of the gusset plate were fixed to a rigid base, while the base was permitted to translate out-of-plane. The connection ultimately failed due to buckling of the gusset plate. Figure 4.8 plots the relationship between the compressive load and the out-of-plane displacement of the test frame. The gusset plate sustained a maximum load of 361 kips (1,606 kN). The response curve indicates that, as out-of-plane deformation increased, the gusset plate gradually softened until eventually strength degradation occurred.

\

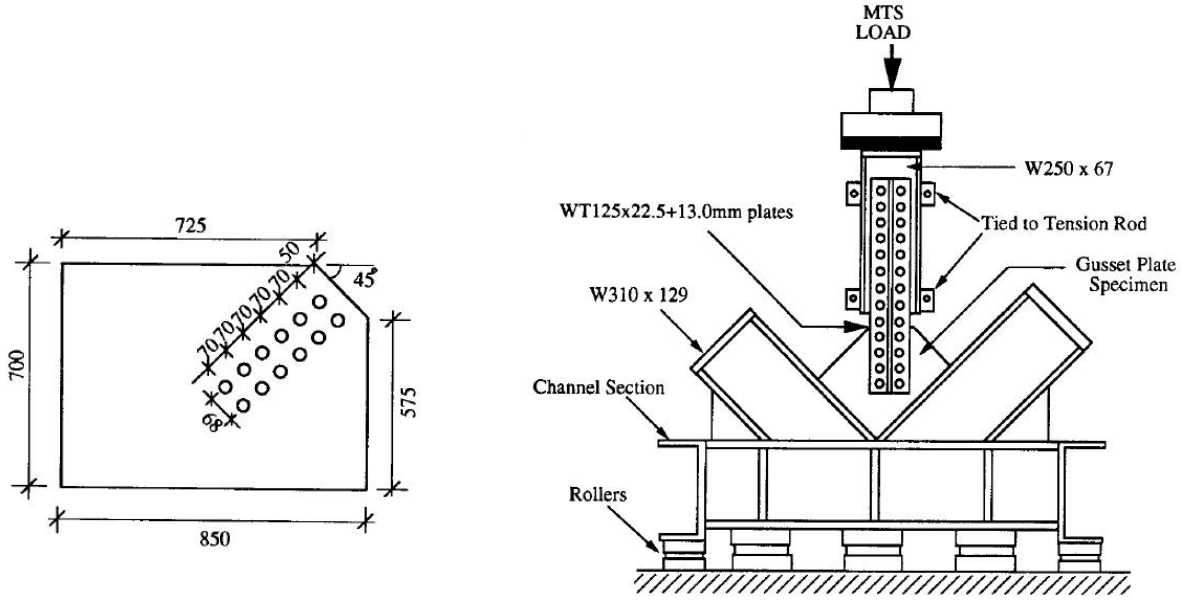

(a) Gusset plate dimensions (unit in mm)

(b) Test setup

Figure 4.7 Schematic of compression test (from Yam and Cheng 1993). Courtesy of J.J. Roger Cheng and Michael Yang.

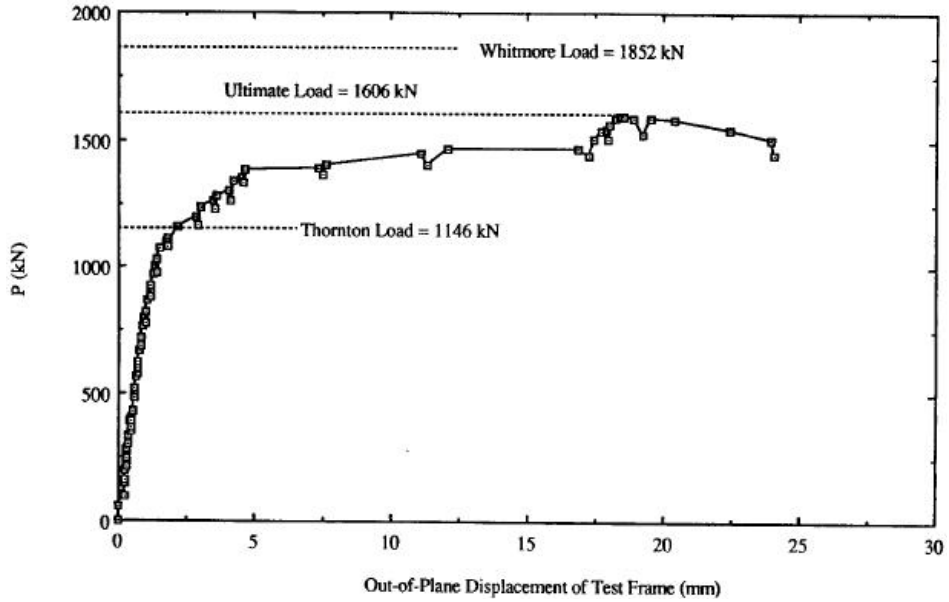

Figure 4.8 Compressive force versus out-of-plane displacement for compression gusset plate connection (from Yam and Cheng 1993). Courtesy of J.J. Roger Cheng and Michael Yang.

Figure 4.9 shows the finite element model before and at the end of the analysis. The model was supplied with boundary conditions reflecting the test setup, as rigid cylindrical shells (representing the bolts) were displaced in the direction toward the gusset plate. Figure 4.10 plots the compressive load versus out-of-plane displacement relationship obtained from three models. The meshing scheme validated from the first study (in Section 4.2) was used, while the number of elements across the thickness of the gusset plate was varied between one and three. The out-of-plane displacement *d* indicated in Figure 4.9 is plotted in the abscissa. Figure 4.10 indicates that the maximum strength and failure due to instability were represented well by using either two or three elements across the thickness of the gusset plate. Using either model, the measured strength of 361 kips (1,606 kN) was predicted within 10%, while the computed out-of-plane displacement was on the same order as that measured during the test: Figure 4.8 indicates that the ultimate load was reached at an out-of-plane displacement of 0.7 inch (18 mm).

4.4 Modeling Procedure for U10 Gusset Plate Connection

Based on the two validation studies described above, the behavior of both tension and compression gusset plate connections may be reproduced reasonably well by using C3D8 elements throughout, 16 elements surrounding the bolt holes, and two elements across the thickness of the plate. The von Mises yield criteria and the isotropic hardening rule was used to model inelastic material behavior, and the large strain-large displacement formulation was used to account for nonlinear geometry. This finite element modeling and analysis procedure was used to model the U10 gusset plate connection in Chapter 5.

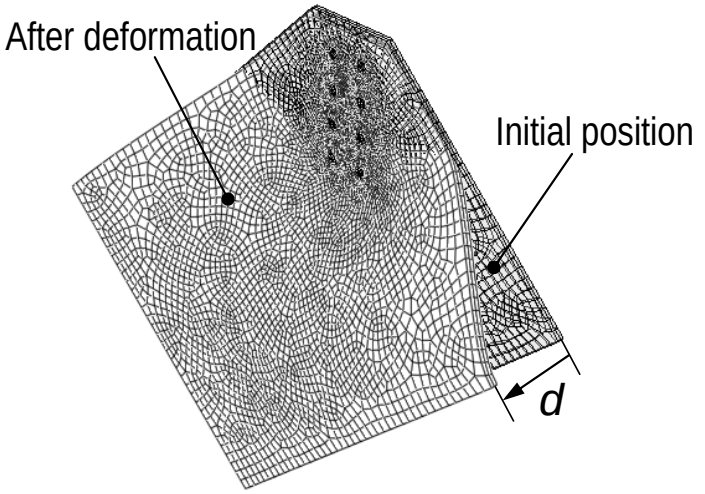

Figure 4.9 Finite element model before and after deformation.

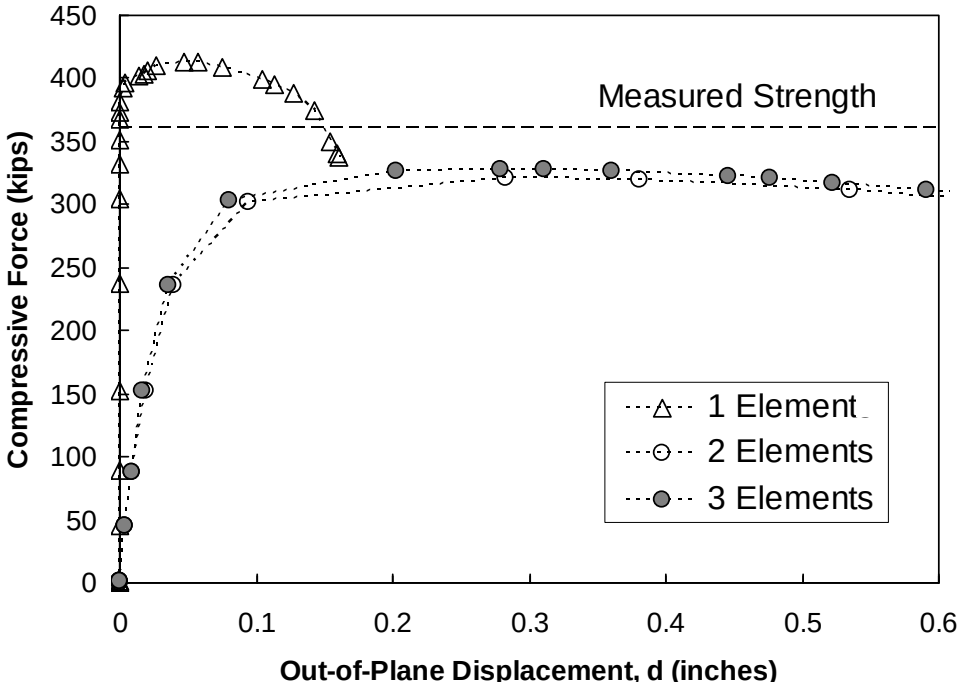

Figure 4.10 Compressive force versus out-of-plane displacement.

CHAPTER 5: U10 GUSSET PLATE CONNECTION ANALYSIS

5.1 Introduction

Chapter 5 focuses on detailed nonlinear finite element analysis of the gusset plate connection at panel point U10. Section 5.2 describes the 3D finite element model, including the dimensions, boundary conditions, and material properties. Section 5.3 introduces the loading steps used in the analysis. Finally, Section 5.4 presents and discusses analysis results. The results are used to gain insight into the behavior of the gusset plates and possible failure mechanism.

5.2 Model Description

The truss forces obtained from the bridge analysis (Chapter 3) supplied the loading conditions for a detailed gusset plate connection model at panel point U10 shown in Figure 5.1. The concept of the loading condition is shown in Figure 3.7(a). The model consisted of five short, stub segments connected through a pair of gusset plates. The dimensions of each component were taken from the original construction drawings (Mn/DOT 2008). A rigid shell plate was attached to the far end of each stub segment and to the top of the upper chords, at the location where the floor truss seated. The vertical load and truss forces were applied to the center of the shell plate, perpendicular to the plate. The truss loading points were allowed to translate only along the original member axis, and the top loading point was restrained from motion in the out-of-plane direction. The transverse reactions computed at the loading points were minimal, which assured that minimal secondary moment was introduced in the primary bending plane or out-of-plane of the model.

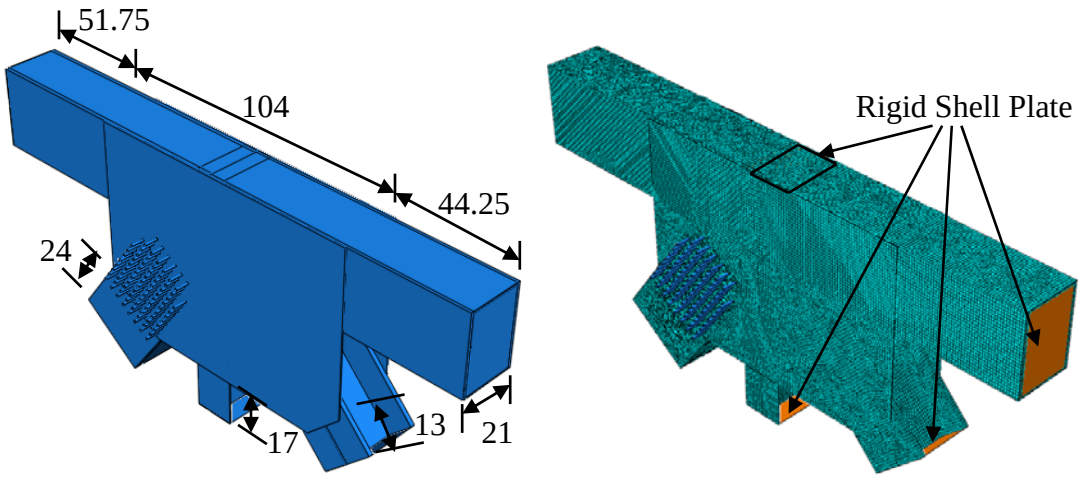

(a) Dimensions (unit in inches) **(b) Finite element mesh**

Figure 5.1 Gusset plate connection model at panel point U10.

The primary objective of the gusset plate connection model analysis was to examine the stress and strain condition that may have led to the failure shown in Figure 2.5. Therefore, the rivet connection was explicitly modeled only between the compression diagonal L9/U10 and the gusset plates. Unlike the other four truss members, which were merged to the gusset plates, the diagonal L9/U10 was modeled as an independent element. Force transfer between the flange plate of L9/U10 and the gusset plates was permitted only in the direction normal to the surface (In other words, friction was neglected). As shown in Figure 5.2, rivets were modeled as rigid cylindrical shells interacting with the periphery of the rivet holes, either in the flange plate of L9/U10 or the gusset plate. A uniform pressure of 8.2 ksi was applied at both sides of the riveted joint within an annular region of 0.3 inches from the edge of holes to produce a pre-tension of 10 kips. This pre-tension is equivalent to the minimum bolt-pretension specified by the Research Council on Structural Connections (RCSC 2004). The pressure was also needed to prevent separation between the diagonal L9/U10 and the gusset plates during analysis.

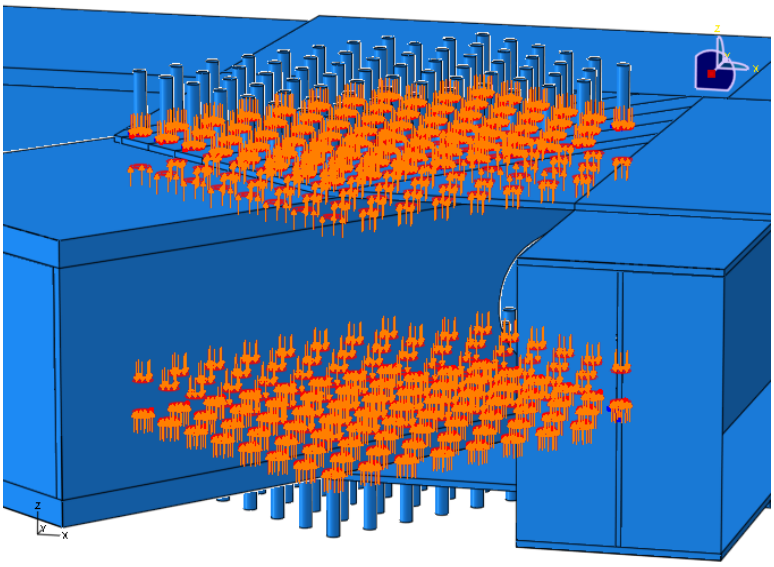

Figure 5.2 Modeling of rivets and pre-tension.

The elasto-plastic steel properties for the gusset plate were based on the tension test data on the actual U10 gusset plates provided by Beshah et al. (2008). The same plastic steel properties were used for other members. Beshah et al. reported a yield strength of 50 ksi and tensile strength of 80 ksi. As plotted in Figure 5.3, the relationship between true stress and logarithmic plastic strain for the gusset plate was approximated as a piecewise linear line with 51.5 ksi at 0 plastic strain, 75 ksi at 0.04, and 88 ksi at 0.1. Beyond the plastic strain of 0.1, the steel behavior was assumed to be perfectly plastic. The meshing strategy was based on the study described in Chapter 4. The model, as shown in Figure 5.1(b), had a total of 119,932 elements and 200,753 nodes. Computations were run on an IBM Power4 system and the Scientific Development and Visualization Laboratory at the University of Minnesota Supercomputing Institute.

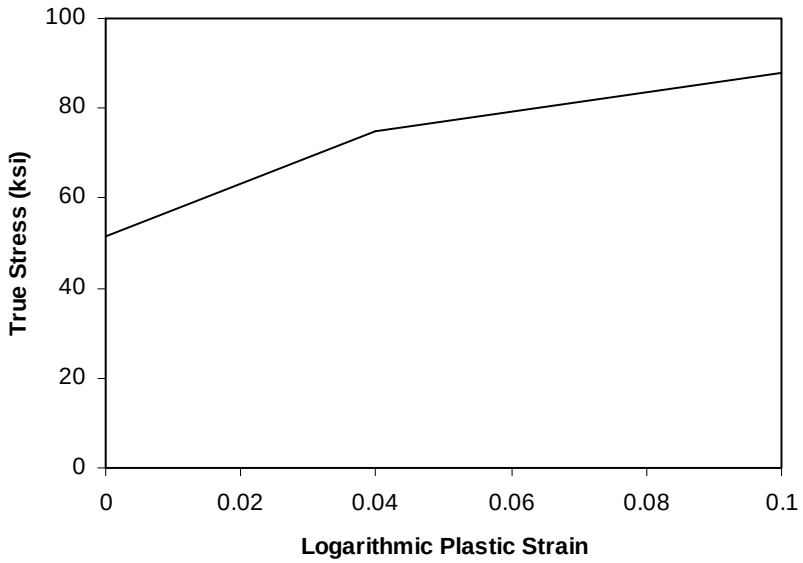

Figure 5.3 True stress versus logarithmic plastic strain for steel material.

5.3 Loading Steps

The analysis was conducted in the five successive steps designated below. The truss forces were increased in four steps, by first introducing the forces for Case 1 of the bridge analysis (Step 1), and increasing the forces, in order, to Case 2 (Step 2), Case 3 (Step 3), and Case 4 (Step 4). Subsequently, as shown in Figure 5.4, a linear thermal gradient of 30 °F was introduced between the surfaces of the two gusset plates by either maintaining the same support conditions (Step 5a) or freezing translation and rotation of the six loading points after completion of Step 4 (Step 5b). In truss bridges, the truss members are supplied with substantial longitudinal restraint by surrounding members (Huckelbridge 2008). The two support conditions should reasonably bound the expected restraints. Step 5a should provide a lower-bound estimate for the effect of restraints and Step 5b should provide an upper-bound estimate.

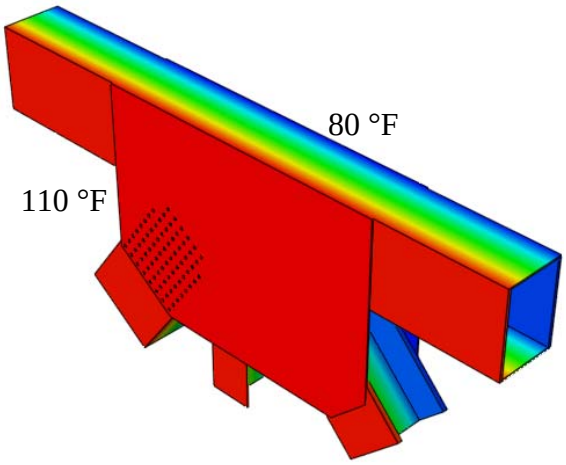

Figure 5.4 Introduced linear thermal gradient of 30 °F for Step 5.

5.4 Results and Discussions

Figure 5.5(a) shows a photographic view of the fracture observed along the compression diagonal L9/U10 (fracture (A) in Figure 2.5(b)). Figure 5.5(b) shows the maximum principal stress field in the gusset plate, near the same perimeter rivet holes, evaluated at completion of analysis Step 4. The bolt hole numbers 5, 6, and 7 indicated in the figure are counted starting at the edge of the gusset plate. On the left edge of the perimeter rivet holes, the maximum principal stress act in the vertical direction. At this location, the principal stress acts nearly perpendicular to the fracture seen in Figure 5.5(a), and indicated by dotted lines in Figure 5.5(b). Therefore, it is suspected that fracture initiated on the left edge of the holes (as viewed in Figure 5.5) due to large normal stresses causing mode I fracture, and propagated straight until the fracture grew large enough to disturb the stress field and change the direction of fracture propagation. The comparison in Figure 5.5 indicates that the detailed nonlinear finite element analysis may provide important insight into the gusset plate failure. In this study, the initiation and propagation of fracture was not examined explicitly. It is reminded that the critical stress and strain values depend substantially on the meshing scheme, as demonstrated in Figure 4.6.

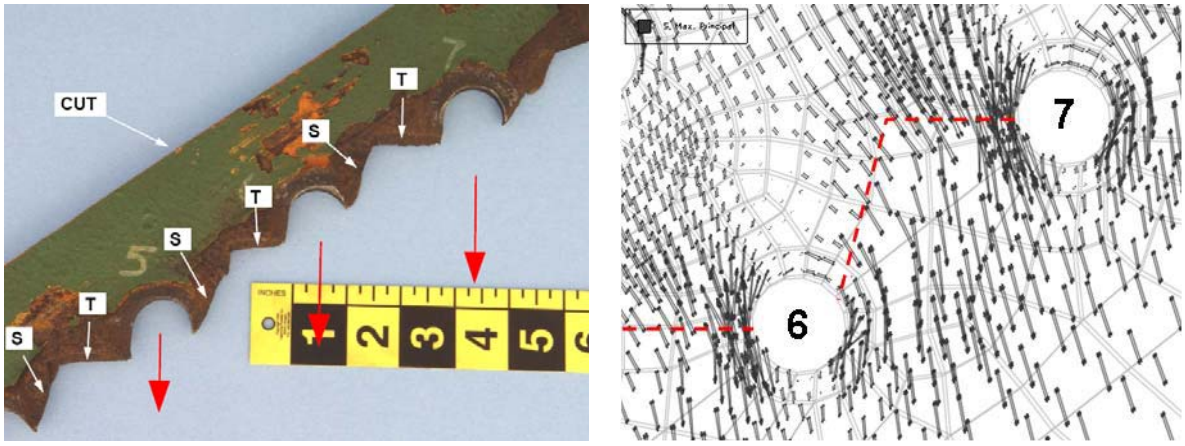

(a) Observed fracture (NTSB 2008d) **(b) Distribution of maximum principal stress**

Figure 5.5 Fracture along L9/U10.

Figure 5.6 shows how yielding of the gusset plates spread as the analysis progressed. The grey to black color indicates the region where the Mises stress exceeds the specified yield stress of 51.5 ksi. The region in white is elastic. At the end of Step 1, localized plasticity was observed adjacent to the upper-left corner of the compression diagonal L9/U10 surrounding rivet holes. In addition, a small region below the upper chords yielded because of the large net shear force along the horizontal section. At the end of Step 2, the yielded region was spread extensively. This result suggests that the dead loads added in years after the original construction stressed the gusset plates beyond a generally accepted level. The standard practice (Kulicki et al. 2006) is to assure that gusset plates remain elastic under design loads. As the analysis progressed to Steps 3 and 4 with increasing load and truss forces, yielding spread along the perimeter of the compression diagonal L9/U10 and the lower edge of the upper chords. While the difference

between Steps 4 and 5a is barely noticeable, Step 5b clearly produced increased area of yielding beyond Step 4. The regions of high stresses coincide with the reported locations of fracture, (A) and (B) in Figure 2.5(b). The substantial yielding shown in Figure 5.6 may have led to the observed failure of the gusset plates.

Figure 5.7 plots the Mises stress versus equivalent plastic strain (PEEQ) measured at a sampling point. As indicated in Figure 5.6, the sampling point is adjacent to an upper-left rivet hole, and was identified as a critical point where large compressive stresses developed. The sampling point was a node point shared by 2 elements, and located along the periphery of a rivet hole. For uniaxial loading cases, the relationship between Mises stress and PEEQ coincides with the true stress versus logarithmic plastic strain material model. Therefore, Figure 5.7 is also a confirmation that the computed stress and strain field agrees with the assumed material plasticity model, indicated in the figure by a piecewise-linear line. At the end of Step 1, the sampling point is already yielded. At the end of Step 4, the Mises stress was as high as 80 ksi and the PEEQ was 0.07. The PEEQ increased by 0.02 between Steps 1 and 2, and between Steps 3 and 4. In other words, loads DL2 and CL produced substantial plastic strains in the gusset plate.The increase in

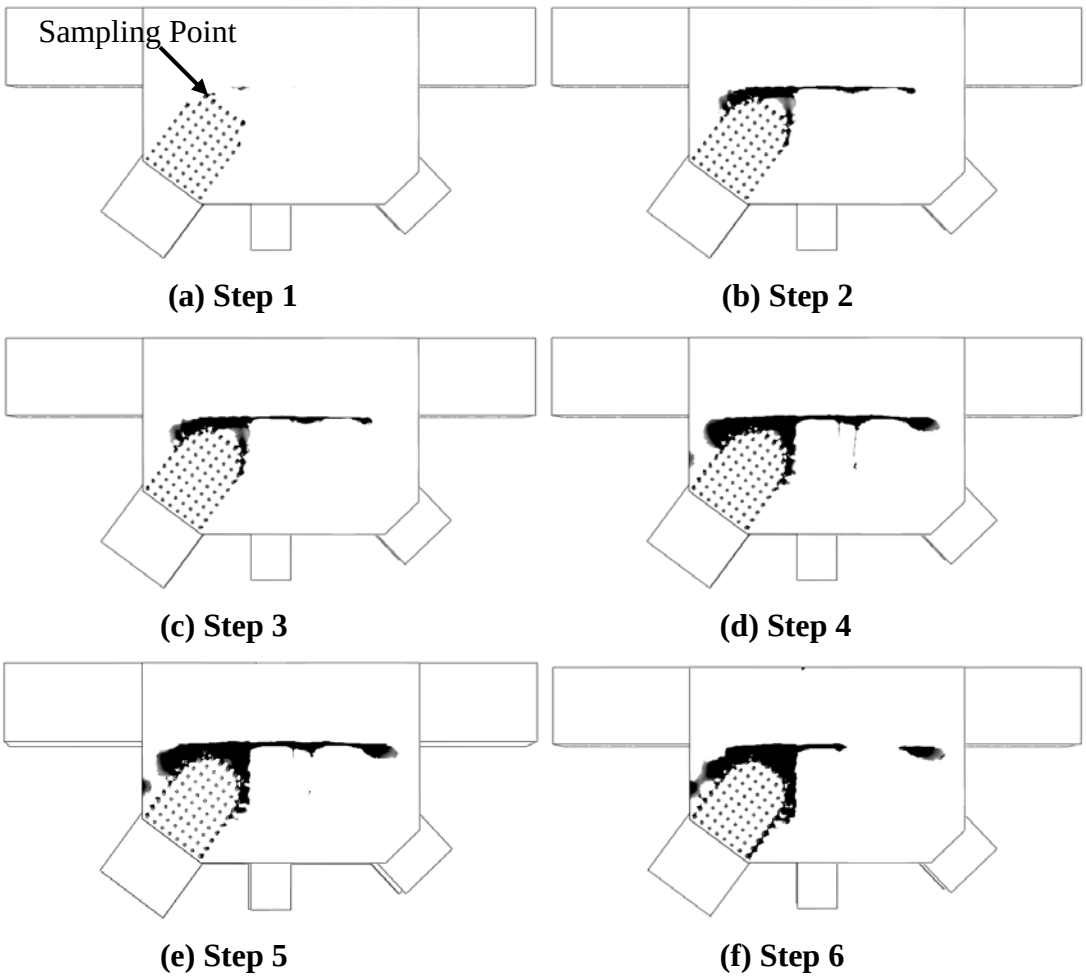

Figure 5.6 Yielding of the gusset plate at the end of each step.

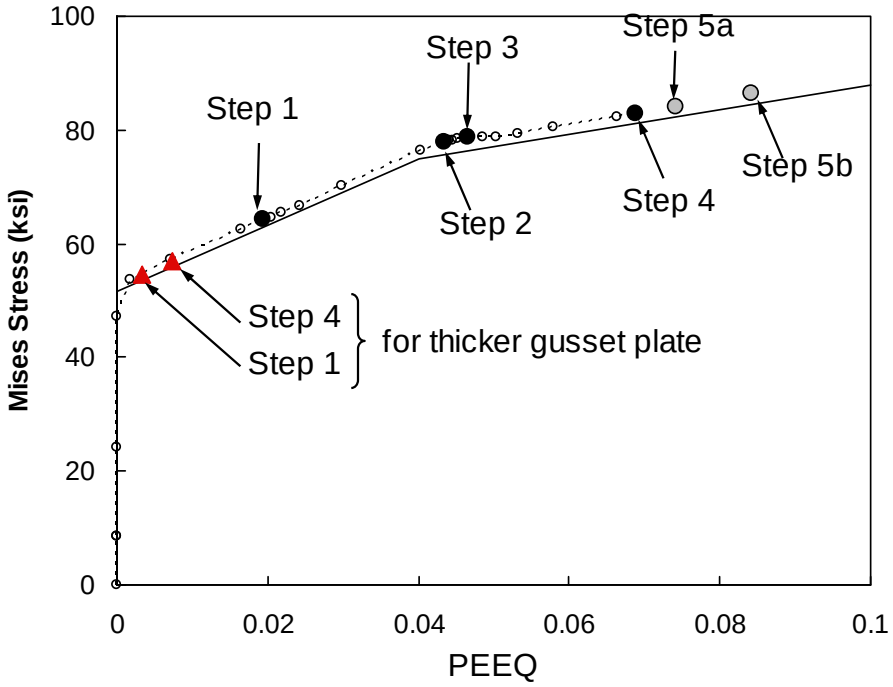

Figure 5.7 Mises stress versus PEEQ at a critical point.

stress and PEEQ caused by temperature gradient was greater than the increase from live loads (LL) but less substantial than that due to the construction loads (CL). The PEEQ produced by the sum of all loading effects was roughly 0.08.

Figure 5.7 also shows data obtained by increasing the gusset plate thickness from 0.5 inches to 1.0 inch. Although the thicker gusset plate also yield at the end of Step 1, the PEEQ at the sampling point at the end of Step 4 was smaller than 0.01. Very limited yielding was observed in the thicker gusset plates except at the immediate vicinity of the sampling point. Such limited yielding is implicitly accepted in steel connection design. Therefore, the thicker gusset plates would have sustained the same load conditions without discernable yielding.

The above analysis results, combined with the observed fracture described by the NTSB (2008c; 2008d), suggest that failure of gusset plate U10 initiated either along the perimeter of the compression diagonal (fracture (A) in Figure 2.5(b)) or along the critical shear plane below the upper chords (fracture (B) in Figure 2.5(b)). The location of yielding suggests that interaction of shear force and compression may have influenced the failure. Consequently, in order to examine the effect of shear-compression interaction, the connection model analysis was repeated for a modified gusset plate connection shown in Figure 5.8 that replaces the top chord U9/U10 and vertical U10/L10 by fixed supports along the edges of the gusset plates. This connection is a compression connection, unlike the U10 connection which is subjected to combined shear and compression, but resembling the specimens studied by Yam and Cheng (1993). However, due to the short unsupported edges of the gusset plate and the short “column” length ahead of the rivet group, buckling is not a concern for this compression connection.

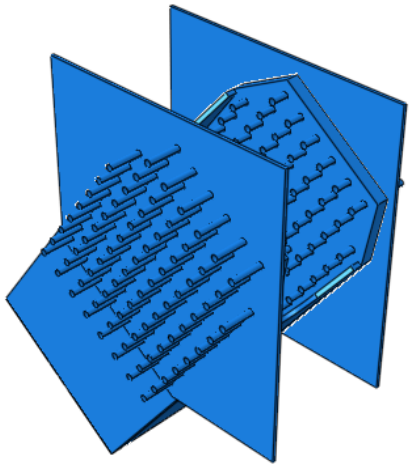

Figure 5.8 Compression gusset plate connection model.

Figure 5.9 compares the response obtained from the two connection models, the U10 connection shown in Figure 5.1 and the compression connection shown in Figure 5.8. The response is represented by the compression in L9/U10 against the displacement of the loading point in L9/U10. Loading for the U10 connection was applied incrementally in proportion to the forces caused by the original dead load (DL1). The Figure shows that the elastic stiffness was 40% smaller for the U10 connection compared to the compression connection. The predicted capacity of the U10 connection, in terms of the compression in L9/U10, was approximately 3,600 kips, while the predicted capacity of the compression connection was approximately 4,000 kips. Here, the capacity is defined by the load at which the response curve completely flattened. The figure also indicates the compression at the end of Step 4 (2,431 kips), which, strictly speaking represents a slightly different loading condition. Disregarding the high likelihood of fracture prior to reaching the capacity (refer to Section 4.2), the simulation result suggests that the U10 connection was able to carry a compressive force in L9/U10 of about 1.5 times that at the end of Step 4.

To further understand the yielding in gusset plates in the region in front of the connection, the response of the two connection models was re-plotted in Figure 5.10, represented by the compression in L9/U10, increased as Steps 1 to 4, against the averaged strain of gauge length *L* indicated in the figure. The elastic stiffness was also 40% smaller for the U10 connection compared to the compression connection. Although the U10 connection softened progressively as the compression exceeded 1,700 kips, the compression connection remained largely elastic when the analysis was terminated at a compression of 2,430 kips. The U10 connection was affected substantially by yielding in the region in front of the connection. Figures 5.6 and 5.10 suggest that, beyond Step 1, the stress was redistributed from the front of the connection to the shear lines along the perimeter rivet holes, resulting in the wide yielded region surrounding member L9/U10. Discernable yielding did not occur in the compression connection at the end of Step 4. Therefore, the failure of the U10 gusset plate might not be addressed in design unless the interaction between shear and compression is accounted for.

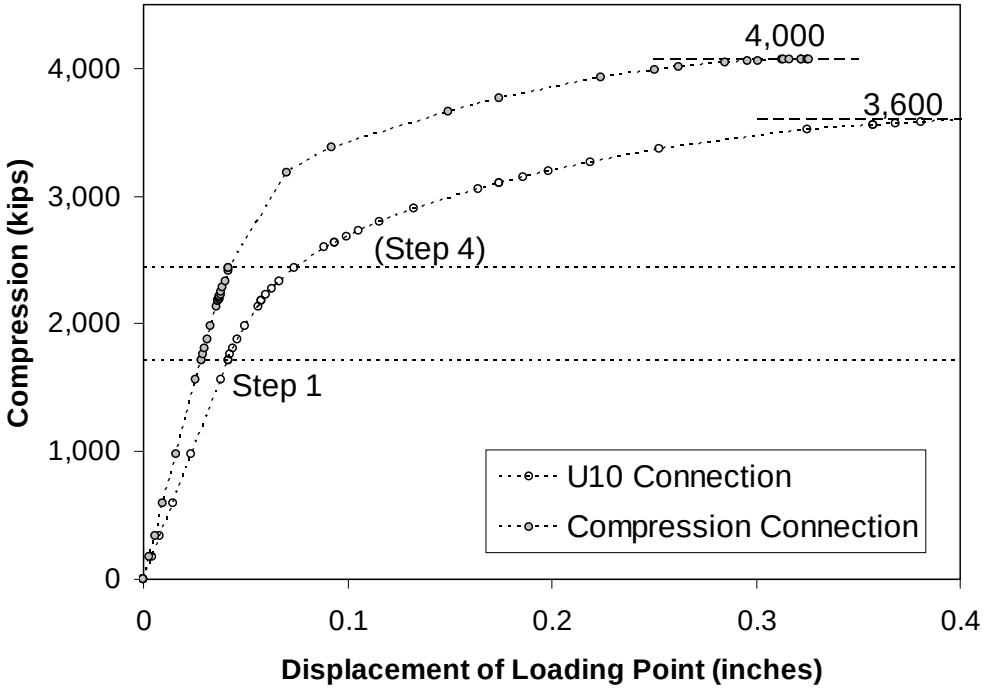

Figure 5.9 Load versus displacement of loading point.

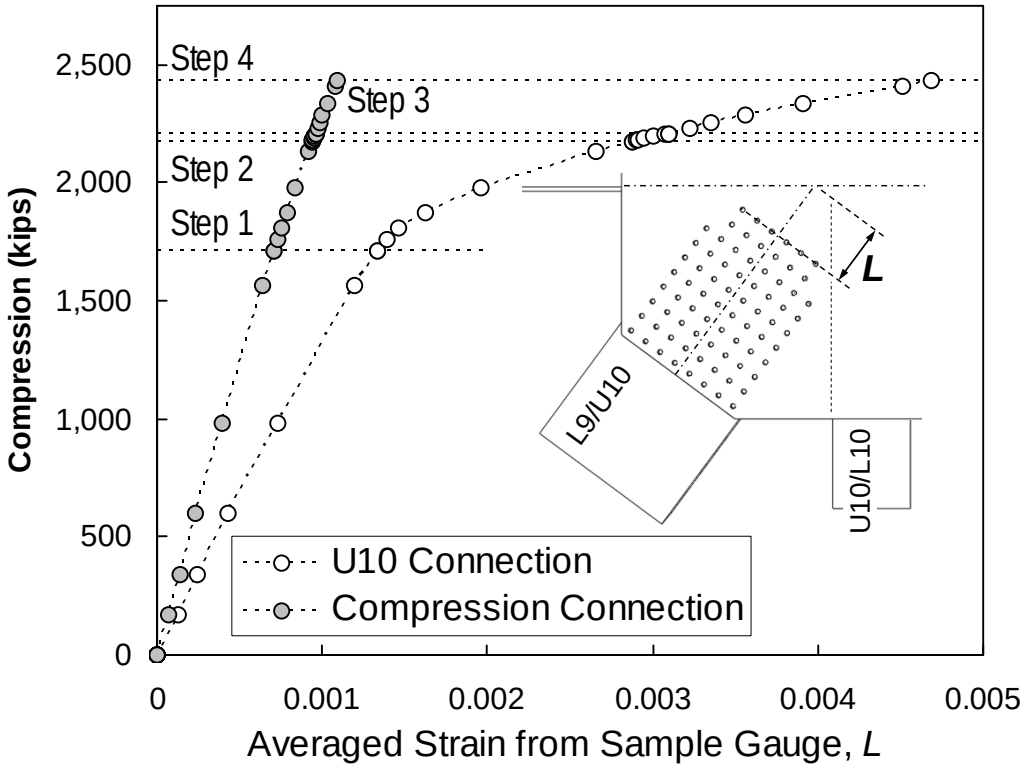

Figure 5.10 Load versus averaged strain measured for sampling gauge.

CHAPTER 6: COLLAPSE SEQUENCE STUDY

6.1 Introduction

The simple design calculations described in Section 3.6 and detailed FE analysis results described in Chapter 5, combined with photographic evidence from the NTSB (2008a) cited in Section 2.2, strongly indicate that the collapse of the I-35W Bridge initiated at panel point U10, and the fracture likely initiated in the portion of the gusset plate that connected to compression diagonal L9/U10. In this chapter, a possible bridge collapse sequence following failure of diagonal L9/U10 is described. Section 6.2 describes how truss forces may have redistributed as L9/U10 lost its load-carrying capacity, due to failure at the gusset plate connection. Section 6.3 explains a possible collapse sequence and compares the prediction to available video proofs.

6.2 Truss Force Redistribution

The 3D model created in Chapter 3 was used to study the truss force redistribution as one of the two U10 panel points gradually failed at the connection with L9/U10. As shown in Table 3.3, the forces transferred to panel point U10W were larger, albeit slightly, than the forces transferred to panel point U10E. Therefore, it was postulated that gusset plate failure occurred first in the U10W gusset plates. Analysis for Loading Case 4 (defined in Section 3.4) was repeated for slightly perturbed models in which the compressive strength limit of diagonal L9/U10W was reduced to 75, 50, 25, or 0% of the compressive force delivered under Case 4, 2,504 kips (see Table 3.3). The strength reduction reflected the process where the gusset plate connection gradually failed at the connection with diagonal L9/U10W. This analysis does not address the rate of gusset plate failure and the resulting dynamic effects.

It was found from the four results that the forces redistribute nearly linearly with strength reduction of diagonal L9/U10W. Figure 6.1 illustrates the analysis results, highlighting how the truss forces redistributed in the west main truss (Figure (a)) and east main truss (Figure (b)) when the strength of diagonal L9/U10W reduced to zero. In the figures, dashed lines represent members which saw force reduction, solid lines represent members which saw up to 500 kips of force increase, and bold solid lines represent members which saw more than 500 kips of force increase. The figure indicates that, as L9/U10W lost its load-carrying capacity, the forces would have redistributed to members near Pier 7 in the west main truss, and to members close to panel point U10E in the east main truss. This is a reasonable redistribution path because failure of L9/U10W causes the west main truss to function close to a cantilever structure which results in large negative bending moment near Pier 7, and the gravity loads applied on the U10 floor truss would find an alternative load path at the other supporting end at U10E. As a result of large force redistribution, the four members indicated by “x” marks were subjected to a force greater than 70% of their nominal strength capacity.

Table 6.1 lists the vertical reaction force at each of the eight piers before and after failure of L9/U10W, and also lists the changes of the reaction forces. Notable reduction in reaction force was observed at west Pier 6, and notable increase was observed at east Pier 6 and west Pier 7. The shift in reaction forces agrees well with the force redistribution indicated in Figure 6.1. Figures 6.1 and 6.2 illustrate the non- symmetrical force redistribution following failure of one

member (or connection) in the west main truss.

Figure 6.2 plots the transition of truss forces in selected members close to panel point U10 or U10'. U10 and U10' are the panel points which had under-designed gusset plates, according to Holt and Hartmann (2008) and NTSB (2008b). The figure indicates the truss force before failure of L9/U10W, after failure of L9/U10W, and the reserve capacity after force redistribution. "C" indicates that the member is in compression, and "T" indicates that the member is in tension. The reserve capacity is calculated by subtracting the force after failure of

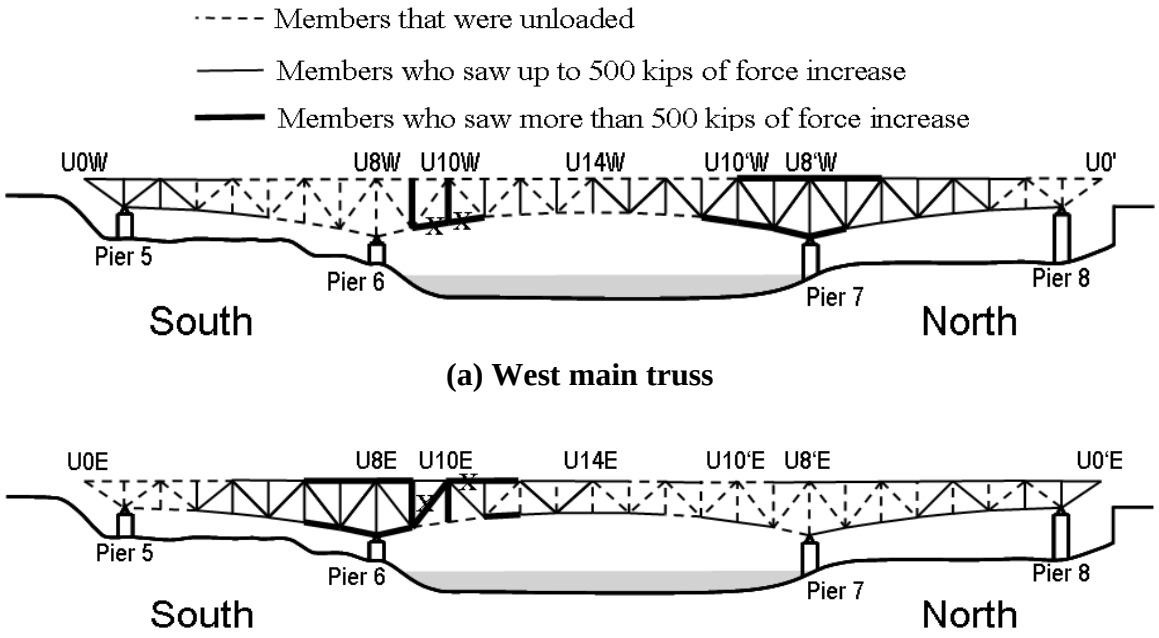

(a) West main truss

(b) East main truss

Figure 6.1 Truss force redistribution.

Table 6.1 Reaction forces before and after force redistribution (unit in kips)

		Before Redistribution	After Redistribution	Changes
Pier 5	West	1490	1650	160
	East	1435	1297	-138
Pier 6	West	5183	4580	-603
	East	4908	5379	471
Pier 7	West	4777	5339	562
	East	4687	4405	-282
Pier 8	West	1812	1693	-119
	East	1771	1721	-50

L9/U10W from the nominal strength capacity. Four of these members, L9/L10W, L10/L11W, U10/U11E, and L9/U10E, are the compression members indicated in Figure 6.2 by an "x" mark. The four members saw an increase in force that was 35% of their nominal strength capacity or larger, and were subjected to a force greater than 70% of their capacity after the force redistribution. It is noted that, after the force redistribution, the force in compression diagonal L9/U10E was 92% of its capacity. This is a compression diagonal that connected to U10E with similarly under-designed gusset plates as those in L9/U10W. It is quite likely that L9/U10E was not capable of carrying the design loads, much less the redistributed forces. Therefore, the gusset plate connection at L9/U10E is suspected as the first location to fail after L9/U10W.

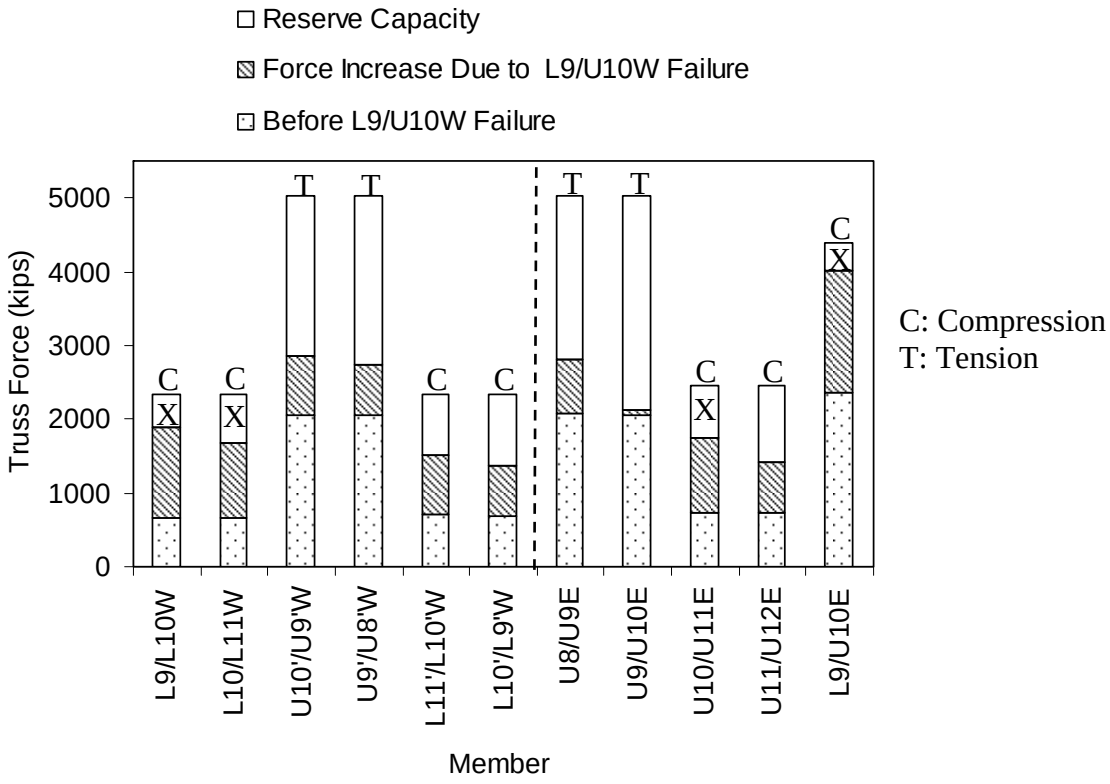

Figure 6.2 Truss forces and reserve capacity.

6.3 Possible Bridge Collapse Sequence

Figure 6.3 shows the elastic deflection of the bridge model when the strength of the diagonal member L9/U10W was set to zero and loading Case 4 was applied. The deflection shown in the figure is enhanced in order to make the deformation visible. The center span of the bridge severely deflected downwards, and the model was distorted and twisted in the region close to panel point U10W. Although material and geometrical nonlinearity were not considered in the model, the distortion and twisting in Figure 6.3 correlates with the photograph of the collapsed bridge shown in Figure 1.1(b).

Figure 6.4 shows a possible collapse sequence of the bridge that is consistent with the

truss force redistribution study in previous section. First, the connection with compression diagonal L9/U10W at panel point U10W fractured, causing L9/U10W to lose its ability of carry force (Stage 1 in the figure). Force redistribution caused overstress and failure of the similar connection between L9/U10E and panel point U10E. After the two members failed, the center truss spans effectively reduced to a cantilever structure (Stage 2). Large negative bending moments were produced near Pier 7. The center span could not carry its self-weight and loads any more. As the center span fell down, the hinge support at Pier 7 was pulled in toward the river (Stage 3). The gusset plates at panel point U10', which were similarly under-designed as the gusset plates at panel point U10, may have fractured as the center span collapsed. The north side span was pulled toward the river with Pier 7 and collapsed (Stage 4).

Figure 6.5 shows highlights of video image taken from a monitoring camera southwest of the bridge center span (Hill et al. 2008). To the knowledge of the author, this is the only video recording of the bridge collapse. The video image suggests that the center span fell with the south side tipping downwards. Large distortion of the main truss is seen in Frame 4, in the region close to Pier 7. Unfortunately, the region near Pier 6, where the collapse is believed to have initiated, was not captured in the video. However, the video image agrees with the postulated collapse sequence, that the failure likely initiated near Pier 6, failure near Pier 7 followed, and the North span collapsed last.

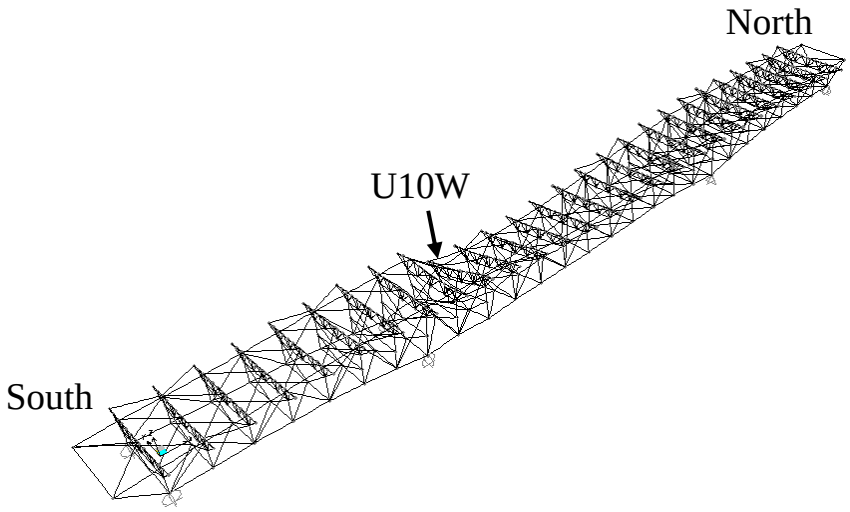

Figure 6.3 Deflection of I-35W Bridge after L9/U10W failure.

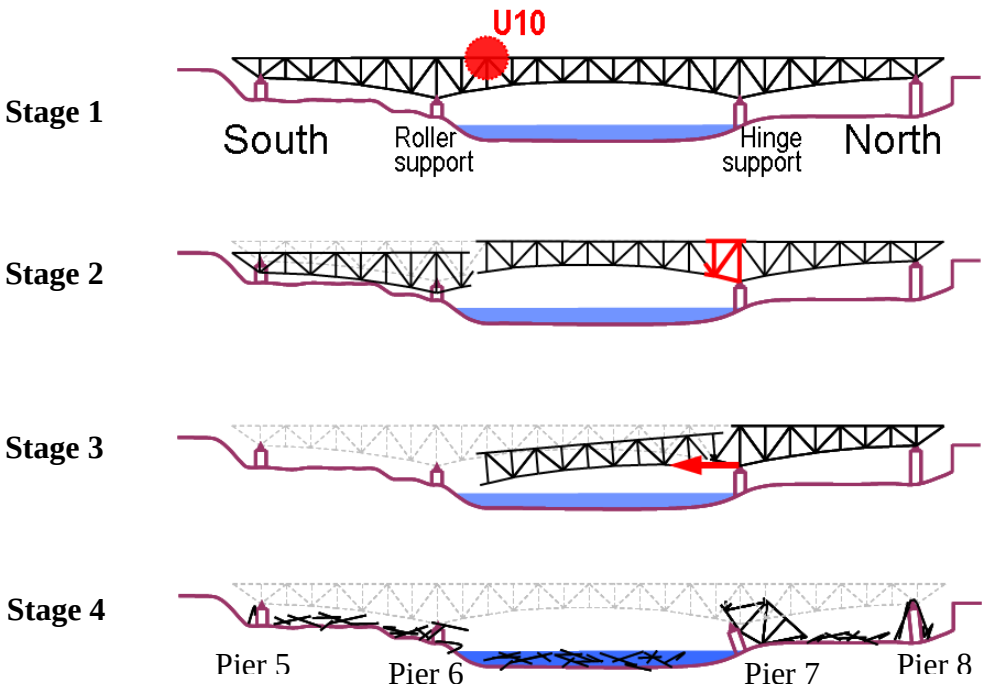

Figure 6.4 Possible bridge collapse sequence.

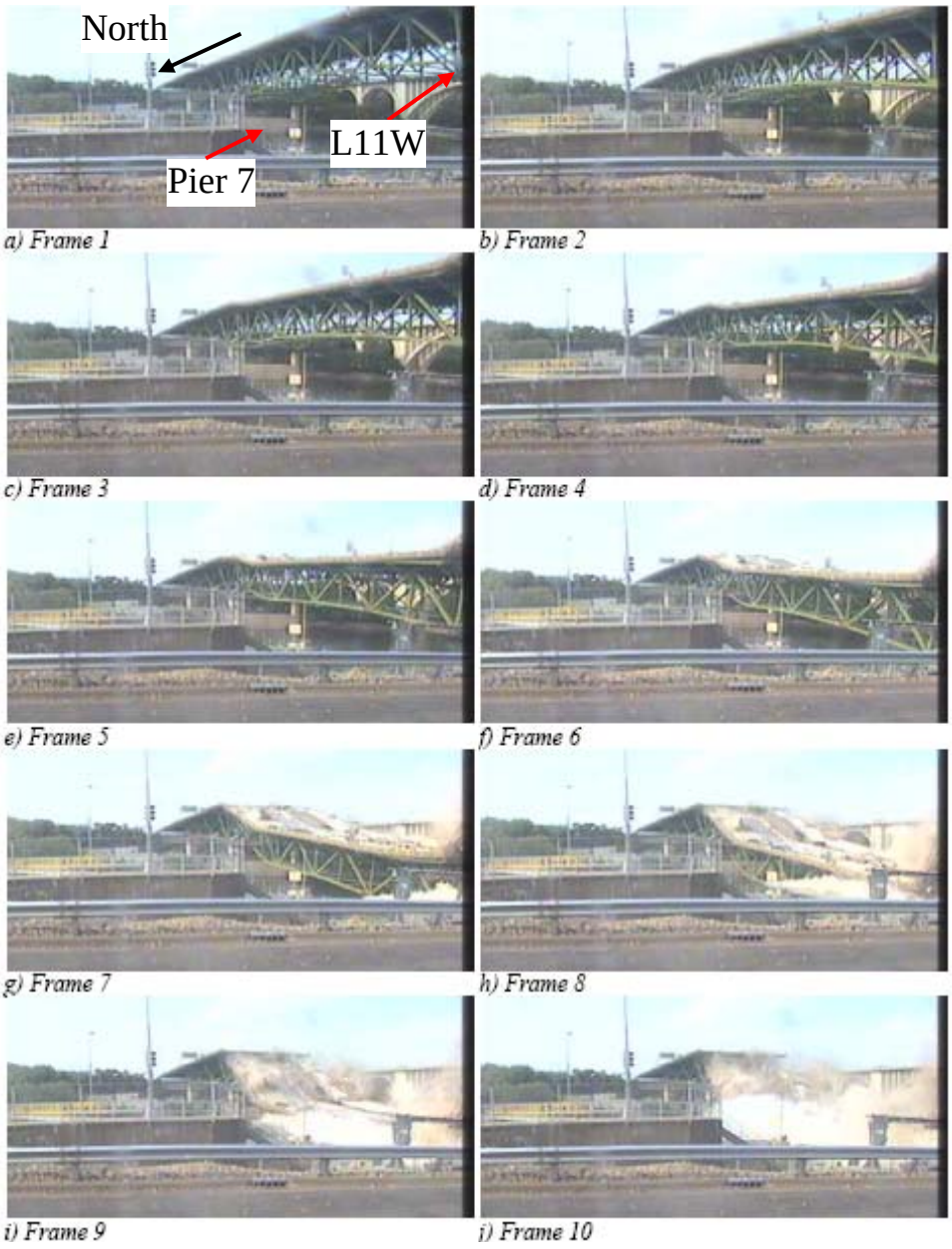

Figure 6.5 Highlight frames from video image (from Hill et al. 2008).

CHAPTER 7: CONCLUSIONS

7.1 Summary

Reported evidence suggests that the collapse of the I-35W Bridge initiated at gusset plate connections at panel point U10. A computational study on these connections was conducted in this report. The study consisted of a bridge fact description and a literature review in Chapter 2, a bridge analysis for estimating truss forces, design checks of individual truss members, and design checks of the U10 gusset plates in Chapter 3, a validation study of a finite element modeling procedure for gusset plates in Chapter 4, a detailed nonlinear, three-dimensional, finite element analysis of the U10 gusset plate connection in Chapter 5, and a collapse sequence study of the bridge in Chapter 6.

The literature study indicated that past and current gusset plate design is based on simple assumptions and calculations. It was noted that very limited research information is available on gusset plates subjected to forces from multiple directions as in gusset plates in truss bridge systems. A bridge analysis model was created using a commercial structural analysis software, SAP 2000 (CSI 2007). Loads applied to the bridge at the time of the collapse were estimated. The truss forces obtained from the bridge analysis were used to check the adequacy of individual truss members and the U10 gusset plates using conventional design methods. The truss members appeared to be reasonably sized. However, it was found that the U10 gusset plate did not have adequate thickness to keep itself in the elastic range. Prior to performing finite element analysis of the U10 gusset plates, the modeling and analysis procedure in ABAQUS version 6.8 was validated using available test data. The same procedure was applied to model the U10 gusset plate connections. Analysis results were scrutinized and compared against fractures observed from the bridge debris. The locations of high plastic stress in the FE model corresponded with the locations of the fractures. In addition, the results suggested that further understanding of interaction between shear and compression might be a key issue to improve gusset plate design. Finally, a possible bridge collapse sequence was proposed and compared against available video image.

7.2 Conclusions

Key findings of this study are summarized as follows:

- The concrete deck overlay and new parapets added in later years after original construction increased the dead loads by 30%.
- The live loads were rather small at the time of the collapse because of the traffic lane closures.
- The construction materials and equipment placed on the day of the collapse caused 10 to 15% increase in the forces applied on the U10 gusset plates.
- Temperature gradient between the two sides of the connection may have produced additional stress and strain in the gusset plates. However, the effect of temperature

gradient is difficult to quantify because the computed results are highly dependent on the assumed boundary conditions for the analysis model.

- A substantial portion of the U10 gusset plates may have yielded at the time of the collapse. Weight increase due to past deck reconstruction and construction materials and equipment staged on the day of the collapse, along with insufficient strength of the gusset plate, were identified as the main contributing factors to the substantial yielding. These results corroborate the findings by the NTSB (2008b) and Hill et al. (2008).
- The bridge collapse might be explained with the following sequence: first, the gusset plates connecting the compression diagonal L9/U10W to panel point U10W failed; force redistribution led to overload and failure of the gusset plates connecting the compression diagonal L9/U10E to panel point U10E; the center span now acted as a cantilever with the south end free and north end fixed; due to large bending moment produced at the north end, the north end of the center span also failed; the entire center span fell and pulled down the north side span in the process.

7.3 Future Research Recommendations

Standard design procedures (Holt and Hartmann 2008; Kulicki et al. 2006) check the gusset plate strength at the compression member and along the critical shear section independently, but do not check the interaction between the forces. On the other hand, results from this study suggest that shear-compression interaction contributed to the substantial yielding of the gusset plates, and therefore, may have played a key role in the I-35W Bridge collapse. Panel points with combined shear and compression generally occur in truss structures that are continuous over multiple spans. Therefore, further research on the behavior of gusset plate connections subjected to combined shear and compression is believed to improve the safety and reliability of steel truss bridges.

REFERENCES

American Association of State Highway Officials (AASHO). (1973). *Standard Specifications for Highway Bridges, 11th edition*. Association General Offices, AASHO, Washington, D.C.

American Institute of Steel Construction (AISC). (2005). *Specification for Structural Steel Buildings*. Chicago, IL.

Barker, R. M., and Puckett, J. A. (2007). *Design of Highway Bridges, An LRFD Approach, 2nd Edition*. John Wiley & Sons, Inc., Hoboken, NJ.

Beshah, F., Wright, W., and Graybeal, B. (2008). "Mechanical property test report (I-35W over the Mississippi River)." *Federal Highway Administration Turner-Fairbank Highway Research Center Report*. <http://www.ntsb.gov/dockets/highway/hwy07mh024/404089.pdf> (Apr. 21, 2009).

Bjorhovde, R., and Chakrabarti, S. K. (1985). "Tests of full-scale gusset plate connections" *J. Struct. Eng.*, ASCE, 111(3), 667-684.

Computers and Structures, Inc. (CSI). (2007). *Basic Analysis Reference Manual*. Berkeley, CA.

Gross, J. L. (1990). "Experimental study of gusseted connections." *Eng. J.*, AISC, 27(3), 89-97.

Hardash, S. G. and Bjorhovde, R. (1985). "New design criteria for gusset plates in tension." *Eng. J.*, AISC, 22(2), 77-94.

Hill, H. J., McGormley, J. C., Koob, M. J., and Nugent, W. J. (2008). *I-35W Bridge over the Mississippi River: collapse investigation – Bridge No. 9340, Minneapolis, Minnesota*. Final Report, Wiss, Janney, Elstner Associates, Inc., Northbrook, IL, prepared for Mn/DOT. <http://www.ntsb.gov/dockets/highway/hwy07mh024/404995.pdf> (Apr. 21, 2009).

Holt, R. and Hartmann, J. (2008). *Adequacy of the U10 gusset plate design for the Minnesota bridge No. 9340 (I-35W over the Mississippi River)*. Final Report. Turner-Fairbank Highway Research Center Report., Federal Highway Administration, McLean, VA. <http://www.ntsb.gov/dockets/highway/hwy07mh024/404084.pdf> (Apr. 21, 2009).

Huckelbridge, A., personal communication, Sep. 15, 2008.

Kulicki, J. M., Prickett, J. E., and LeRoy, D. H. (2006). "Chapter 13. Truss bridges." *Structural Steel Designer's Handbook, 4th Edition*. Edited by Brockenbrough, R. L. and Merritt, F. S., ASCE, McGraw-Hill Professional.

Minnesota Department of Transportation (Mn/DOT). (2008). *I-35W Bridge original plans & details*. <http://www.dot.state.mn.us/i35wbridge/history.html> (Apr. 21, 2009).

National Transportation Safety Board (NTSB). (2007). *Loads on the bridge at the time of the accident*. Modeling Group Study Report No. 07-115. <http://www.ntsb.gov/dockets/highway/hwy07mh024/385259.pdf> (Apr. 21, 2009).

National Transportation Safety Board (NTSB). (2008a). Photos of I-35W Bridge. <http://www.ntsb.gov/dockets/highway/hwy07mh024/387406.pdf> (Apr. 21, 2009).

National Transportation Safety Board (NTSB). (2008b). *Collapse of I-35W Highway Bridge, Minneapolis, Minnesota, August 1, 2007*. Accident Report NTSB/HAR-08/03. <http://www.dot.state.mn.us/i35wbridge/ntsb/finalreport.pdf> (Apr. 21, 2009).

National Transportation Safety Board (NTSB). (2008c). *Structural investigation group chairman factual report*. Report No. 08-015. <http://www.ntsb.gov/dockets/highway/hwy07mh024/387408.pdf> (Apr. 21, 2009).

National Transportation Safety Board (NTSB). (2008d). *Materials laboratory factual report*. Report No. 07-119. <http://www.ntsb.gov/dockets/highway/hwy07mh024/386200.pdf> (Apr. 21, 2009).

Research Council on Structural Connections (RCSC). (2004). *Specification for Structural Joints Using ASTM A325 or A490 Bolts*. Chicago, IL.

Simulia (2008). *ABAQUS Version 6.8 Documentation Collection*, Simulia Corp., Dassault Systèmes, Providence, RI.

Tajima, J., Takena, K., and Miki, C. (1984). "Fatigue strengths of truss made of high strength steels." *Proc. JSCE*, 341, 1-10.

Thornton, W. A. (1984). "Bracing connections for heavy construction." *Eng. J.*, AISC, 21(3), 139-148.

URS Corp. (2006). *Fatigue evaluation and redundancy analysis – Bridge No. 9340 (I-35W over Mississippi River)*. Bridge 9340 Study, Prepared by URS Corp. for Mn/DOT, Minneapolis, MN.

Yam, M. C. H. and Cheng, J. J. R. (1993). "Experimental investigation of the compressive behavior of gusset plate connections." *Struct. Eng. Rep. No. 194*, University of Alberta, Alberta, Canada.

Yamamoto, K., Akiyama, N., and Okumura, T. (1985). "Elastic analysis of gusseted truss joints." *J. Struct. Eng.*, ASCE, 111(12), 2545-2564.

Yamamoto, K., Akiyama, N., and Okumura, T. (1988). "Buckling strength of gusseted truss joints." *J. Struct. Eng.*, ASCE, 114(3), 575-590.

APPENDIX A:

DETAILED DESCRIPTION OF THE BRIDGE SYSTEM

A.1 Primary Structural Features

Figure A.1 shows photographs of the I-35W Bridge over the Mississippi River in Minneapolis, Minnesota. The bridge is designated as Bridge 9340 by the Minnesota Department of Transportation (Mn/DOT). As shown in Figure 2.1, the bridge was composed of a three-span deck-truss system and approach spans connecting to the south and north ends of the deck-truss system. The center portion of the bridge, spanning 456 feet over the Mississippi River, was a deck-truss system. The concrete deck placed on the bridge was separated in the middle between the two traffic directions. Near the south end of the bridge, the traffic lanes curved toward the west. Near the north end of the bridge, an exit lane was placed at the right end of the northbound traffic lanes. However, within the truss segment of the bridge, the concrete deck was roughly symmetric between the two traffic directions.

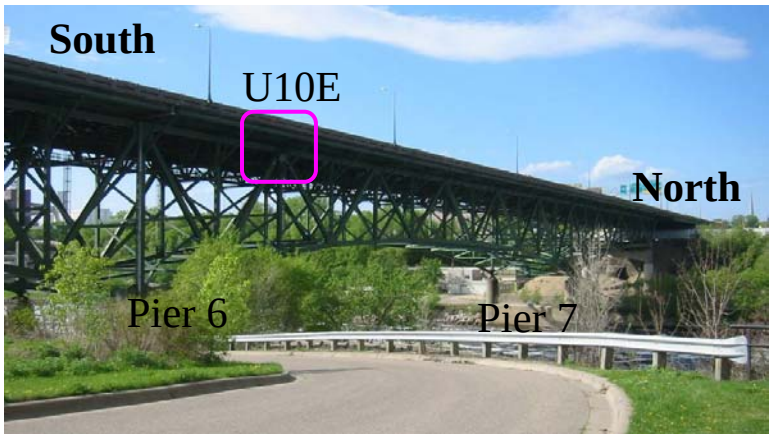

(a) Viewed from south-east (from wikipedia[#])
http://en.wikipedia.org/wiki/File:I-35W_Bridge_2.jpg

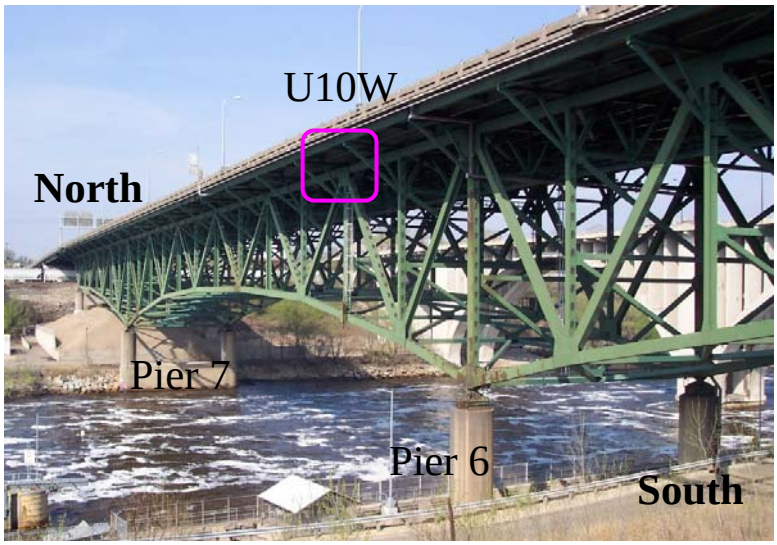

(b) Viewed from south-west (from NTSB 2008a)

Figure A.1 Photographs of I-35W Bridge before collapse.

The two main trusses were placed at the west and east edges of the system, 72 feet 4 inches apart. The west and east main trusses were nearly identical. The nomenclature of the panel points are indicated in Figure 2.1. The distance between panel points were 38 feet. The only exception to this distance was between panel points U0 and U1, where the curve of the traffic at the south end needed to be accommodated. The overall distance between the south and north ends of the truss was roughly 1,064 feet. The main trusses were supported at the bottom at four lower chord panel points. The four support points, L1, L8, L8', and L1', were placed at Piers 5, 6, 7, and 8, respectively.

Figure A.2 shows section views of the deck-truss system. A system of concrete deck and steel stringers supported the traffic lanes. The stringers were supported by floor trusses, placed perpendicular to the main trusses. The floor trusses were supported by the main trusses at panel points along the upper chord of the main truss. Out-of-plane stability of the main truss was supplied by braced frame systems, referred to in the construction plan drawing as the "sway frames." The sway frames were placed directly underneath the floor trusses. Near Piers 6 and 7, the sway frame comprised two layers of braced frames. Otherwise, the sway frame was composed of a single layer of braced frame.

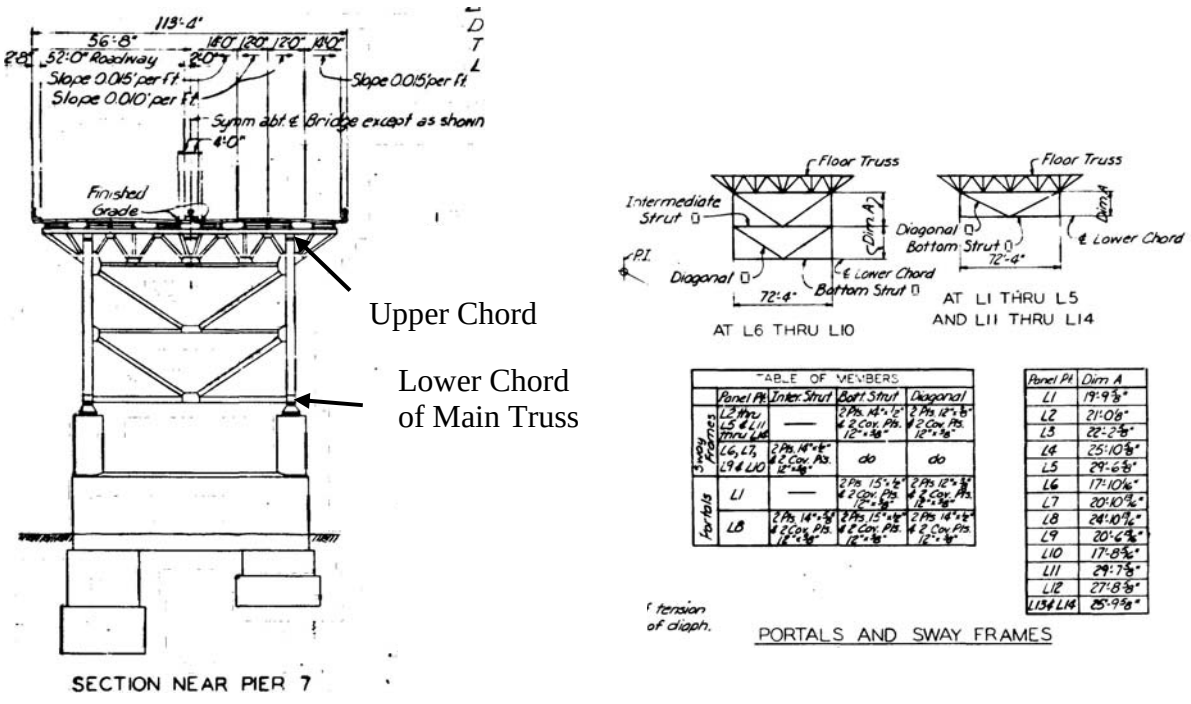

Figure A.2 Section view and sway frames (from Mn/DOT 2008).

The main trusses were supported by a roller bearing at Piers 5, 6, and 8, and by a hinge bearing at Pier 7. Figure A.3 shows photographs of the roller and hinge bearings. Based on field inspection, URS (2006) reports "relatively poor" conditions of bearings at Pier 6 and 7, which were directly underneath the expansion joints, and also states that "[all] the roller bearings seem to have thick coating of paint and did not appear to be functioning as intended under live load."

Judging from the mechanism of the bearings, out-of-plane motion (perpendicular to the primary plane of the main trusses) was restrained at the support points.

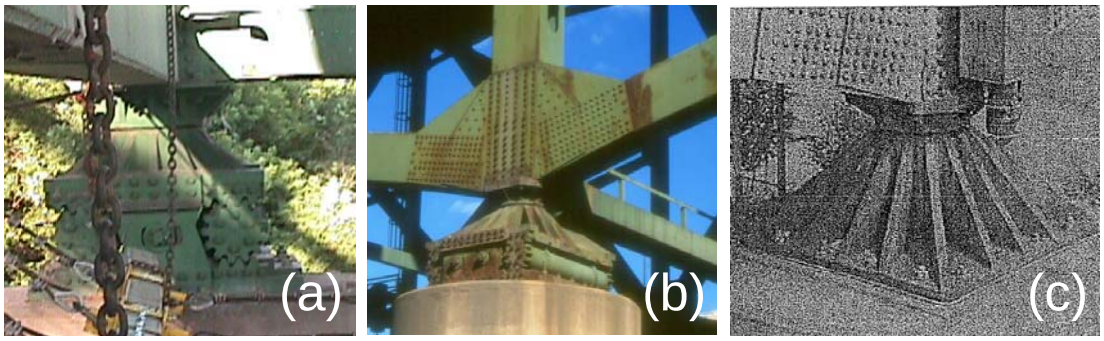

(from Prof. Robert Dexter) **(from wikipedia#)** **(from URS 2006)**

http://en.wikipedia.org/wiki/File:MN-I35-SW-pier.jpg

Figure A.3 Photographic view of bearing supports.

Figure A.4 shows the placement of stringers that directly supported the concrete decks. Each concrete deck (supporting the southbound and northbound traffic) was supported by seven stringers, spaced evenly, 8 feet-2 inches apart. The W27×94 stringers ran continuously between expansion joints, through either four or six panel point spans. The stringers were laterally braced by L15×33.9 "stringer diaphragms" (a single channel used at each bracing point). The stringer

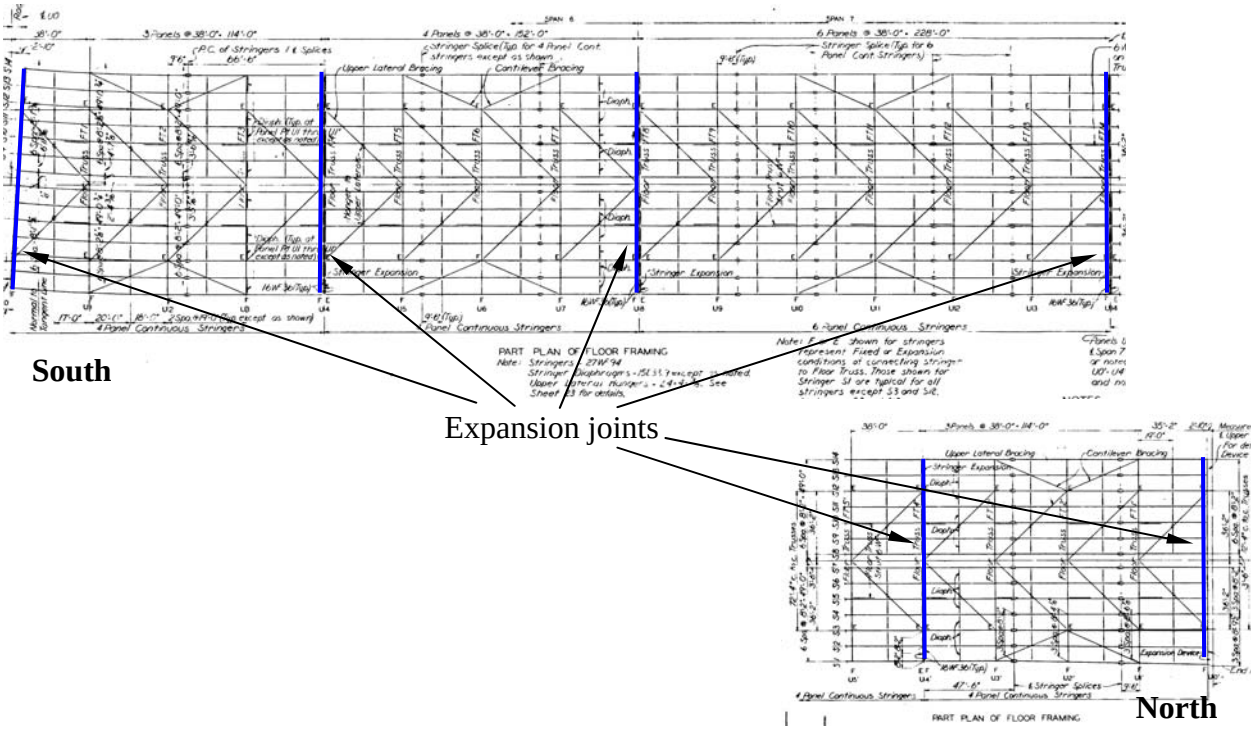

Figure A.4 Plan view of stringer placement (from Mn/DOT 2008).

diaphragms were paced above each floor truss, as shown in Figure A.5, and at the middle of adjoining floor trusses. Therefore, the unbraced length of the stringers was generally 19 feet. As indicated in Figure A.4, expansion joints were placed at the south and north ends of the truss systems (panel points U0 and U0') and at five locations within the truss system at panel points U4, U8, U14, U8', and U4'.

Figure A.5 shows the east half of a floor truss. As mentioned previously, the concrete deck is separated at mid-width. At the third panel point counted from the edge, the upper chord of the floor truss rests on the upper chord of the main truss. The figure indicates how the traffic load and weight of the concrete deck is delivered through the stringers to the upper chord panel points of the floor truss.

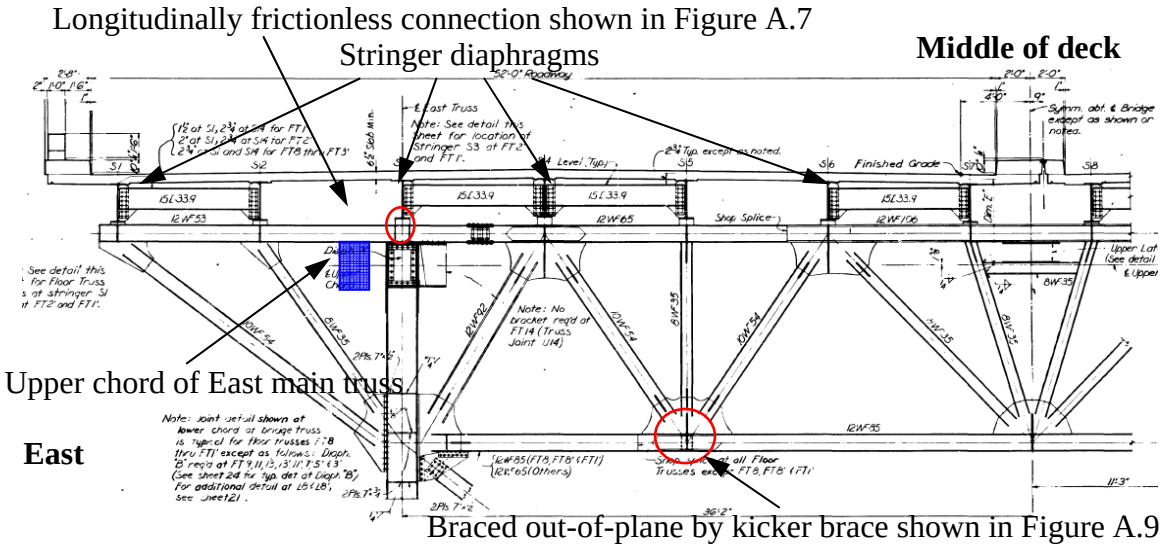

Figure A.5 Cross-sectional view of concrete deck and floor truss (from Mn/DOT 2008).

A.2 Key Details

In addition to the primary structural features described above, a number of particular details need to be examined in order to understand the structural behavior of the bridge. Some of the details described below were interpreted and incorporated in the computational models developed in this study.

A.2.1 Standard Connections between Stringers and Floor Truss

The majority of stringers (with the exception of stringers above main trusses) were bolted directly to the upper chord of the floor trusses. As shown in Figure A.6, the connection was achieved by using four, 7/8-inch diameter high-strength bolts. Spacer plates with thickness ranging between 1 inch and 5.5 inches were used in the bolted connections between the stringer and top flange of the upper chord.

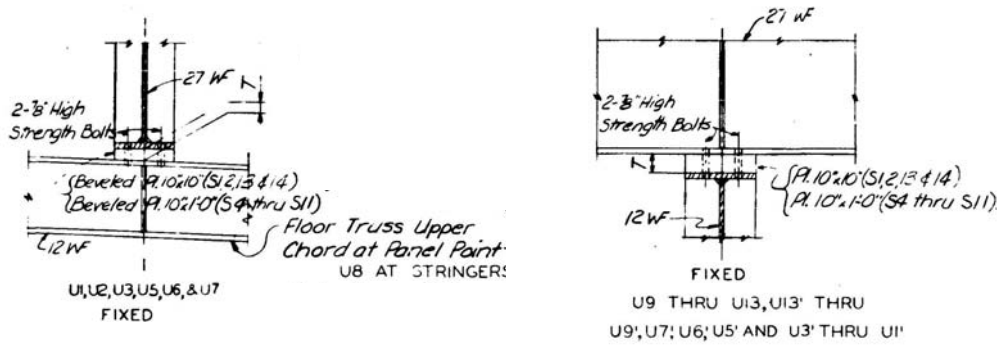

Figure A.6 Connection between stringer and upper chord of floor truss (from Mn/DOT 2008).

A.2.2 Connections between Stringers and Floor Truss at Panel Points of the Main Truss

Two stringers were placed directly above the east main truss and west main truss, respectively. Figure A.7 shows a steel spacer plate inserted between the bottom flange of the stringer and upper chord of the floor truss. While the assembly of steel plates prevented out-of-plan motion of the bottom flange of the stringer, the stringer was not fastened to either the spacer plate or upper chord. The figure further indicates a bronze plate inserted between the spacer block and stringer, presumably to reduce friction between these pieces. Therefore, the stringers were permit differential displacement in the longitudinal direction, and the displacement could occur with relatively small friction.

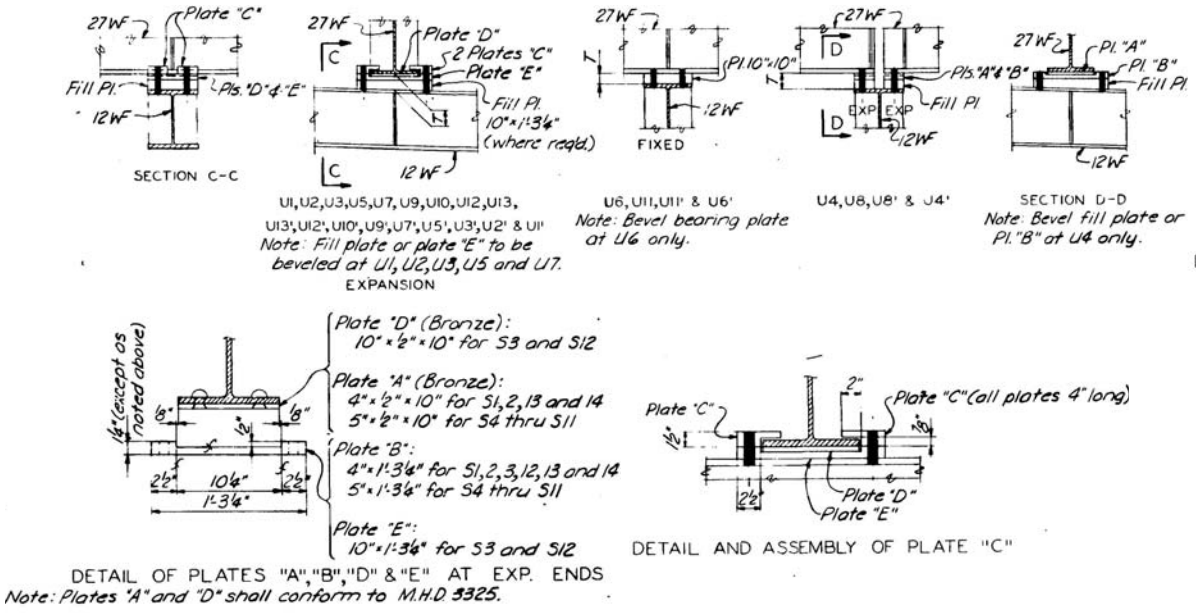

Figure A.7 Stringer seats on upper chord of main trusses (from Mn/DOT 2008).

A.2.3 End Floor Beams

At each end of the deck-truss system, the floor truss was replaced by a varying-depth plate girder shown in Figure A.8. The plate girders are referred to in the construction plan drawing as "end floor beams." The end floor beam had a constant flange width of 12 inches, a constant web thickness of 3/8 inches, and was 70-inch deep on average. The flange thickness varied between 3/4 inches in the edge portions and 1-3/4 inches near the middle portion. As shown in Figure A.8(a), the depth of the south end floor beam varied substantially (deeper in the east edge and shallower in the west edge) in order to accommodate the tilt of the roadway. The end floor beams spanned between the two main trusses, supported an overhang over each side edge, and was supported at the bottom by upper chords of the main trusses.

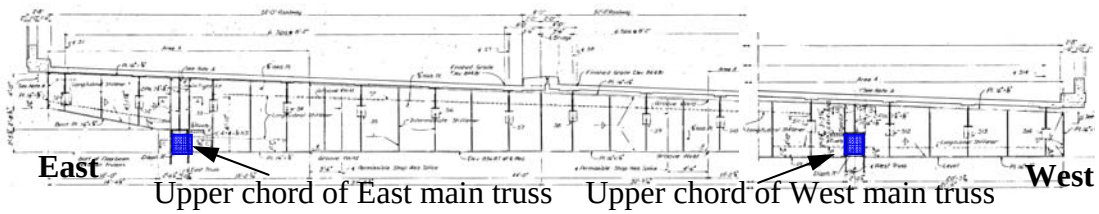

(a) At south end (Panel point U0) viewed from north

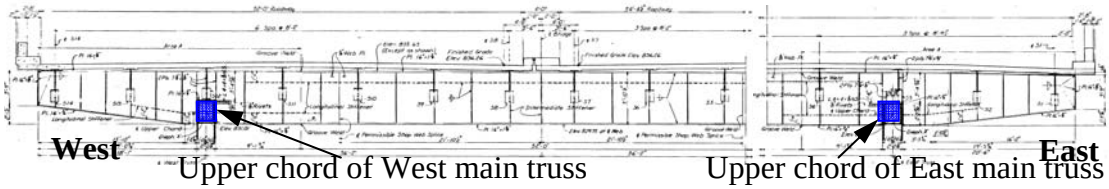

(b) At north end (U0') viewed from south

Figure A.8 End floor beams (from Mn/DOT 2008).

A.2.4 Floor Truss Bracing

The floor trusses were provided with lateral bracing (in the longitudinal direction of the bridge) at two of the five panel points in the lower chord. As shown in Figure A.9, a diagonal brace member was placed in a 45° angle between the braced point in the lower chord and the bottom flange of a W27×94 stringer.

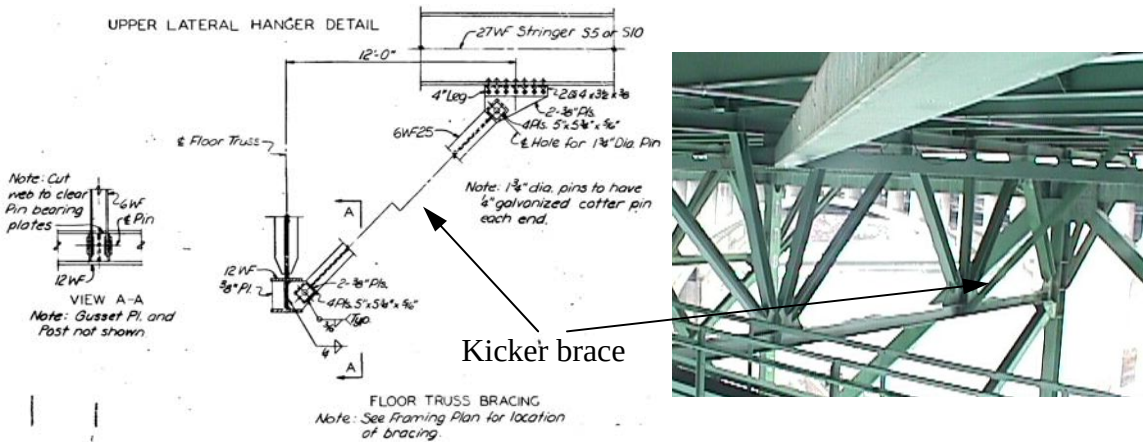

(from Mn/DOT 2008) **(from Prof. Robert Dexter)**

Figure A.9 Lateral bracing of bottom chord of floor truss.

A.2.5 Composite Action between Stringers and Concrete Deck

Shear studs were welded to all stringers, but only in the region close to the expansion joints. Figure A.10 shows that 153 shear studs were placed in the region between the end support point at the expansion joint, and 31 feet from the end support point. Three 7/8-inch diameter, 4-inch long studs were placed in the same cross-section, 3.5 inches apart in the transverse direction. Figure A.11 shows the continuous stringer span between U0 and U4. The photograph was taken on August 31, 2007, roughly one month after the bridge collapse, and after the concrete deck was removed from this segment. The photographs show that shear studs were placed only between U0 and U1 and between U3 and U4, but not between U1 and U3. Judging from the placement pattern, it is suspected that the shear studs were used not to achieve composite action in flexure, but to increase integrity of the concrete deck near the expansion joints, where the concrete deck may be subjected to substantial compression when the deck expands thermally.

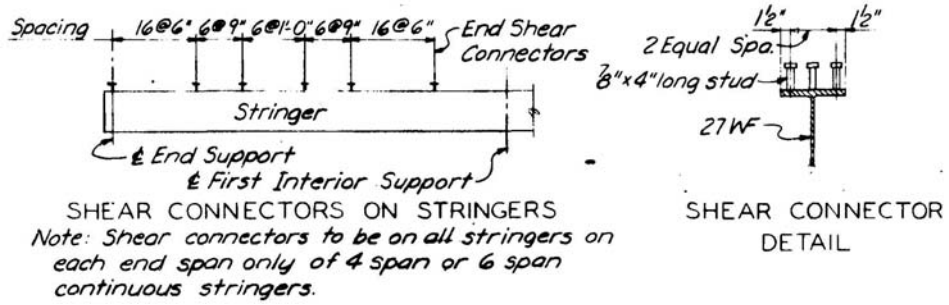

Figure A.10 Location of shear studs on top flange of stringers (from Mn/DOT 2008).

Figure A.11 Shear studs in stringers placed only in the first span of the continuous span (from Prof. Taichiro Okazaki).

A.2.6 Expansion Joints

As described previously, expansion joints were placed at the two ends of the truss system, and at five locations along the deck-truss system. As indicated in Figure A.4, the expansion joints were placed above panel points U4, U8, U14, U8' and U4'. Panel points U8 and U8' were directly above Piers 6 and 7. Figure A.12 shows details of the stringer expansion. Similar to the connection between stringers and the floor truss, bronze insert plates were used, presumably to minimize friction at the stringer expansion joints. At both sides of the expansion joints, the concrete deck was supported transversely by W16×36 beams. Figure A.13 shows photographs of two expansion joints viewed from underneath the concrete deck. The corrugated metal deck in the middle portion of the concrete deck was placed for drainage.

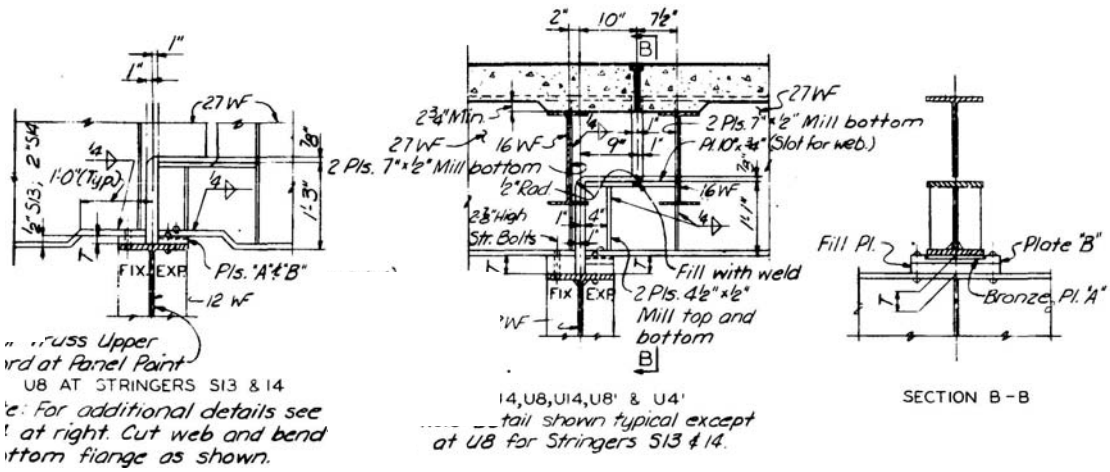

Figure A.12 Details of stringer expansions (from Mn/DOT 2008).

Figure A.13 Photographs of stringer expansions viewed from below (from Prof. Robert Dexter).

A.2.7 Approach Span

Similar to the stringers above the truss system, the approach spans were composed of plate girders supporting the concrete deck. Seven plate girders, placed 8 feet-2 inches apart, supported a composite deck carrying the northbound or southbound traffic.

As shown in Figure A.14, the south approach span is curved according to curve of the roadway. The far south span between the south abutment and Pier 1 is simply supported at the ends, and thus should not transfer load to any other span of the bridge. Across the entire span between Pier 2 and the cross girder (described later in Section A.2.8) near Pier 5, the web plate of the plate girder was 3/8 inches thick and 48 inches deep. The flange was either 12 or 14 inches

wide, and between 3/4 and 1.5 inches thick. Shear studs were placed across the span for composite action.

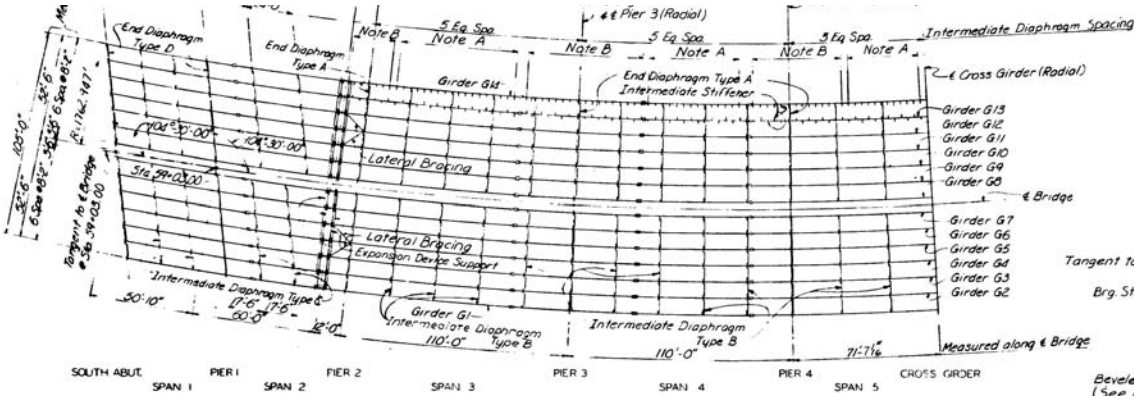

(a) Plan view

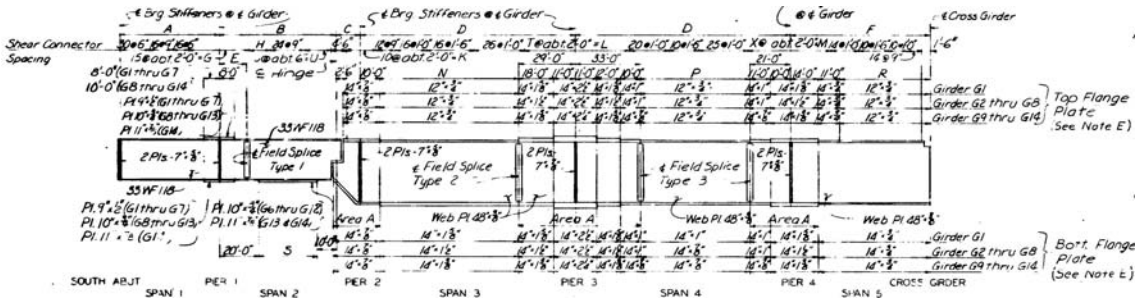

(b) Elevation and section dimensions

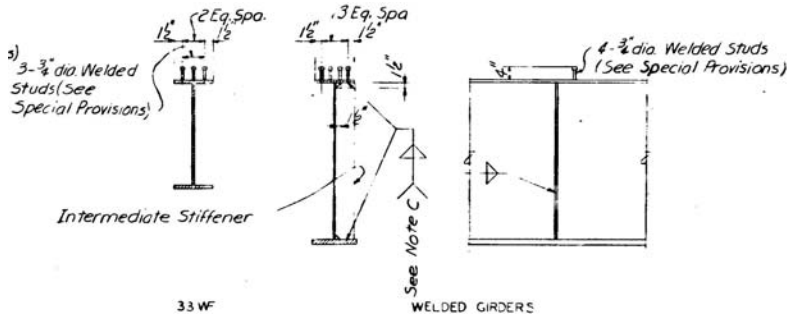

(c) Shear stud placement

Figure A.14 Plate girders in south approach span (from Mn/DOT 2008).

Figure A.15 shows the north approach span between the cross girder near Pier 8 and Pier 11. Girders are added to the east edge of the deck to support the spread of roadway near the north end. Unlike the south approach span, diagonal braces are added to brace the plate girders laterally. The section of the plate girder varied substantially. The web plate varied from 48

inches by 5/8 inches adjacent to the cross girder and 14 inches by 1.25 inches at the north end. The flange was 12, 14, 16, or 20 inches wide, and between 1 and 2 inches thick. Shear studs were placed across the span.

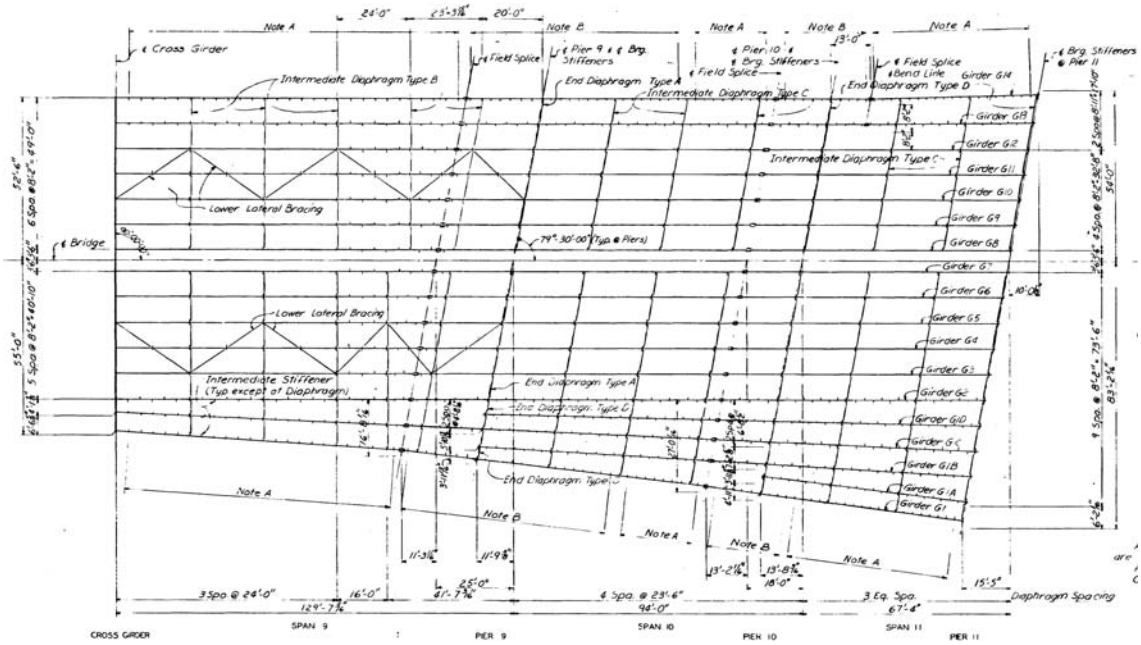

(a) Plan view

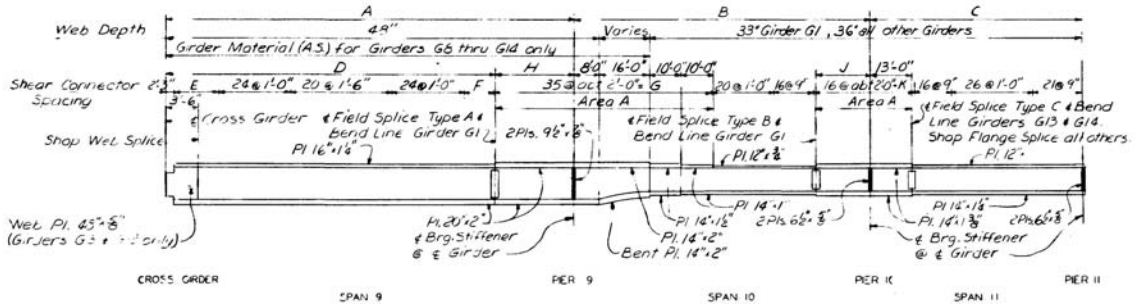

(b) Elevation and section dimensions

Figure A.15 Plate girders in north approach span (from Mn/DOT 2008).

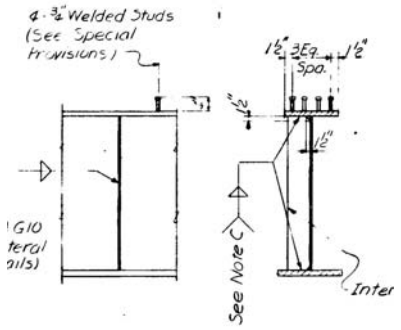

(c) Shear stud placement

Figure A.15 Plate girders in north approach span (from Mn/DOT 2008, continued).

A.2.8 Cross Girder of Approach Span

The end of the approach span was connected to a deep plate girder, referred to as the "cross girder." Figure A.16 shows the cross girders at the south and north approach spans. The cross girders were supported by the main trusses at panel point U0 and U0'. Cast expansion bearings shown in Figure A.17 were placed at node U0 and U0' of the main trusses, which in turn, supported the cross girder. The cross girder had a constant flange width of 16 inches, a constant web thickness of 3/8 inches, and was 80 inches deep on average. A thicker, 3/4-inch thick web was used in the region immediately adjacent to the bearings. The flange thickness varied between 3/4 inches in the edge portions and 2 inches near the middle portion.

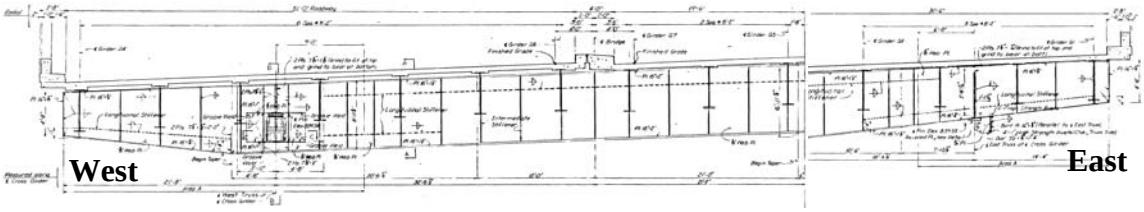

(a) At end of south approach span (panel point U0) viewed from south

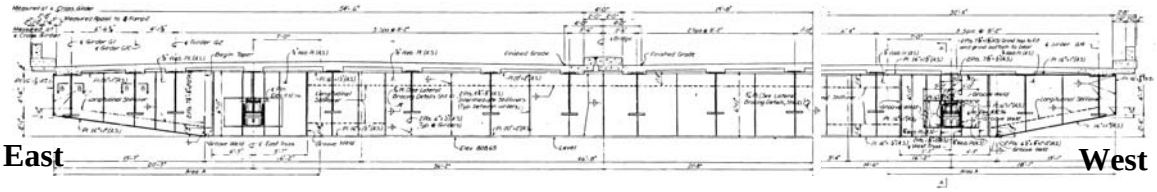

(b) At end of north approach span (U0') viewed from north

Figure A.16 Cross girders (from Mn/DOT 2008).

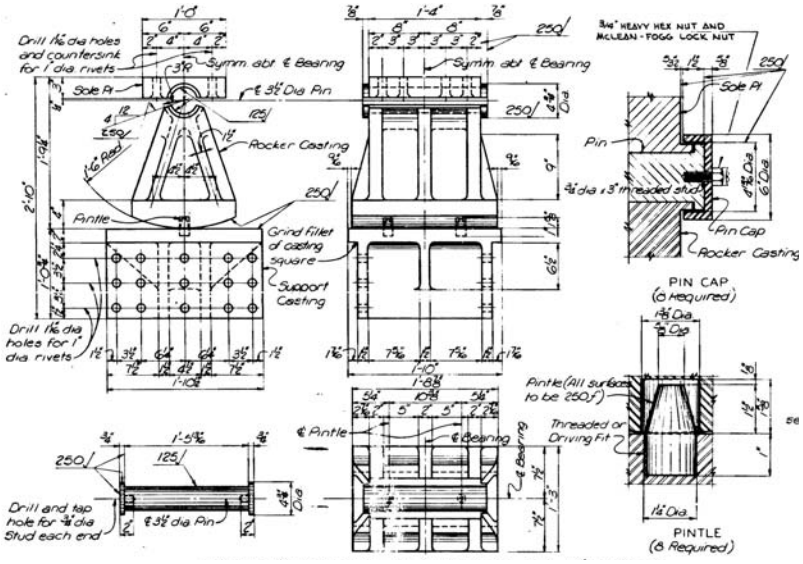

Figure A.17 Expansion bearings between approach span and main truss at panel points U0 and U0' (from Mn/DOT 2008).

APPENDIX B

LOAD ESTIMATION

B.1 Original Design Dead Load (DL1) for 2D Model

The original design dead load (DL1) for the 2D model included the weight of major concrete and steel components, except the self-weight of main truss that was explicitly assigned to the modeled members. Using the layout of the main truss members and the cross-sectional areas provided in the drawings, the net weight of each of the two main trusses was evaluated as 1,260 kips. This section describes the procedure used to evaluate the following components of the dead loads:

Concrete slab

Floor trusses

Sway frames

Lateral bracing system (Upper and Lower)

End floor beams (South and North)

Cross girders (South and North)

W27x94 stringers

C15x33.9 stringer diaphragms

Steel spacer plates between stringer and floor truss

W6x25 kicker braces attached to floor truss

Expansion finger joints

W16x36 beams at expansion joints

Roller bearings placed at U0 and U0'

Miscellaneous steel weight

Loads transferred from the approach spans

B.1.1 Concrete Slab (one deck)

The weight of concrete components was computed based on the cross-sectional dimensions shown in Figure A.5. The weight of concrete, carried by one of the two main trusses, per unit length of the bridge was computed as follows:

- Cross-sectional area of concrete deck = (52' + 2' + 2' 6") × 6.5" = 30.6 ft^2
- Cross-sectional area of concrete parapet = (10" × 2' 8") + (1' × 1' 6") + (2' × 10¼") = 5.39 ft^2
- Total weight of concrete components = (30.6 + 5.39) ft^3 × 0.150 kcf = 5.4 kips/ft

Therefore, the net weight of concrete slab per panel point was evaluated as:

5.4 kips/ft × 38 ft = **205.2 kips**

B.1.2 Floor Trusses (one half)

Each one half of the floor trusses is composed of the following members:

Top chord		W12×53	length 245"
		W12×65	length 196"
		W12×106	length 196"
Diagonals	U1-L3	W10×54	length 174"
	U2-L3	W8×35	length 174"
	U4-L3	W12×92	length 174"
	U4-L5	W10×54	length 174"
	U5-L5	W8×35	length 174"
	U6-L5	W10×54	length 174"
	U6-LC	W8×35	length 174"
	U7-LC	W8×35	length 174"
Bottom chord		W12×65	length 172"
		W12×85	length 270"

The net weight of the above components is computed as: **12.4 kips**

B.1.3 Sway Frames

Each one half of a single-layer sway frame was composed of the following box-section members:

Diagonals	2 plates of 14" × 1/2" and 2 plates of 12" × 3/8"
Intermediate strut	2 plates of 14" × 5/8" and 2 plates of 12" × 3/8"
Bottom strut	2 plates of 15" × 1/2" and 2 plates of 12" × 3/8"

Sway frames had double layers between panel points 6 and 10 and between 6' and 10', and a single layer at the remaining panel points. The height of the sway frame varied between different panel points. The intermediate strut occurred only at double-layer sway frames.

B.1.4 Upper and Lower Braces

Cantilever bracing	W6×18
Upper lateral diagonals	2 plates of 12" × 3/8" and 2 plates of 12" × 3/8"
Lower lateral diagonals	2 plates of 12" × 3/8" and 2 plates of 14" × 3/8"

B.1.5 South End Floor Beam

Flange plate	16" × 3/4"	over	28' 9"	
(top and bottom)	16" × 1-1/4"	over	44'	
	16" × 7/8"	over	36' 3.5"	Total length of 109' 1/2"
Web plate	Depth varying linearly from 9' 2.25" to 5' 5-13/16"			
	Constant thickness of 3/8"			
	Length of 109' 1/2" (neglect taper)			
Intermediate stiffeners	32 double-sided, 3/8"			
Longitudinal stiffeners	Single-sided, 3/4" thick (assumed), 120' long (assumed)			

Net weight: **32.7 kips**

B.1.6 North End Floor Beam

Flange plates	16" × 3/4"	over	28' 3"	
(top and bottom)	16" × 1-1/4"	over	52'	
	16" × 7/8"	over	30' 8"	Total length of 110' 11"
Web plate	Constant depth of 5' 10-1/2"			
	Constant thickness of 3/8"			
	Length of 110' 11" (neglect taper)			
Intermediate stiffeners	32 double-sided, 3/8"			
Longitudinal stiffeners	Single-sided, 3/4" thick (assumed), 120' long (assumed)			

Net weight: **30.2 kips**

B.1.7 South Cross Girder

Flange plate	16" × 3/4"	over	17' 2"	
(top and bottom)	16" × 1"	over	24' 12-7/8"	
	16" × 1-1/2"	over	33'	
	16" × 1"	over	11'	
	16" × 7/8"	over	22' 2-7/8"	
Web plate	Depth varying linearly from 9' 2.25" to 5' 5-13/16"			
	Constant thickness of 3/8"			
	Length of 108' 5-3/4" (neglect taper)			
Intermediate stiffeners	32 double-sided, 3/8"			
Longitudinal stiffeners	Single-sided, 3/4" thick (assumed), 120' long (assumed)			

Net weight: **37.3 kips**

B.1.8 North Cross Girder

Flange plate	16" × 1"	over	15' 7"
(top and bottom)	16" × 1-1/4"	over	82' 4"
	16" × 1"	over	13' 1"
Web plate	Constant depth of 6' 7"		
	Constant thickness of 3/8"		
	Length of 111' (neglect taper)		
Intermediate stiffeners	32 double-sided, 3/8"		
Longitudinal stiffeners	Single-sided, 3/4" thick (assumed), 120' long (assumed)		

Net weight: **36.1 kips**

B.1.9 W27x94 Stringers

7 stringers were for either southbound or northbound.

Total weight of stringers per unit length = 7 × 0.094 kips/ft = 0.658 kips/ft

Weight per panel point of each main truss = 0.658 kips/ft × 38 ft = **25.0 kips**

B.1.10 C15x33.9 Stringer Diaphragms

From Figure A.5, four 98" stringer diaphragms were placed at each panel point. And six 98" stringer diaphragms were placed in the middle of each panel.

Total weight at each panel point = 4 × (98'/12) × 0.0339 kips/ft = 1.11 kips

Total weight in the middle of each panel = 6 × (98'/12) × 0.0339 kips/ft

= 1.66 kips

The stringer diaphragms were placed at totally 22 panel points with the exception of expansion joints, and 28 middle points of each panel.

Total weight per panel point of each main truss = 1.11 + 1.66 = **2.77 kips**

B.1.11 Steel Spacer Plate between Stringer and Floor Truss

The average thickness of spacer plates was estimated as 3". At each panel point, there were totally 7 spacer plates.

Total weight at each panel point = 7 × 10" × 12" × 3" × 0.284 pci = **0.72 kips**

B.1.12 W6x25 Kicker Brace Attached to Floor Truss

One 17' kicker brace was placed at all floor trusses from panel points 1 through 14 and from panel points 13' to 1'. Two kicker braces were used for each floor truss.

Total weight at each panel point = 17' × 0.025 kips/ft = **0.425 kips**

B.1.13 Expansion Finger Joints

The weight of a typical cast finger joint unit was estimated as 1.48 kips. Seventeen casting units were placed at each side of the expansion joint in each deck. Consequently, the net weight of the expansion finger joints at the expansion joint was: 1.48 kips × 34 = **50.4 kips**.

B.1.14 W16x36 Beams at Expansion Joints

Six W16x36 beams, 98" long, were placed at both side of each expansion joint (U4, U8, U14, U8’ and U4’). The total weight of these beams at each expansion joint was: 12 × (98/12 ft) × 0.036 kips/ft = **3.5 kips**.

B.1.15 Roller Bearings Placed at U0 and U0'

From Figure A.17, the weight of the bearing was estimated as **1.5 kips**.

B.1.16 Other Miscellaneous Steel Weight

10% of the sum of steel weight calculated above was used as an estimate of miscellaneous weights, including secondary elements that were not included in the above calculations such as gusset plates, splice plates, and stiffener plates, and the rivets and welds. It is noted here that the self-weight of the main truss was multiplied by a factor of 1.1 in order to account for the same miscellaneous weights.

B.1.17 Load Transferred from Approach Spans

The south approach spans between Piers 2 and 5 was modeled as a three-span, continuous girder, where the far-north support corresponded to panel point U0. Therefore, the reaction at the far-north support was used as an estimate of the load transferred from the south approach spans to the main truss. Similarly, the north approach spans between Piers 8 and 11 was modeled as a continuous girder that yielded the load transferred to the main truss.

A uniformly distributed load was assumed for the continuous girders, which was composed of the following:

- Concrete slab

  As evaluated previously, total weight of concrete components per unit length was 5.4 kips/ft.

- Seven plate girders

Average cross-sectional area of each plate girder was estimated as 45.1 in^2. The net weight of seven girders = 45.1 × 0.284 pci × 7 = 1.08 kips/ft.

- Intermediate diaphragms and intermediate stiffeners

  Six W24×68 beams were used to connect the plate girders laterally, at thirteen locations. The net weight = 0.068 kips/ft × (98/12 ft) × 6 × 13 = 43.3 kips. For simplicity, assume that this weight was uniformly distributed between the three spans, as 43.3 / 298 ft = 0.15 kips/ft.

- Miscellaneous steel weight (intermediate web stiffeners, shear studs, splice plates, bolts, etc.) = 10% of net steel weight = (1.08 + 0.15) × 0.1 = 0.12 kips/ft.

Consequently, the uniformly distributed load was evaluated as: 5.4 + 1.08 + 0.15 + 0.12 = 6.75 kips/ft. Using three moment equation, the load transferred from south approach spans was **170.7 kips**.

Similarly, for the north approach spans between Piers 8 and 11, the uniformly distributed load was evaluated as: 5.4 + 1.5 + 0.14 + 0.16 = 7.2 kips/ft. Therefore, the load transferred from north approach spans was **379.0 kips**.

The loads representing each of the above components are summarized in Table B.1.

B.2 Dead Load After Renovations (DL1 + DL2) for 2D Model

After renovations, the average thickness of the concrete slab was increased by about 2 inches, and new parapets were added on the bridge. Therefore, the weight of concrete components was increased. This also caused additional loads transferred from approach spans. These two loads were recalculated as follows. The weight of steel components was not changed.

B.2.1 Concrete Slab (one deck)

From Figure 3.4, the weight of concrete (carried by one of the two main trusses) per unit length of the bridge was computed as follows:

Cross-sectional area of concrete deck = (52' + 2' + 2' 6") × 8.5" = 40.0 ft^2

Cross-sectional area of concrete parapet = (10" × 2' 8") + (1' × 1' 6") + (2' × 2' 8")
+ (10" × 2' 8")
= 11.3 ft^2

Total weight of concrete components = (40.0 + 11.3) × 0.150 kcf = 7.7 kips/ft

Weight of concrete slab per panel point of each main truss = 7.7 kips/ft × 38 ft
= **292.6 kips**

Table B.1 DL1 applied to 2D model at panel points

Panel Point	Itemized Weight (kips) for Each Category									Total Weight (kips)
	A	B	C	D	E	F	G	H	I	
U0	209.5	102.6	0.0	32.7	0.0	1.6	13.3	50.4	9.8	419.9
U1	0.0	205.2	13.6	0.0	6.6	6.2	27.8	0.0	5.4	264.8
U2	0.0	205.2	13.6	0.0	6.7	9.2	27.8	0.0	5.7	268.2
U3	0.0	205.2	13.6	0.0	6.8	8.0	27.8	0.0	5.6	267.0
U4	0.0	205.2	13.6	0.0	7.0	6.7	26.7	54.0	10.8	324.0
U5	0.0	205.2	13.6	0.0	7.2	8.0	27.8	0.0	5.7	267.5
U6	0.0	205.2	13.6	0.0	11.3	9.8	27.8	0.0	6.3	274.0
U7	0.0	205.2	13.6	0.0	11.8	8.0	27.8	0.0	6.1	272.5
U8	0.0	205.2	13.6	0.0	12.5	6.7	26.7	54.0	11.4	330.1
U9	0.0	205.2	13.6	0.0	11.8	6.7	27.8	0.0	6.0	271.1
U10	0.0	205.2	13.6	0.0	11.3	8.0	27.8	0.0	6.1	272.0
U11	0.0	205.2	13.6	0.0	7.2	9.3	27.8	0.0	5.8	268.9
U12	0.0	205.2	13.6	0.0	7.1	8.0	27.8	0.0	5.7	267.4
U13	0.0	205.2	13.6	0.0	7.0	6.7	27.8	0.0	5.5	265.8
U14	0.0	205.2	13.6	0.0	7.0	5.1	26.7	54.0	10.6	322.2
U0'	416.6	102.6	0.0	30.2	0.0	0.0	13.3	50.4	9.4	622.5

Load categories

A: Load transferred from approach spans (including cross girder and roller bearings)
B: Concrete slab
C: Floor trusses (including kicker braces and weight of steel spacers)
D: End floor beams
E: Sway frames
F: Lateral system
G: W27x94 stringers and C15x33.9 stringer diaphragms
H: Expansion joints (At panel points U4, U8, and U14, the weight of W16x36 beams are included)
I: Miscellaneous = Take 10% of total steel weight including all of C to H

B.2.2 Load Transferred from Approach Spans

As evaluated previously, total weight of concrete components per unit length was 7.7 kips/ft. For south approach spans, the uniformly distributed load was evaluated as: 7.7 + 1.08 + 0.15 + 0.12 = 9.0 kips/ft. Using three moment equation, the load transferred from south approach spans was **228.0 kips**. For north approach spans, the uniformly distributed load was evaluated as: 7.7 + 1.5 + 0.14 + 0.16 = 9.5 kips/ft. Using three moment equation, the load transferred from north approach spans was **500.0 kips**.

Table B.2 summarizes the load values after renovations and distributes them to panel points as concentrated loads.

Table B.2 (DL1 + DL2) applied to 2D model at panel points

Panel Point	Itemized Weight (kips) for Each Category									Total Weight (kips)
	A	B	C	D	E	F	G	H	I	
U0	266.8	146.3	0.0	32.7	0.0	1.6	13.3	50.4	9.8	520.9
U1	0.0	292.6	13.6	0.0	6.6	6.2	27.8	0.0	5.4	352.2
U2	0.0	292.6	13.6	0.0	6.7	9.2	27.8	0.0	5.7	355.6
U3	0.0	292.6	13.6	0.0	6.8	8.0	27.8	0.0	5.6	354.4
U4	0.0	292.6	13.6	0.0	7.0	6.7	26.7	54.0	10.8	411.4
U5	0.0	292.6	13.6	0.0	7.2	8.0	27.8	0.0	5.7	354.9
U6	0.0	292.6	13.6	0.0	11.3	9.8	27.8	0.0	6.3	361.4
U7	0.0	292.6	13.6	0.0	11.8	8.0	27.8	0.0	6.1	359.9
U8	0.0	292.6	13.6	0.0	12.5	6.7	26.7	54.0	11.4	417.5
U9	0.0	292.6	13.6	0.0	11.8	6.7	27.8	0.0	6.0	358.5
U10	0.0	292.6	13.6	0.0	11.3	8.0	27.8	0.0	6.1	359.4
U11	0.0	292.6	13.6	0.0	7.2	9.3	27.8	0.0	5.8	356.3
U12	0.0	292.6	13.6	0.0	7.1	8.0	27.8	0.0	5.7	354.8
U13	0.0	292.6	13.6	0.0	7.0	6.7	27.8	0.0	5.5	353.2
U14	0.0	292.6	13.6	0.0	7.0	5.1	26.7	54.0	10.6	409.6
U0'	537.6	146.3	0.0	30.2	0.0	0.0	13.3	50.4	9.4	787.2

Load categories

A: Load transferred from approach spans (including cross girder and roller bearings)
B: Concrete slab
C: Floor trusses (including kicker braces and weight of steel spacers)
D: End floor beams
E: Sway frames
F: Lateral system
G: W27x94 stringers and C15x33.9 stringer diaphragms
H: Expansion joints (At panel points U4, U8, and U14, the weight of W16x36 beams are included)
I: Miscellaneous = Take 10% of total steel weight including all of C to H

B.3 Live Load (LL) for 2D Model

Based on vehicle data at the time of the collapse released by NTSB (2007), vehicle loads were assumed to be uniformly distributed in the following five portions separately: south approach spans, panel points 0 through 8, panel points 8 through 8', panel points 8' through 0', and north approach spans. After calculations, the distributed load on each portion was estimated as 0.22 kips/ft, 0.31 kips/ft, 0.13 kips/ft, 0.12 kips/ft, and 0.225 kips/ft, respectively. Consequently, using three moment equation, the live load transferred from south approach spans was 5.5 kips, and the live load transferred from north approach spans was 11.9 kips. Table B.3 distributes the live loads to panel points based on tributary area calculations. Each load was multiplied by a factor of 1.3 to consider the impact effects.

Table B.3 LL applied to 2D model at panel points

Panel Point	LL (kips)
U0	14.8
U1-U7	15.3
U8	10.9
U9-U9'	6.4
U8'	6.2
U7'-U1'	5.9
U0'	18.4

B.4 Construction Load (CL) for 2D Model

Construction load was computed based on construction materials and equipment weight report (NTSB 2007). From Figure 3.2, the coarse and fine aggregate piles and construction equipment were located on the inside two southbound lanes close to panel point U10. The coarse aggregate pile was "assumed to extend from 10 feet to 70 feet north of pier 6", and the fine aggregate pile "was assumed to extend from 70 feet to 125 feet north of pier 6". The size of the coarse aggregate pile was estimated to be "60 feet long and about 16 feet wide at the south end and 14 feet wide at the north end". The fine aggregate pile was estimated to be "55 feet long and about 14 feet wide at the south end and 12 feet wide at the north end". The estimated weights of the coarse and fine aggregate piles were 184,380 lbs and 198,820 lbs, respectively.

The coarse and fine aggregate piles crossed panel points U9 through U11. Therefore, the construction material loads were approximated as concentrated loads at those panel points. The concentrated load at each panel joint was calculated proportional to the volume of aggregate piles carried by that panel joint as follows:

U9: 184,380 lbs × 38'/60' = 116.8 kips

U10: 184,380 lbs × 13'/60' + 198,820 lbs × 25'/55' = 130.3 kips

U11: 198,820 lbs × 30'/55' = 108.4 kips

Construction equipment weight (B11-B16, B21, D15 and D16 indicated in Figure 3.2) was shared by two close panel points proportional to the reciprocal of the distance.

U11: 8.955 × 21/38 + 48.2 × 29/38 + 0.2 × 20/38 = 41.8 kips

U12: 8.955 × 17/38 + 48.2 × 9/38 +0.2 × 18/38 + 51.4 × 23/38
+ 24.745 × 31/38 + 48.035 × 11/38 + 0.2 × 11/38 + 0.2 × 4/38
= 80.8 kips

U13: 51.4 × 15/38 + 24.745 × 7/38 + 48.035 × 27/38 + 0.2 × 27/38
+ 0.2 × 34/38 + 2.2 × 31/38 + 2.2 × 19/38 + 1.8 × 1/38
+ 2.2 × 9/38 + 3.3 × 16/38 + 0.2 × 4/38
= 64.2 kips

U14: $2.2 \times 7/38 + 2.2 \times 19/38 + 1.8 \times 37/38 + 2.2 \times 29/38 + 3.3 \times 22/38 + 0.2 \times 34/38 + 0.2$

$= 7.2$ kips

When applied to panel points, above loads were divided by 2 to account for the assumption that the loads were shared by the two main trusses evenly.

B.5 Load Estimation for 3D Model

Loads for 3D model could be obtained based on loads for 2D model with minor modifications. When applying DL1 or (DL1 + DL2) to 3D model, since floor trusses, end floor beams, sway frames, and lateral braces were explicitly modeled, the values for categories C, D, E, and F in Tables B.1 and B.2 became zero. The values for other categories remained. Similar to 2D model, the loads applied to panel points were calculated. Subsequently, the loads were distributed to each upper-chord panel point of the floor trusses proportional to the volume of concrete components carried by that panel point. It is reminded that heavy outside and median parapets were located on the bridge, a larger proportion of loads were carried by end and middle parts of the floor trusses. Live load (LL) and construction load (CL) for 3D model were assigned to specific upper-chord panel points of the floor trusses. The idea of tributary area was employed. Tables B.4 to B.7 summarize the four load conditions for the 3D model. The upper-chord panel points of each floor truss were numbered 1 through 14 from west to east.

Table B.4 DL1 applied to 3D model (unit in kips)

Main Truss Panel Point	Upper-chord Panel Point of Floor Truss				
	1	2-6	7-8	9-13	14
U1-U3 U5-U7 U9-U13 U13'-U9' U7'-U5' U3'-U1'	39.4	30.9	42.0	30.9	39.4
U4 U8 U14 U8' U4'	49.1	38.5	52.4	38.5	49.1

Table B.5 (DL1+DL2) applied to 3D model (unit in kips)

Main Truss Panel Point	Upper-chord Panel Point of Floor Truss				
	1	2-6	7-8	9-13	14
U1-U3 U5-U7 U9-U13 U13'-U9' U7'-U5' U3'-U1'	56.7	38.8	72.5	38.8	56.7
U4 U8 U14 U8' U4'	67.0	45.8	85.6	45.8	67.0

Table B.6 Live load (LL) applied to 3D model (unit in kips)

Main Truss Panel Point	Upper-chord Panel Point of Floor Truss		
	1	2-4	8-10
U1-U7	3.0	6.0	3.3
U8	2.0	4.0	2.6
U9-U9'	1.0	2.0	1.9
U8'	1.1	2.1	1.7
U7'-U1'	1.1	2.2	1.4

Table B.7 Construction load (CL) applied to 3D model (unit in kips)

Main Truss Panel Point	Upper-chord Panel Point of Floor Truss
	5-7
U9	39.0
U10	43.4
U11	50.0
U12	27.0
U13	21.4
U14	2.4